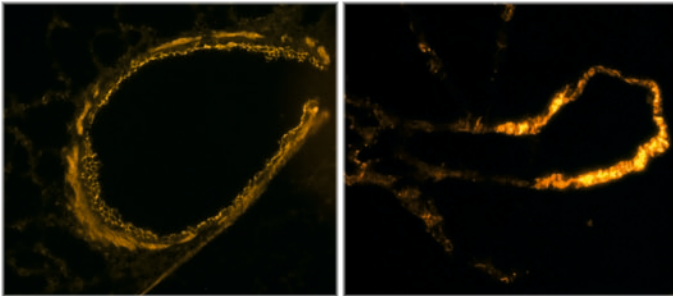


Expression and role of TASK-1 channels in pulmonary vessels and airways

Ghulam Murtaza



INAUGURALDISSERTATION zur Erlangung des Grades eines **Doktors der Humanbiologie**
des Fachbereichs Medizin der Justus-Liebig-Universität Gießen



édition scientifique
VVB LAUFERSWEILER VERLAG

Das Werk ist in allen seinen Teilen urheberrechtlich geschützt.

Jede Verwertung ist ohne schriftliche Zustimmung des Autors oder des Verlages unzulässig. Das gilt insbesondere für Vervielfältigungen, Übersetzungen, Mikroverfilmungen und die Einspeicherung in und Verarbeitung durch elektronische Systeme.

1. Auflage 2012

All rights reserved. No part of this publication may be reproduced, stored in a retrieval system, or transmitted, in any form or by any means, electronic, mechanical, photocopying, recording, or otherwise, without the prior written permission of the Author or the Publishers.

1st Edition 2012

© 2012 by VVB LAUFERSWEILER VERLAG, Giessen
Printed in Germany



édition scientifique
VVB LAUFERSWEILER VERLAG

STAUFENBERGRING 15, D-35396 GIESSEN
Tel: 0641-5599888 Fax: 0641-5599890
email: redaktion@doktorverlag.de

www.doktorverlag.de

**Expression and role of TASK-1 channels
in pulmonary vessels and airways**

Inauguraldissertation
zur Erlangung des Grades eines
Doktors der Humanbiologie
des Fachbereichs Medizin
der Justus-Liebig-Universität Gießen

vorgelegt von

Ghulam Murtaza

aus Daska, Pakistan

Giessen 2012

Aus dem Institut für Anatomie und Zellbiologie
des Fachbereichs Medizin der Justus-Liebig-Universität Giessen
Leiter/Direktor: Prof. Dr. Wolfgang Kummer

Gutachter: Prof. Dr. Wolfgang Kummer
Gutachter: Prof. Dr. Klaus-Dieter Schlüter

Tag der Disputation: 10.09.2012

To

My Parents

I TABLE OF CONTENTS

I	TABLE OF CONTENTS	I
II	LIST OF FIGURES.....	IV
III	LIST OF TABLES	V
IV	LIST OF ABBREVIATIONS	VI
1	INTRODUCTION.....	1
1.1	TASK-1 channels	1
1.2	TASK-1 and NOX4.....	4
1.3	Mucociliary clearance	6
2	MATERIALS AND METHODS	9
2.1	Animals	9
2.2	Immunohistochemistry.....	9
2.3	Western blot	10
2.4	Two-dimensional gel electrophoresis.....	11
2.5	PCR	11
2.5.1	RT-PCR.....	11
2.5.2	Laser-assisted microdissection and subsequent RT-PCR	12
2.5.3	Real-Time RT-PCR.....	13
2.6	Videomorphometry	14
2.6.1	Preparation of precision cut lung slices.....	14
2.6.2	Videomorphometric analysis of precision cut lung slices.....	15
2.6.3	Statistical analysis of videomorphometric data.....	16
2.7	Particle transport speed	16
2.7.1	Preparation of the trachea and imaging.....	16
2.7.2	Particle tracking.....	17
2.7.3	Statistical analysis of PTS data	17
3	RESULTS.....	19

3.1	Immunohistochemistry.....	19
3.1.1	TASK-1 immunohistochemistry in the lung.....	19
3.1.2	TASK-1 immunohistochemistry in the cerebellum.....	21
3.1.3	NOX4 immunohistochemistry in lung, kidney, and cerebellum.....	22
3.1.4	Aldosterone synthase immunohistochemistry in the adrenal gland..	25
3.2	Western blot analysis.....	26
3.2.1	Western blot analysis with anti-TASK-1, lot # AN 03.....	26
3.2.2	Western blot analysis with anti-TASK-1, lot # AN 08.....	27
3.2.3	Western blot analysis with anti-TASK-1, lot # AN 02.....	27
3.2.4	Western blot analysis with anti-NOX4, Santa Cruz.....	28
3.2.5	Western blot analysis with anti-NOX4, Biomol.....	30
3.3	Validity of anti-TASK-1 lot # AN 02, analysed by 2-D gel electrophoresis.....	33
3.4	Qualitative and quantitative RT-PCR.....	33
3.4.1	Expression of TASK-1, TASK-2, and TASK-3, analysed by RT-PCR.....	33
3.4.2	Expression of TASK-1 mRNA in manually dissected tracheal epithelium and trachealis muscle.....	34
3.4.3	Laser-assisted microdissection and RT-PCR for TASK-1 mRNA detection in pulmonary cells.....	35
3.4.3.1	Laser-assisted cell picking.....	35
3.4.3.2	Expression of TASK-1 mRNA in pulmonary structures.....	36
3.4.3.3	Expression of TASK-1 mRNA in tracheal epithelium.....	37
3.4.4	Expression of TASK-1 mRNA, analysed by real-time RT-PCR.....	38
3.4.5	Expression of NOX4 mRNA in NOX4 KO mice, analysed by RT-PCR.....	39
3.5	Videomorphometric analysis of PCLS.....	40
3.5.1	Videomorphometric analysis of pulmonary vessels in response to hypoxia in TASK-1 KO mice.....	41
3.5.2	Videomorphometric analysis of pulmonary vessels in response to anandamide.....	43
3.5.3	A293 causes contractions of vessels independent from TASK-1 channels.....	45

III

3.5.4	Videomorphometric analysis of pulmonary vessels in response to hypoxia in NOX4 KO mice.....	48
3.5.5	Effect of hypoxia and anandamide on bronchoconstriction.....	50
3.6	Measurement of cilia-driven PTS	51
3.6.1	Inhibition of TASK-1 channels does not affect cilia-driven PTS	51
3.6.2	Effect of anesthetics on the cilia-driven PTS	52
3.6.3	Avertin-induced decrease in PTS persisted in the presence of TASK-1 inhibitors and in TASK-1 KO mice	53
4	DISCUSSION	56
4.1	Antibodies and TASK-1 KO mice validity	56
4.2	TASK-1 channels	57
4.3	Relationship between TASK-1 and TASK-3	61
4.4	NOX4	62
4.5	Particle transport speed	65
4.6	Conclusions	66
5	SUMMARY	68
6	ZUSAMMENFASSUNG.....	70
7	REFERENCES.....	73
8	DECLARATION	94
9	CURRICULUM VITAE	95
10	ACKNOWLEDGEMENTS	100

II LIST OF FIGURES

Fig. 1	TASK-1 immunohistochemistry, lung.	20
Fig. 2	TASK-1 immunohistochemistry, cerebellum.	22
Fig. 3	NOX4 immunohistochemistry in the lung, kidney, and cerebellum.....	24
Fig. 4	Aldosterone synthase immunohistochemistry, adrenal gland.....	25
Fig. 5	Western blot, TASK-1 antibody, lot # AN 03.....	26
Fig. 6	Western blot, TASK-1 antibody, lot # AN 08.....	27
Fig. 7	Western blot, TASK-1 antibody, lot # AN 02.....	28
Fig. 8	Western blot, NOX4 antibody, Santa Cruz.	30
Fig. 9	Western blot, NOX4 antibody, Biomol.....	32
Fig. 10	Expression of TASK-1, TASK-2, and TASK-3, RT-PCR, agarose gel.....	34
Fig. 11	Expression of TASK-1 in manually dissected tracheal epithelium and trachealis muscle, RT-PCR, agarose gel.	35
Fig. 12	Laser-assisted cell picking, larger pulmonary vessel.	36
Fig. 13	Laser-assisted microdissection and RT-PCR, agarose gel.	37
Fig. 14	Expression of TASK-1 in laser-microdissected tracheal epithelium, RT-PCR, agarose gel.....	38
Fig. 15	Real-Time RT-PCR analysis of TASK-1 in cerebellum and lung.	39
Fig. 16	Expression of NOX4 mRNA in NOX4 KO mice, RT-PCR, agarose gel.	40
Fig. 17	Videomorphometry, HPV in TASK-1 KO and WT mice.....	42
Fig. 18	Videomorphometry, effect of anandamide on PV under normoxia and hypoxia in TASK-1 WT mice.	44
Fig. 19	Videomorphometry, effect of A293 on PV under normoxia and hypoxia in TASK-1 WT mice.	46
Fig. 19	Videomorphometry, effect of A293 on PV under normoxia in TASK-1 KO mice.	47
Fig. 20	Videomorphometry, HPV in NOX4 KO and WT mice.	49
Fig. 21	Videomorphometry, effect of hypoxia and anandamide on bronchial diameter.....	50
Fig. 22	Inhibition of TASK-1 channel does not affect the cilia-driven PTS.....	51
Fig. 23	Effect of anesthetics on the cilia-driven PTS.	53
Fig. 24	Avertin-induced decrease in PTS in the presence of TASK-1 inhibitors and in TASK-1 KO mice.	55

III LIST OF TABLES

Table 1	Primer pairs used for RT-PCR	14
---------	------------------------------------	----

IV LIST OF ABBREVIATIONS

[Ca ²⁺] _i	intracellular calcium concentration
AA	arachidonic acid
Ach	acetylcholine
AT	adipose tissue
ATP	adenosine triphosphate
BSA	bovine serum albumin
cAMP	cyclic adenosine monophosphate
CBF	ciliary beat frequency
CCD	charge-coupled device
cGMP	cyclic guanosine monophosphate
COPD	chronic obstructive pulmonary disease
DMSO	dimethyl sulfoxide
dNTPs	deoxynucleotid triphosphate
DTT	dithiothreitol
EDTA	ethylenediaminetetraacetic acid
FA	fatty acids
FAD	flavin adenine dinucleotide
FITC	fluorescein isothiocyanate
G-proteins	guanine nucleotide-binding proteins
H ₂ O ₂	hydrogen peroxide
HEK	human embryonic kidney
HEPES	hydroxyethyl piperazine ethane sulphonic acid
HPV	hypoxic pulmonary vasoconstriction
HRP	horseradish peroxidase
K _{2P}	2 pore domain k ⁺ channels
KCNK	potassium channel, subfamily K
kDa	kilodalton
MCC	mucociliary clearance
MEM	minimum essential medium
MLC	myosin light chain
MuLV	moloney murine leukemia virus
NADPH	nicotinamide adenine dinucleotide phosphate

VII

NEB	neuroepithelial body
NO	nitric oxide
NOX	NADPH oxidases
O ₂ ⁻	superoxide
P	pore
PAGE	polyacrylamide gel electrophoresis
PAP	pulmonary artery pressure
PASMC	pulmonary arterial smooth muscle cells
PBS	phosphate buffered saline
PCLS	precision cut lung slices
PCR	polymerase chain reaction
PH	pulmonary hypertension
PMSF	phenylmethylsulfonylfluorid
PTS	particle transport speed
PV	pulmonary vessels
PVDF	polyvinylidene fluoride
RNA	ribonucleic acid
RT-PCR	reverse transcription polymerase chain reaction
SDS	sodium dodecyl sulphate
SEM	standard error of mean
SMC	smooth muscle cells
SPSS	statistical package for the social sciences
TASK	TWIK related acid sensitive K ⁺ channels
TBS	tris-buffered saline
TGF	transforming growth factor
TMS	transmembrane segments
TRAAK	TWIK related arachidonic acid-stimulated K ⁺ channel
TREK	TWIK related K ⁺ channels
TWIK	tandem of P domains in weak inward rectifier K ⁺ channels
αSMA	alpha smooth muscle actin

1 INTRODUCTION

1.1 TASK-1 channels

An increase in pulmonary artery pressure (PAP) is known as pulmonary hypertension (PH). It is a complex disease which is characterized by the thickening of the arterial wall built up by pulmonary arterial smooth muscle cells (PASMC), increased pulmonary vascular resistance due to vasoconstriction and elimination of pulmonary microvasculature. These processes lead to decrease in exercise tolerance and right heart failure and ultimately death ^[1-5]. It also contributes to the morbidity (a diseased state, disability, or poor health due to any cause) and mortality of patients with various lung and heart diseases ^[6-13]. Tightening of blood vessels under certain conditions, diseases like pneumonia, blocking of blood vessels due to some parasites, blood clots and tumors, unknown chemicals or toxins and low supply of oxygen to lungs are a few examples of PH causing agents ^[14].

Pulmonary vasoconstriction (PV) induced by reduced pulmonary arterial pO_2 is known as hypoxic pulmonary vasoconstriction (HPV). This is a physiological phenomenon in which blood is shifted from poorly oxygenated to better ventilated areas of lung. In this way, systemic O_2 delivery ^[15] and ventilation-perfusion matching is optimized while reducing shunt fraction ^[16]. Persistent or intermittent hypoxia contributes to obstructive sleep apnea (obstruction of the upper airway during sleep), pickwickian syndrome also known as obesity hypoventilation syndrome (a condition when overweight people fail to breathe rapidly or deeply enough resulting in low blood oxygen and high blood carbon dioxide levels) and injury or damage to the respiratory center. Chronic hypoxia occurs in obstructive pulmonary disease (COPD, a disease characterized by narrowing of airways), cystic fibrosis (thick, sticky mucus is built up in the lungs and digestive tract), diffuse interstitial pulmonary fibrosis (characterized with swollen and scarred deep lung tissues), radiation fibrosis (lungs get scarred from radiations) and infiltrative lung tumors ^[6-12]. Hypoxia-induced pulmonary vascular remodelling decreases luminal area of the vessels and increases vascular resistance. It leads to PH and right ventricular hypertrophy ^[4]. Under hypoxic conditions deposition of collagen, elastin, fibronectin and tenascin in pulmonary vessels ^[17-19] and an increased expression of transforming growth factor was observed ^[20-24].

Changes in oxygen concentration affect PASMC proliferation and ion transport across the plasma membrane. In PASMC, chronic, acute, and subacute hypoxia induce intrinsic changes in the ionic balance and calcium homeostasis, resulting in membrane depolarization and elevation in resting intracellular calcium concentration $[Ca^{2+}]_i$ ^[25-28]. Cytosolic Ca^{2+} triggers smooth muscle cell (SMC) contraction via the actin-myosin apparatus and expression of immediate early genes, thus inducing a proliferative response ^[29] and PV ^[27, 30]. The extent of SMC contraction depends upon phosphorylation of 20-kDa myosin light chain (MLC₂₀). An increase in MLC₂₀ phosphorylation will increase the contraction of SMC ^[31]. The pore-forming proteins which help to establish and control the small voltage gradient across the plasma membrane and allow movement of ions according to their electrochemical gradient are described as ion channels. A living cell contains more than 300 types of these channels ^[32] and among these potassium (K^+) channels are most widely distributed ^[33].

K^+ channels are protein complexes present in biological membranes. They form potassium-selective pores and allow the passive movement of K^+ across membranes. They are considered as therapeutic targets in the treatment of pain ^[34] and play an obligatory role in controlling K^+ homeostasis and cell volume. They contribute to modifications of the electrical membrane potential, neurotransmitter and hormone secretion, and neuronal and muscular excitability ^[35]. K^+ channels have different numbers of transmembrane segments (TMS) and pore (P) domains. Two pore domain K^+ channels or K_{2P} channels with 4 TMS can be briefly divided into following categories: (1) TWIK-1 (Tandem of P domains in Weak Inward rectifier K^+ channels), also known as KCNK1 (potassium channel, subfamily K, member 1) ^[36] is involved in the regulation of cardiac excitability ^[37, 38], (2) TREK-1 (TWIK-Related K^+ channel), also known as KCNK2 ^[39], is involved in thermosensation ^[40, 41], (3) TASK-1 (TWIK-related Acid-Sensitive K^+ channels), also known as KCNK3 ^[42, 43], (4) TRAAK (TWIK-Related Arachidonic Acid (AA)-stimulated K^+ channels), also known as KCNK4 ^[44], is also involved in thermosensation ^[40, 41], (5) TASK-2, also known as KCNK5 ^[45], is important for osmotic volume regulation in kidney ^[46], (6) TWIK-2 ^[47], is also involved in the regulation of cardiac excitability ^[9], (7) KCNK6, (8) KCNK7 ^[48], both are thought to be silent subunit and their activation depends upon the presence of a partner ^[49, 50], (9) TASK-3, also known as KCNK9 ^[51] has 54% same amino acid sequence as that of TASK-1, but less than 30% with those of other tandem pore K^+ channels and regulates

membrane potential and neuronal firing in the cerebellum ^[52-54], (10) TASK-4, also known as KCNK17 ^[55], is expressed predominantly in adrenal glands and pancreas and is sensitive to alkaline pH ^[55, 56], (11) TASK-5, also known as KCNK15, being mainly expressed in adrenal glands and pancreas is suggested to be involved in the regulation of hormone secretions ^[56]. Amongst the above stated K_{2P} channels, TASK-1 and TASK-3 channels are present in oxygen sensing bodies like the rat carotid body. TASK-1 is an oxygen sensitive channel and has a structure containing two inward-rectifier α subunits and may form dimer with TASK-3 ^[57].

Oxygen tension, pH, mechanical stretch and G-proteins are involved in the regulation of TASK-1 channel open probability ^[50]. Their expression has been reported in rabbit ^[58], rat ^[59, 60], and human ^[61] PASM. The arterial tone is also regulated by the membrane potential of PASM. The closing of K^+ channels in the membrane of PASM decreases K^+ efflux, which causes membrane depolarization and as a result voltage-dependent Ca^{2+} channels will open. Entry of Ca^{2+} will cause vasoconstriction. On the other hand, opening of K^+ channels will lead to increase in K^+ efflux, membrane hyperpolarization and restrict Ca^{2+} entry into the cells. Thus, hyperpolarization of the PASM membrane will cause vasodilation ^[61, 62]. Oxidants and reducing agents may alter the function of K^+ channels ^[63]. Oxidants mimic normoxia and dilate pulmonary vessels, and reducing agents mimic hypoxia and cause constriction to the pulmonary vessels ^[64]. There are certain elements in animal bodies which exhibit altered activity in response to changes in O_2 tension. Mitochondrial complex II ^[65], NOX4 ^[66, 67], and several oxygen-sensitive K^+ channels subunits which open under hypoxia and reversibly close by hypoxia ^[68-78] are examples of such elements.

The pulmonary trunk branches into left and right pulmonary arteries. The pulmonary arteries gradually extend towards the periphery of the lung and further divide by two ways: (1) The stem branch bifurcates into two equal sized branches and the sum of the diameters of both branches is greater than the stem branch, (2) the stem branch collaterally divides into two branches, one of which has same size as the stem and runs in the same direction and the other is of smaller size. Arteries are divided into small and large arteries according to their diameter, Reid et al. classified arteries as small arteries having size up to 1 mm ^[79]. Hislop et al. classified them as small with 50-1000 μm in external diameter and the smaller arteries present specifically in alveolar region as intra-

acinar arteries with diameter $< 100 \mu\text{m}$ [80]. Tabuchi et al. divided arteries into medium-sized arterioles (30-50 μm diameter), and small arterioles ($< 30 \mu\text{m}$) [81]. Pulmonary vessels with different lumen diameter are different in their muscularization. Vessels with diameter $< 100 \mu\text{m}$ are partially muscular [82, 83] and in the rat vessels with diameter $< 50 \mu\text{m}$ have been described as having no muscle at all. Vessels being different in muscularization and size have been investigated independently [81, 84-86]. Tabuchi et al. observed prominent HPV in medium-sized arterioles (30-50 μm diameter), minor in small arterioles ($< 30 \mu\text{m}$), and it was absent in venules in a mouse model [81]. We also divided arteries into small intra-acinar arteries (lumen diameter 25-40 μm) and larger arteries (lumen diameter 41-60 μm) and investigated the role of TASK-1 channels in response to hypoxia separately. Drexler et al. also described mechanical differences between pulmonary trunk and right and left main extrapulmonary arteries and assumed an independent and different behaviour of every section of extrapulmonary arteries [87].

The first aim of present study was to investigate the role of TASK-1 channels in the contraction of pulmonary vessels and airways under hypoxia, as amongst the $\text{K}_{2\text{P}}$ channels this one has been reported as being O_2 sensitive and its opening being regulated by O_2 tension [52, 59]. To carry out this study, bronchoconstriction and PV were investigated under normoxic and hypoxic conditions using precision cut lung slices (PCLS). Intra-acinar and larger pulmonary arteries were studied separately. TASK-1 KO mice and inhibitors (anandamide and A293) were used. In a parallel study, PAP under hypoxia and normoxia was also measured using isolated perfused and ventilated lungs from KO and WT mice.

1.2 TASK-1 and NOX4

The NOX (nicotinamide adenine dinucleotide phosphate, NADPH, oxidases,) family of membrane proteins consists of 7 known members, i.e. NOX1, NOX2, NOX3, NOX4, NOX5, DUOX1 and DUOX2 [88-90]. They are characterized by NAD(P)H and FAD (flavin adenine dinucleotide) binding domains in their C-terminal ends that produce superoxide ($\text{O}_2^{\cdot-}$) by transferring an electron from NADPH (or NADH) to O_2 [90]. According to recent studies, NOX4 predominantly produces hydrogen peroxide (H_2O_2) instead of $\text{O}_2^{\cdot-}$ [91-94]. NOX1 expression has first been described in colon [95]. NOX proteins are present only in specific tissues except NOX4 which was initially reported to be highly expressed in the kidney [96, 97]. NOX4 is also highly expressed in endothelial

cells ^[98], SMC ^[99], cardiomyocytes ^[100, 101], placenta, pancreas, bone, lung ^[88], human airway and PASMC ^[102, 103]. Furthermore, immunohistochemical studies show that NOX components are present in carotid bodies ^[104], pulmonary neuroepithelial bodies (NEB) ^[105], and PASMC ^[106].

NOX1 is suggested to be involved in mitogenesis (mitosis induction) ^[95]. NOX2 is thought to produce a burst of $O_2^{\cdot-}$ and thus kills bacteria ^[2]. This classical leukocyte NOX plays an important role in host defense against bacterial and fungal pathogens ^[107, 108]. It contributes to the development of cardiac hypertrophy and contractile malfunctioning induced by angiotensin II, myocardial infarction (tissue death) or pressure overload ^[109-114]. NOX1 and NOX4 are thought to play a role in vascular pathology ^[115, 116]. In the heart, expression of NOX4 is highly increased during pressure overload ^[110]. NOX4 distinguishes from other NOX family members in that it is regulated mainly at expression level. Further, its activation is not dependent upon agonist stimulation or regulatory subunits ^[91, 92, 117]. It is also upregulated under chronic hypoxic conditions in pulmonary microvasculature ^[118, 119].

NOX4 has also been linked to K_{2P} function. Several subunits assemble to form functional K_{2P} channels. In case of TASK-1, dimerisation of subunits forms a functional channel but this is not containing any structure capable of sensing changes in oxygen and regulating opening and closing of the channel pore ^[62]. Therefore, it is thought that TASK-1 may have a partner protein which primarily senses oxygen tension and then regulates the opening of the TASK-1 channel. A heme protein is reported to be associated with NOX activity. Spectral analysis ^[120] detected the heme signal, and hypoxia induced FAD and $NADP^+$ reduction. These effects were inhibited by NOX inhibitors. In HEK293 (human embryonic kidney) cells, co-localization of TASK-1 and NOX4 has been observed in plasma membranes using fluorescence fusion proteins (combination of two different genes, which originally coded for separate proteins, to create a new protein). TASK-1 channel activity was inhibited by hypoxia and augmented by increasing NOX4 expression. Moreover, TASK-1 responses to changes in pO_2 were abolished by using NOX4 siRNA and NOX inhibitors. Thus, NOX4 is considered as an important partner of TASK-1 in regulating its response to oxygen tension ^[121].

The second objective of the present study was to investigate the functional relationship between TASK-1 and NOX4. The study was performed using TASK-1 and NOX4 KO mice. Contraction of pulmonary small and large vessels in TASK-1 WT and KO mice in response to normoxia and hypoxia was investigated and these results were then compared with results under the same conditions as used previously with NOX4 WT and KO mice.

1.3 Mucociliary clearance

Mucociliary clearance (MCC), also known as mucociliary apparatus, is the process by which bronchi get rid of foreign particles and bacteria and clean themselves. The respiratory epithelium consists of basal cells, unicellular glands known as goblet cells and ciliated cells and dark cytoplasmic non-ciliated cells. A basal membrane is present beneath the epithelium for its support. The basal cells lie near the basal membrane and are considered as stem cells which grow into different kinds of cells. The goblet cells have a shape like a glass and produce mucus. The ciliated cells are equipped with motile cilia, and dark cytoplasmic non-ciliated cells contain secretory granules ^[122]. Brush cells are also reported in respiratory epithelium in lower airways, characterized by an apical tuft of microvilli. They are reported to be involved in chemosensation ^[123], regulating the mucous viscosity ^[124], taste sensing ^[125] and the regulation of respiration ^[126]. The ciliated cells line the main bronchi down to the smallest bronchioli. Mucus fluid in the airways captures the foreign objects such as allergens, bacteria, dust particles, and pollutants. Cilia move in coordination and push the mucus towards the pharynx where it is either swallowed or expelled out through the mouth. MCC depends upon the number, structure, activity and coordinated movement of cilia. Optimum activity of cilia is achieved at a temperature of 37 °C and an absolute humidity of 44 mg/dl³ corresponding to a relative humidity of 100% ^[127-129].

The name cilium is derived from the Latin word for "eyelash" because cilia resemble the tiny projections from cell bodies. Cilia are of two types: motile cilia, usually present on cell surface and beating in a coordinated pattern, and non-motile, also known as primary cilia, having sensory functions. They contain a microtubule-based cytoskeleton known as axoneme. There is also a difference between primary and motile cilia on the basis of the axoneme. In case of primary cilia, the axoneme contains a ring of nine outer microtubule doublets, and in motile cilia, the axoneme has two central microtubule

singlets and nine outer doublets. The axoneme provides support to cilia and serves to provide binding sites to molecular motor proteins. In this way, movement of proteins up and down the microtubules becomes possible. Dynein is an example of molecular motor proteins. A large amount of energy is required for high ciliary beat frequency (CBF). Under normal conditions, cilia of most mucosal surfaces either remain at rest or beat with very slow frequency. However, a variety of receptor-mediated stimuli can dramatically change CBF. For example, when purinergic P1 and P2 ^[130, 131], cholinergic ^[132-134] and adrenergic receptors ^[135], present on ciliated frog palate and esophagus cells, are activated, a profound and prolonged enhancement of CBF is recorded. Acetylcholine (Ach), a neurotransmitter, is also known to accelerate CBF in mammals ^[136-140] and non-mammals ^[130, 131].

Calcium ions are considered very important for participating in regulation of virtually all cell processes. They act by binding and regulating the activity of a large number of cellular proteins, including protein kinases and phosphatases, calmodulin (CaM), phosphodiesterases, adenylate cyclase, ATPases, membrane channels, cytoskeleton elements and many others ^[141]. They also exert their effect on CBF. In ciliated cells, an increase in CBF is recorded with an increase in $[Ca^{2+}]_i$ ^[142, 143]. Moreover, cytosolic Ca^{2+} also regulates the direction and movement of paramecium ^[144]. Cholinergic stimulation in sheep trachea leads to increase in $[Ca^{2+}]_i$ and this subsequently results in increase in CBF ^[145, 146]. Shear stress also causes a large increase in CBF via increase in $[Ca^{2+}]_i$ ^[147]. In addition to cytosolic Ca^{2+} , other components like cAMP and cGMP are also important in enhancing CBF ^[148-150]. These three second messengers (Ca^{2+} , cAMP, and cGMP) directly interact with the axoneme ^[149]. When K^+ channels in the plasma membrane of PASMC are inhibited, a decrease in K^+ efflux is observed and membrane depolarization is resulted. Due to this depolarization, voltage-dependent Ca^{2+} channels get opened and Ca^{2+} enters into the cells. Conversely, opening of K^+ channels increases K^+ efflux, which causes membrane hyperpolarization. It will cause closing of voltage-dependent Ca^{2+} channels and, consequently, a decrease in Ca^{2+} entry ^[61, 62, 25-28].

Inhibition of K^+ channels causes membrane depolarization, opening of Ca^{2+} channels and, consequently, it will facilitate an increase in Ca^{2+} entry into the cells. In ciliated cells, this is expected to rise CBF which is directly related to the amount of Ca^{2+} present within the cells. So the third aim of our study was to explore the role of TASK-1

channels in cilia driven particle transport speed (PTS) in mouse trachea. TASK-1 channels blockers (anandamide and A293) and activators (isoflurane and avertin) were used, and changes in PTS were recorded from isolated trachea from mouse. The role of TASK-1 channels in PTS was further investigated in TASK-1 KO mice and recordings from these animals were compared with corresponding WT animals.

Taken together, there are the following aims of this study:

1. To investigate the role of TASK-1 channel in HPV and bronchial constriction in mice.
2. To find out the functional relation between TASK-1 and NOX4 for sensing changes in O₂ tension.
3. To explore the role of TASK-1 channel in cilia driven PTS in mice.

2 MATERIALS AND METHODS

2.1 Animals

Animals of both sexes were used and maintained under standard laboratory conditions. All experiments were carried out according to guidelines on the care and use of experimental animals provided by National Institutes of Health and after the approval of Regierungspräsidium Giessen. For bronchoconstriction study, FVB mice were used, and for HPV studies, mice were of the C57BL/6 background. Knockout (KO) mice, deficient in *kcnk3* (TASK-1) described in detail previously ^[151] were a kind gift from Prof. W. Wisden, Imperial College London, and NOX4-null mice, described previously ^[101], were from Prof. Ralf Brandes, Goethe University, Frankfurt. KO Mice from the colony were compared to age-matched, WT mice housed in similar conditions. Genotyping of the animals was carried out by polymerase chain reaction (PCR). Genomic DNA used for genotyping was extracted from ear biopsies as template. Mice used were 14-16 weeks old and sacrificed by cervical dislocation or administration of an overdose of inhaled isoflurane or CO₂ asphyxiation.

2.2 Immunohistochemistry

TASK-1, NOX4 WT and KO mice were sacrificed by administration of an overdose of inhaled isoflurane (Abbott, Wiesbaden, Germany), then perfused via the left ventricle with Zamboni's fixative (15% saturated picric acid, 2% paraformaldehyde in 0.1 M phosphate buffer) and proceeded by rinsing solution ^[152]. Tissues were also put in Zamboni's fixative directly after dissection. Another way of fixing organs was to fill the lungs first with cryoembedding medium (Tissue Tek, Sakura, Netherlands) in 0.1 M phosphate buffer, pH 7.4, via a tracheal cannula, and then organs were freshly dissected and shock-frozen in isopentane cooled with liquid nitrogen. Specimens were sectioned with a cryostat (Leica CM 1900, Germany) at 10 µm thickness, mounted on SuperFrost Plus slides (R. Langenbrinck, Emmendingen, Germany), air-dried and subsequently fixed in acetone for 10 min at -20 °C. Next, sections were either first treated with microwaves or directly saturated with blocking solutions. Saturation of nonspecific protein binding sites was done by incubating cryosections for 1 h in blocking medium consisting of either (a) 10% normal swine serum, 0.5% tween, 0.1% bovine serum albumin (BSA) in phosphate buffered saline (PBS), (b) 5% BSA, 5% normal goat serum

in PBS, or of 0.1 M Tris, 5% normal horse serum, 0.5% sodium dodecyl sulfate (SDS), 1% BSA followed by overnight incubation at room temperature with one of the following antibodies: polyclonal rabbit-anti-TASK-1 antibodies (lot # AN 02 and 06, Alomone Labs. Jerusalem, Israel), three different polyclonal rabbit anti-TASK-1 antibodies were a gift from Prof. Rüdiger Veh, Charité - Universitätsmedizin Berlin, monoclonal rabbit anti-NOX4 antibody (cat # 3187-1, Epitomics, Burlingame, California, USA), mouse monoclonal anti-aldosterone synthase antibody was a gift from Prof. Celso E. Gomez-Sanchez, University of Mississippi Medical Center, Jackson, USA. The above mentioned antibodies except the last one, were used individually in combination with monoclonal FITC-labelled anti- α -smooth muscle actin (α SMA) antibody (1:500, clone 1A4, Sigma Aldrich, Steinheim, Germany). Then the samples were washed in PBS, followed by incubation for 1 h with either Cy3-conjugated donkey anti-rabbit Ig (Millipore, California, USA) or Cy3-conjugated donkey anti-mouse Ig (Dianova, Hamburg, Germany). Sections were washed in PBS, postfixed for 10 min in 4% paraformaldehyde, and then washed again in PBS. Mowiol 4-88 (pH 8.6; Merck, Darmstadt, Germany) was applied on the sections, and glass coverslips were placed over them. Sections were evaluated with a Zeiss Axioplan 2 epifluorescence microscope (Jena, Germany) equipped with appropriate filter sets.

2.3 Western blot

TASK-1, NOX4 WT and KO mice were killed with isoflurane and different organs [lung, cerebellum, heart, trachea, kidney, adipose tissue (AT)] were removed. Tissue were weighed and the 5-fold volume of extraction buffer (7 M urea, 10% glycerol, 10 mM Tris-HCl pH 6.8, 1% SDS), 5 mM dithiothreitol (DTT), 0.5 mM phenylmethylsulfonylfluorid (PMSF), and 1x concentrated Complete Mini Protease Inhibitor Cocktail (Roche Diagnostics, Mannheim, Germany) was added to homogenize the tissues. The samples which were later analyzed with rabbit monoclonal anti-NOX4 antibody were also treated without Protease Inhibitor cocktail. After disintegration of the tissues by a ball mill (Mixer Mill MM300; Retsch GmbH, Haan, Germany) total protein concentrations were determined using Bio-Rad Protein assay (Bio-Rad Laboratories, Munich, Germany). Thirty microgram protein per lane was resolved by 10% SDS polyacrylamide gel electrophoresis (PAGE) and transferred onto polyvinylidene fluoride (PVDF) membranes (Millipore, Schwalbach, Germany). The

membranes were first incubated with blocking solution (Tris-buffered saline (TBS), 0.01% Tween 20, and 10% milk powder) for 1 h at room temperature, then overnight at room temperature with following different antibodies: polyclonal rabbit anti-TASK-1 (lot # AN 02, 03, 08), (H-300, Santa Cruz Biotechnology, Germany), monoclonal rabbit anti-NOX4 (cat # 3187-1, Biomol GmbH, Hamburg, Germany), 1:2,000 diluted in TBS, 0.01% Tween 20, and 5% milk powder. After washing the membranes with TBS, 0.01% Tween 20, they were incubated with horseradish peroxidase (HRP)-conjugated goat anti-rabbit IgG (1:10,000 in TBS, 0.01% Tween 20, and 2.5% milk powder; Pierce, Rockford, Illinois, USA). One volume of Super Signal West Dura Extended Duration Substrate (Pierce/Perbio Science Deutschland, Bonn, Germany) mixed with 9 volumes of Super Signal West Pico Chemiluminescent Substrate and X-ray film (Amersham) were used for visualization of bound antibody.

2.4 Two-dimensional gel electrophoresis

Specificity of anti-TASK-1 lot # AN 02 antibody was investigated by two-dimensional (2-D) gel electrophoresis analysis. Antibody along with cerebellum extracts from TASK-1 WT and KO mice were sent to protein analysis laboratory, Institute of Biochemistry, Justus-Liebig University, Giessen, where this experiment was conducted.

2.5 PCR

2.5.1 RT-PCR

TASK-1, NOX4 WT and KO mice were sacrificed by administration of an overdose of inhaled isoflurane. Expression levels of TASK-1, TASK-2, TASK-3 and NOX4 transcripts from lung, cerebellum, heart, AT, kidney, trachea (at least $n = 3$ for each organ or tissue) were determined by RT-PCR. Total RNA was extracted using RNeasy Micro Kit (Qiagen) and was reverse-transcribed by applying following conditions: 8 μ l of RNA was incubated with DNase and 10x DNase reaction buffer, 1 μ l of each for 15 min at 25 °C, then 1 μ l ethylenediaminetetraacetic acid (EDTA) (25 mM) for 10 min at 65 °C, samples were then directly placed on ice and RT mix [1 μ l Oligo (dt), 1 μ l dNTPs (10 mM), 1 μ l super script II reverse transcriptase (200 U/ μ l), 4 μ l 5x first strand buffer, 2 μ l DTT (0.1 M; all reagents were from Invitrogen except dNTPs which were from Qiagen)] was added. The samples were then PCR-amplified using TASK-1,

TASK-2, TASK-3 and NOX4 primers (Table 1). The following conditions were applied: 1 μ l cDNA as template, 2.5 μ l 10x PCR buffer II, 2 μ l MgCl₂ (25 mM), 0.75 μ l dNTPs (10 mM), 0.75 μ l of each primer, 0.2 μ l AmpliTaq Gold DNA Polymerase (5 U/ μ l; all reagents from Applied Biosystems), and 15.3 μ l H₂O. The PCR was conducted using a thermal cycling profile of 95 °C for 12 min, followed by 39 cycles of 20 s at 95 °C, 20 s at 60 °C, and 20 s at 72 °C. The absence of any contaminating genomic DNA was verified via the inclusion of reactions without reverse transcriptase during the first round of cDNA synthesis. Samples were also processed without template. The products were analysed on a 2% agarose gel, which was stained by ethidium bromide and visualized by UV transillumination.

2.5.2 Laser-assisted microdissection and subsequent RT-PCR

Laser-assisted microdissection was used to isolate cardiomyocytes, tracheal epithelium (n = 5), bronchi (n = 1), and SMC from cryosections of small intra-acinar (n = 2) and large pulmonary arteries (n = 3) of TASK-1 WT mice using a MicroBeam System (P.A.L.M. Microlaser Technologies, Bernried, Germany). Animals were killed with isoflurane and lungs were filled with Tissue Tek in 0.1 M phosphate buffer. Organs were freshly dissected and shock-frozen in isopentane cooled with liquid nitrogen. The membrane slides (P.A.L.M. Microlaser Technologies) were radiated with UV light (254 nm) for 30 min and cryosections with 6 μ m thickness were collected on them. The lid of cups was covered with a film of mineral oil and within 1 h after collecting cryosections, tissue was picked and captured into that lid. RNeasy Micro Kit (Qiagen) was used for further RNA isolation and purification according to the protocol provided by manufacturer. Ten microliter RNA were incubated at 70 °C for 10 min. RT mix was added [2 μ l 10x PCR buffer II, 4 μ l MgCl₂ (25 mM), 1 μ l dNTPs (10 mM), 1 μ l random hexamers (50 mM), 0.5 μ l RNase inhibitor (20 U/ μ l), 1 μ l Moloney Murine Leukemia Virus (MuLV) RT (50 U/ μ l), 0.5 μ l H₂O; all reagents were obtained from Applied Biosystems, Darmstadt, Germany]. RNA was reverse-transcribed into cDNA for 75 min at 43 °C and RT was inactivated by heating the samples for 5 min at 99 °C. PCR was performed using gene-specific intron spanning primers for TASK-1 and β -actin (Table 1). Four microliter cDNA, 2.5 μ l 10x PCR buffer II, 2 μ l MgCl₂ (25 mM), 0.5 μ l dNTPs (10 mM), 0.5 μ l of each primer, 0.2 μ l AmpliTaq Gold DNA Polymerase (5 U/ μ l; all reagents from Applied Biosystems), and 15.3 μ l water were applied. The following

conditions were used for PCR: one cycle of 4 min at 95 °C for initial denaturation, followed by 50 cycles with 20 s at 95 °C, 20 s at 59 °C, 20 s at 73 °C, and a final extension of 7 min at 72 °C. Negative controls were run without RT step in sample processing and control reactions for primers included water instead of cDNA. The PCR products were then analyzed using 2% Tris-acetate-EDTA agarose gel electrophoresis.

2.5.3 Real-Time RT-PCR

Total RNAs from lung (n = 3), cerebellum (n = 3) and heart (n = 6) from TASK-1 WT and KO mice were extracted using the RNeasy method according to the protocol described by the manufacturer (Qiagen). Contaminating DNA was digested using 1 unit of DNase I (Invitrogen, Karlsruhe, Germany) per microgram total RNA. RT-PCR was performed for 50 min at 42 °C using 200 units of SuperScript II RT (Invitrogen, Karlsruhe, Germany) per microgram RNA. Real-Time PCR was conducted in an iCycler (Bio-Rad, Munich, Germany) with QuantiTect SYBR Green PCR Kit (Bio-Rad). Gene specific intron spanning primer sets for TASK-1, β -actin, and β -2-microglobulin (β 2M) were used (Table 1). The following PCR conditions were used: one cycle of 10 min at 95 °C for initial denaturation; followed by 40 cycles of 20 s at 95 °C, 20 s at 60 °C, and 20 s at 72 °C. Control reactions were followed in the absence of DNA and RT. Expression of TASK-1 mRNA was calculated in above mentioned samples by comparing their cycle threshold (CT) values to CT values of β -actin, or β 2M, used as reference genes. Relative expression was calculated by using following formula: $2^{-(KO\Delta ct-WT\Delta ct)}$, where Δct is the difference in CT values between the gene of interest and the housekeeping gene. The values obtained from WT animals were set as 100% and the values from KO were expressed as percentage of that. The amplicons were analysed by 2% Tris-acetate-EDTA agarose gel electrophoresis.

Target	Sequence	Length (bp)	Gene Bank Accession No.
TASK-1	For CCTTCTACTTCGCCATCACC Rev GACACGAAACCGATGAGCAC	250	NM_010608
TASK-2	For TGTGCCTGACATGGATCAGT CAATGGTGGAGATGGTGATG	240	NM_021542
TASK-3	For CGCCCTCGAGTCGGACCATG Rev ACCAGCGTCAGGGGGATACCC	288	NM_001033876
NOX4	For TGTTGGGCCTAGGATTGTGTT Rev AGGGACCTTCTGTGATCCTCG	126	NM_015760
β -Actin	For GTGGGAATGGGTCAGAAGG Rev GGCATACAGGGACAGCACA	300	NM_007393
β -2-Microglobulin	For ATGGGAAGCCGAACATACTG Rev CAGTCTCAGTGGGGGTGAAT	177	NM_009735

Table 1 Primer pairs used for RT-PCR.

For: forward primer, Rev: reverse primer.

2.6 Videomorphometry

2.6.1 Preparation of precision cut lung slices

Animals were killed by cervical dislocation and precision cut lung slices (PCLS) were prepared using protocols described by Martin et al. ^[153] and Pfaff et al. ^[154]. For videomorphometric analysis of pulmonary vessels, the pulmonary vasculature was made free from blood by in situ perfusion with 37 °C hydroxyethyl piperazine ethane sulphonic acid (HEPES)-Ringer buffer (10 mM HEPES, 5.6 mM KCl, 136.4 mM NaCl, 11 mM glucose, pH 7.4) containing heparin, 250 I.U./ml (Ratiopharm, Ulm, Germany) and penicillin/streptomycin, (PAA Laboratories, Austria) 1% via the right ventricle. The lungs were filled with 1.5% low melting point agarose (Bio-Rad Laboratories GmbH, Munich, Germany) via the cannulated trachea to stabilize the lung and facilitate the cutting. Thoracic viscera were rapidly excised *en bloc* and transferred in ice-cold HEPES-Ringer buffer and the agarose was solidified. Lobes of lungs were separated and 200 μ m thick slices were cut using a vibratome (VT 1000 S, Leica, Bensheim, Germany). The solidified agarose was removed from the PCLS by incubating them at

37 °C in a humid atmosphere in phenolred-free minimal essential medium (MEM, Invitrogen, Germany) continuously bubbled with a gas containing 21% O₂, 5% CO₂, 74% N₂ for 2-6 h.

2.6.2 Videomorphometric analysis of precision cut lung slices

Experiments on PCLS were carried out in a flow-through superfusion chamber (Hugo Sachs Elektronik, March-Hugstetten, Germany) mounted on an inverted microscope. For investigating hypoxic effects, the chamber was filled with phenolred-free MEM, and for investigating effect of drugs on bronchoconstriction, it was filled with HEPES buffer. Images of intrapulmonary vessels with inner diameters between 25 and 60 µm and of bronchi 150-250 µm were recorded using a charge-coupled device (CCD)-camera (Stemmer Imaging, Puchheim, Germany). The PCLS were placed in the chamber and held with a platinum ring containing nylon strings. Images were recorded every 2 min for pulmonary vessels and every minute for bronchi. Optimas 6.5 software (Stemmer Imaging, Puchheim, Germany) was used for this purpose. Area of the lumen of vessels or airways was set as 100% at the beginning of the experiment. The constriction and dilatation of the lumen were expressed as relative decrease or increase of that area. In case of pulmonary vessels, the value obtained before exposure to reduced oxygen content was set as 100%. In that way, the effects of different substances on hypoxia were presented on the graphs. At the beginning of each experiment, the viability of the vessels was tested with 0.1 µM U46619, a thromboxane analog (Sigma Aldrich, Deisenhofen, Germany), and 25 µM sodium nitroprusside (Nipruss, Schwarz Pharma GmbH Deutschland, Monheim, Germany). That initial phase of the experiments testing the viability of the vessels was not incorporated in the graphs. In case of bronchi, viability was tested by stimulation with 1 µM muscarine (Sigma Aldrich, Deisenhofen, Germany). Only those vessels or bronchi were included in the study, which responded to a stimulus of U46619 (0.1 µM) or muscarine (1 µM), respectively, with at least 20% reduction of the area of lumen. The flow rates through the perfusion chamber were 0.7 ml/min under normoxia (21% O₂, 74% N₂, 5% CO₂) or hypoxia (1% O₂, 94% N₂, 5% CO₂) and 6 ml/min for washing steps. There was no flow through the perfusion chamber during the application of muscarine, U46619 and nipruss, and when other substances were applied, the flow rates were low (0.7 ml/min).

2.6.3 Statistical analysis of videomorphometric data

Data in the figures are given as means \pm standard error of the mean (SEM) of 7-13 intra-acinar and 8-13 larger pre-acinar pulmonary arteries per condition. Only one vessel or bronchus per PCLS was analysed. PCLS for intra-acinar arteries were obtained from 3-0 mice and for large arteries from 5-9 mice. SPSS 11.5.1 software was used for statistical analysis. Analysis of differences among experimental groups was with the Kruskal-Wallis-test followed by the Mann-Whitney-test. P values ≤ 0.05 and ≤ 0.01 were considered as significant, and highly significant, respectively. For bronchoconstriction study, 3-5 PCLS were obtained from 1-2 mice.

2.7 Particle transport speed

2.7.1 Preparation of the trachea and imaging

Mice were killed by exposure to carbon dioxide environment. The submandibular gland and the infrahyoid musculature were removed after the thorax being opened with scissors. The trachea was cut caudal to the larynx and cranial to the bifurcation, and then transferred to a Delta T culture dish (Biotech, Butler, PA, USA). The Sylgard polymer (Dow Corning, Wiesbaden, Germany) was used to fill the bottom of the dish which was filled with 2 ml cold HEPES-Ringer solution. The blood vessels and connective tissues from the trachea were detached and discarded and it was oriented with the trachealis muscle facing upward. Two insect needles were inserted through trachea in Sylgard polymer on opposite sides for its fixation.

The trachealis muscle was cut using Vannas-Tübingen spring scissors (Fine Science Tools, Heidelberg, Germany) and rinsed with HEPES. Then, the HEPES-Ringer solution was replaced by 1-2 ml fresh warm buffer and the trachea was submerged in it. Then the culture dish was transferred to the Delta T Stage holder 30 min after the death of animal. The temperature of the dish was kept constant at 30 °C during the experiment. To conduct the experiments where application of isoflurane was involved, an isoflurane vaporizer (Abbott, Wiesbaden, Germany) was used. Imaging was proceeded with a Till Vision imaging system (Till Photonics, Gräfelfing, Germany) based on an Olympus BX50 WI microscope (Olympus, Hamburg, Germany), which was equipped with an Imago CCD camera having 1280 x 960 pixels (Till Photonics).

Prior to measurements, 1.5-2.3 μl of a polystyrene bead suspension (mean diameter 2.8 μm , Invitrogen Dynal AS, Oslo, Norway) were added to Delta dish and mixed well and gently. The tracheal epithelial surface was imaged in bright field mode using a 20x water immersion objective (Olympus). Polystyrene beads were recognized by their round structure and brownish colour. An area between two cartilages was chosen for imaging and recordings to avoid large differences in image brightness. Two hundred images were taken for each time point. The exposure time for each image was 20 ms and delay between two images was 85 ms. At the end of each experiment the viability of the ciliated cells was tested with 100 μM ATP, which stimulates CBF via purinergic receptors. Fifty five mice were sacrificed for the experiments. The number of mice for each experiment is shown in the respective figures and legends.

2.7.2 Particle tracking

An average of 200 images of an individual series was calculated and subtracted to remove non-moving objects in the images. It was done on the basis of pixel-by-pixel from each image in the series. If the subtraction value was negative, then the absolute value was taken. The above mentioned procedure facilitated in obtaining a bright image of the formerly darker polystyrene beads. A binary picture was obtained from the copy of series by a thresholding procedure and the image of polystyrene beads was adjusted to bright and the background to dark. A reduction of original film was made from 12 to 8 bit grayscale. Both series were further used for particle tracking by an automatic tracking procedure. TILLvisTRAC software (Till Photonics) was used for this purpose. Only those tracks were included in further calculations which were measured over a length of at least 10 frames. The average of the mean speed of all tracks was calculated.

2.7.3 Statistical analysis of PTS data

Effects of substances on PTS were measured at the first time interval after their application. Moreover, Δ values of substances and vehicles were also compared. SPSS 11.5.1 software was used to conduct statistical analysis. Normal distribution of data was tested with Kolmogorov-Smirnov test, showing no significant difference of the data set to normal distribution. To compare the difference between two points from one experiment and to compare the same time point from different experiments, analysis

was carried out with paired t-test and ANOVA test, respectively. P values ≤ 0.05 were regarded as being statistically significant.

3 RESULTS

3.1 Immunohistochemistry

3.1.1 TASK-1 immunohistochemistry in the lung

Five different anti-TASK-1 antibodies were used to locate the TASK-1 protein in the lung. Immunohistochemical studies were also performed on specimens taken from TASK-1 KO mice and staining was compared with the corresponding WT mice. Anti- α SMA antibody was also used in all the samples to visualize SMC. Rabbit polyclonal anti-TASK-1 (lot # AN 06) antibody labelled SMC of vessels and airways. It also intensively labelled bronchial epithelium (Fig. 1A). Amongst the rabbit polyclonal anti-TASK-1 antibodies (gift from Prof. Rüdiger Veh, Charité), labelling with one antibody was strong in bronchial epithelium as compared to bronchial and vascular SMC (Fig. 1C), and with two other antibodies, a very weak staining was observed both in vessels and airways (Figs. 1E, G). Rabbit polyclonal anti-TASK-1 (lot # AN 02) antibody resulted in labelling only in large but not in small arteries (Fig. 1K). It also stained airway SMC, but only weakly the bronchial epithelium (Fig. 1F). All TASK-1 antibodies showed equal staining intensity in KO mice samples (Figs. 1B, D, F, H, J) when compared with corresponding WT (Figs. 1A'-J'). Labelling was absent in the sample treated without primary antibody (Fig. 1L). Different patterns of labelling with the above described antibodies and the presence of staining in KO mice demonstrated the nonspecific binding of these antibodies.

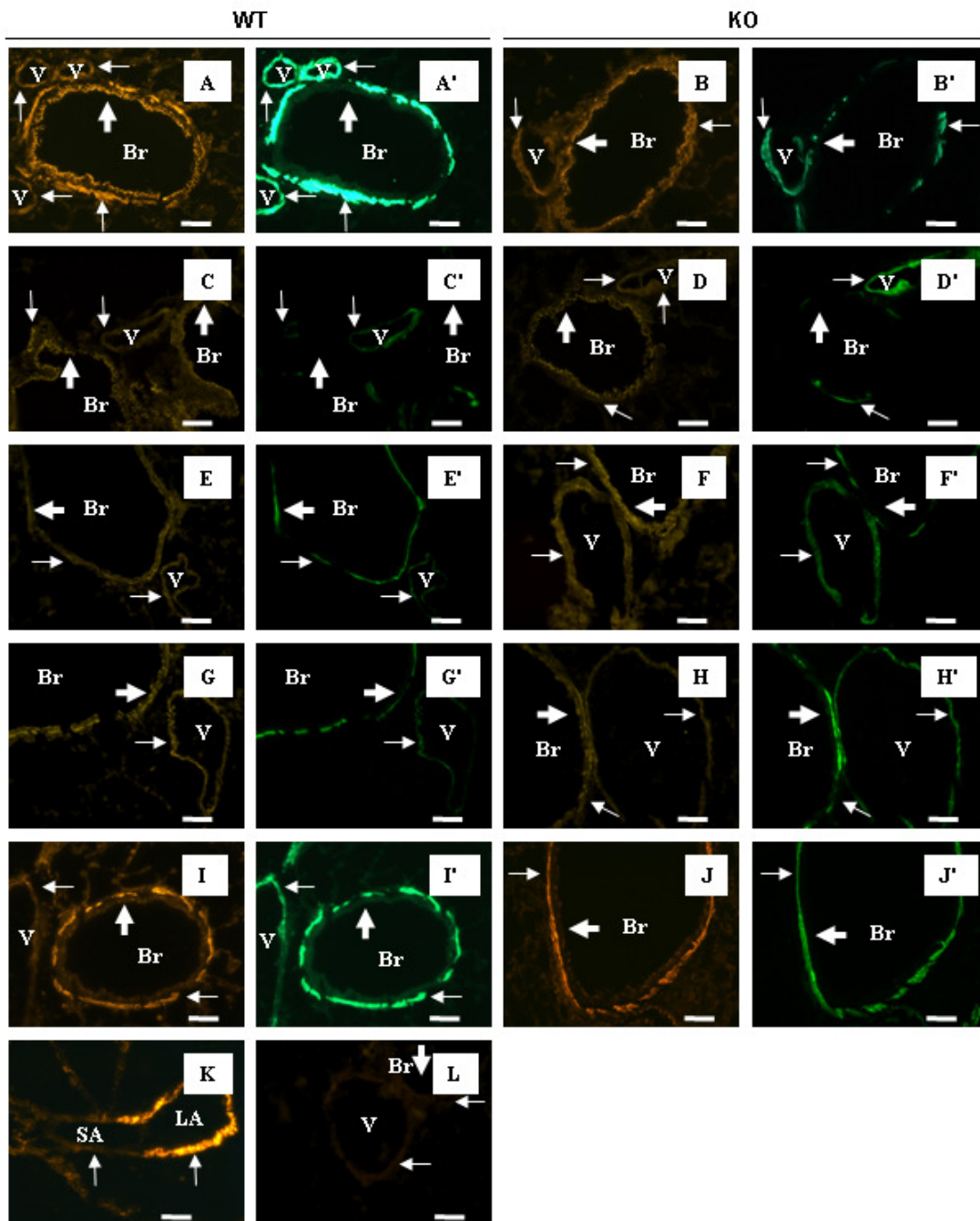


Fig. 1 TASK-1 immunohistochemistry, lung.

Staining patterns with different TASK-1 antibodies were different. KO samples also showed similar staining results when compared to WT. A'-J' represent anti- α SMA staining to demonstrate SMC. The sample treated without primary antibody showed no labelling (L). First row represents labelling with anti-TASK-1 antibody lot # AN 06. Second, third, and fourth with anti-TASK-1 antibodies gifted by Prof. Rüdiger Veh, Charité. Fifth row and K with anti-TASK-1 antibody lot # AN 02. *Thick arrows*: bronchial epithelium, *thin arrows*: smooth muscle cells. Abbreviations: V: vessel, Br: bronchus, SA: small artery, LA: large artery, WT: wild-type, KO: knockout, bar: 50 μ m.

3.1.2 TASK-1 immunohistochemistry in the cerebellum

In the cerebellum of TASK-1 WT and KO mice, labelling was observed in pia mater, molecular layer, Purkinje cell layer and granule cell layer with rabbit polyclonal anti-TASK-1 (lot # AN 02) antibody (Fig. 2A). Amongst the TASK-1 antibodies provided by Prof. Rüdiger Veh, Charité, one antibody did not show staining in cerebellum (Fig. 2C), while the other two antibodies labelled only pia mater (Figs. 2E, G). All TASK-1 antibodies tested also produced identical immunohistochemical labelling patterns in the cerebellum taken from KO (Figs. 2B, D, F). Secondary reagent control treated under the same experimental conditions but without TASK-1 antibodies was without any staining (Fig. 2I). Different staining patterns and the presence of identical staining in KO mice demonstrated nonspecific binding of TASK-1 antibodies.

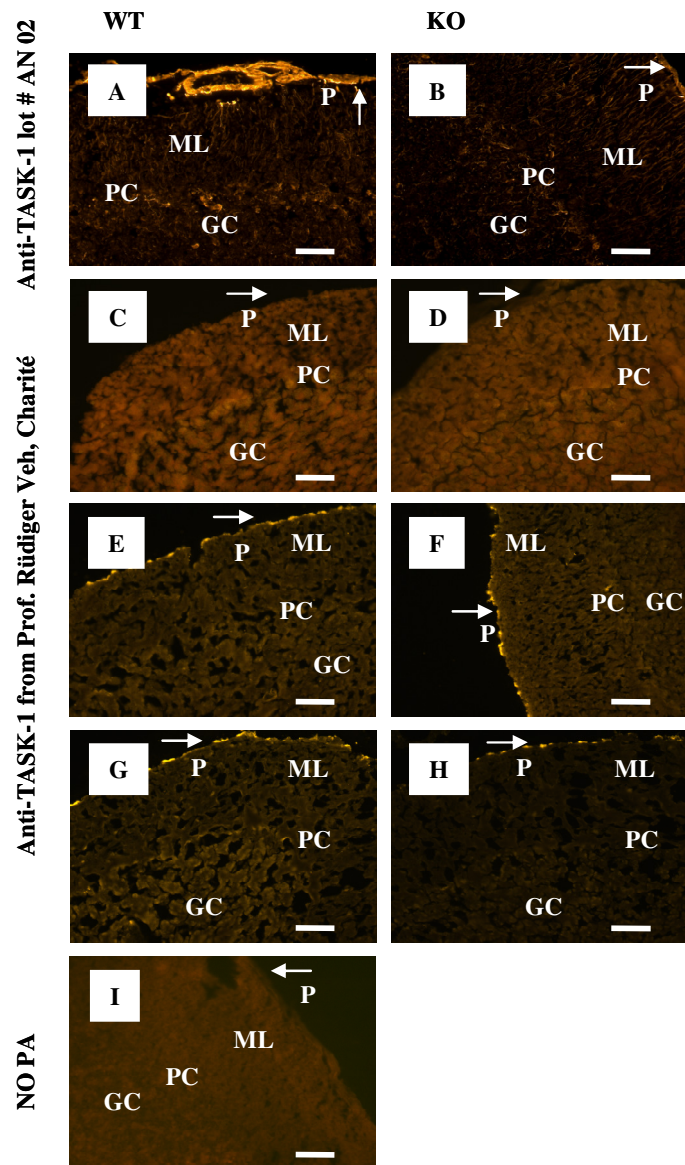


Fig. 2 TASK-1 immunohistochemistry, cerebellum.

All antibodies produced different labelling patterns. Abbreviations: P: pia mater, ML: molecular layer, PC: Purkinje cell layer, GC: granule cell layer, WT: wild-type, KO: knockout, PA: primary antibody, *arrows*: pia mater, bar: 50 μm.

3.1.3 NOX4 immunohistochemistry in lung, kidney, and cerebellum

Monoclonal rabbit anti-NOX4 antibody was used to investigate the localization of NOX4 protein in the lung, kidney, and cerebellum. Anti- α SMA antibody was used to visualize SMC. The NOX4 WT and KO mice used were perfused with and samples subsequently immersed in Zamboni's fixative. Samples were also treated with

microwave/proteinase K/proteinase K plus microwave. Treatment of samples with proteinase K was carried out in an attempt to reduced nonspecific binding to other proteins since NOX4 itself is more resistant to digestion (Prof. R. Brandes, personal communication). Different patterns of labelling with anti-NOX4 antibody in different tissues and under different experimental conditions were observed. In microwave treated lung samples, from both KO and WT mice, labelling with NOX4 antibody in vessels and bronchial SMC was either absent or too weak to be observed. However, in bronchial epithelium, staining was detected although it was not prominent (Figs. 3A, B). Still strong staining with α SMA antibody was observed in vessels and bronchial SMC (Figs. 3A', B'). In microwave plus proteinase K treated lung samples from WT and KO mice, staining with anti-NOX4 (Figs. 3C, D) and anti- α SMA (Figs. 3C', D') antibodies was absent or very weak. No staining was observed from the secondary reagent control lung sample, where it was treated in the same way (microwave treatment) but without primary antibody (Fig. 3O).

The kidney samples, from NOX4 WT and KO mice, were treated with microwave/proteinase K/microwave plus proteinase K. Labelling with anti-NOX4 antibody was very weak or absent in microwave (Figs. 3E, F), proteinase K (Figs. 3G, H) and microwave plus proteinase K (Figs. 3I, J) treated samples. Staining was also absent from the sample treated under the same conditions (microwave) but without primary antibody (Fig. 3P). A weak labelling with NOX4 antibody was observed in cerebellar molecular, Purkinje and granule cell layers in microwave (Fig. 3K) and microwave plus proteinase K (Fig. 3M) treated samples from NOX4 WT mice. In microwave treated cerebellum from NOX4 KO mice, staining was intense (Fig. 3L) and in microwave plus proteinase K treated KO cerebellum it was weak as compared to WT sample (Fig. 3N). The kidney, cerebellum and lung samples from NOX4 WT mice showed expression of NOX4 mRNA in RT-PCR analysis, and this expression was absent in KO mice. Therefore, presence of immunohistochemical labelling in lung and cerebellum samples from NOX4 KO mice and the absence of labelling in the kidney from both WT and NOX4 KO animals, pictured the unspecific binding of antibodies in the tissues. Immunolabelling was absent from the cerebellum treated under same conditions (microwave treatment) but without primary antibody, demonstrating that nonspecific labelling was not caused by the secondary antibody (Fig. 3Q).

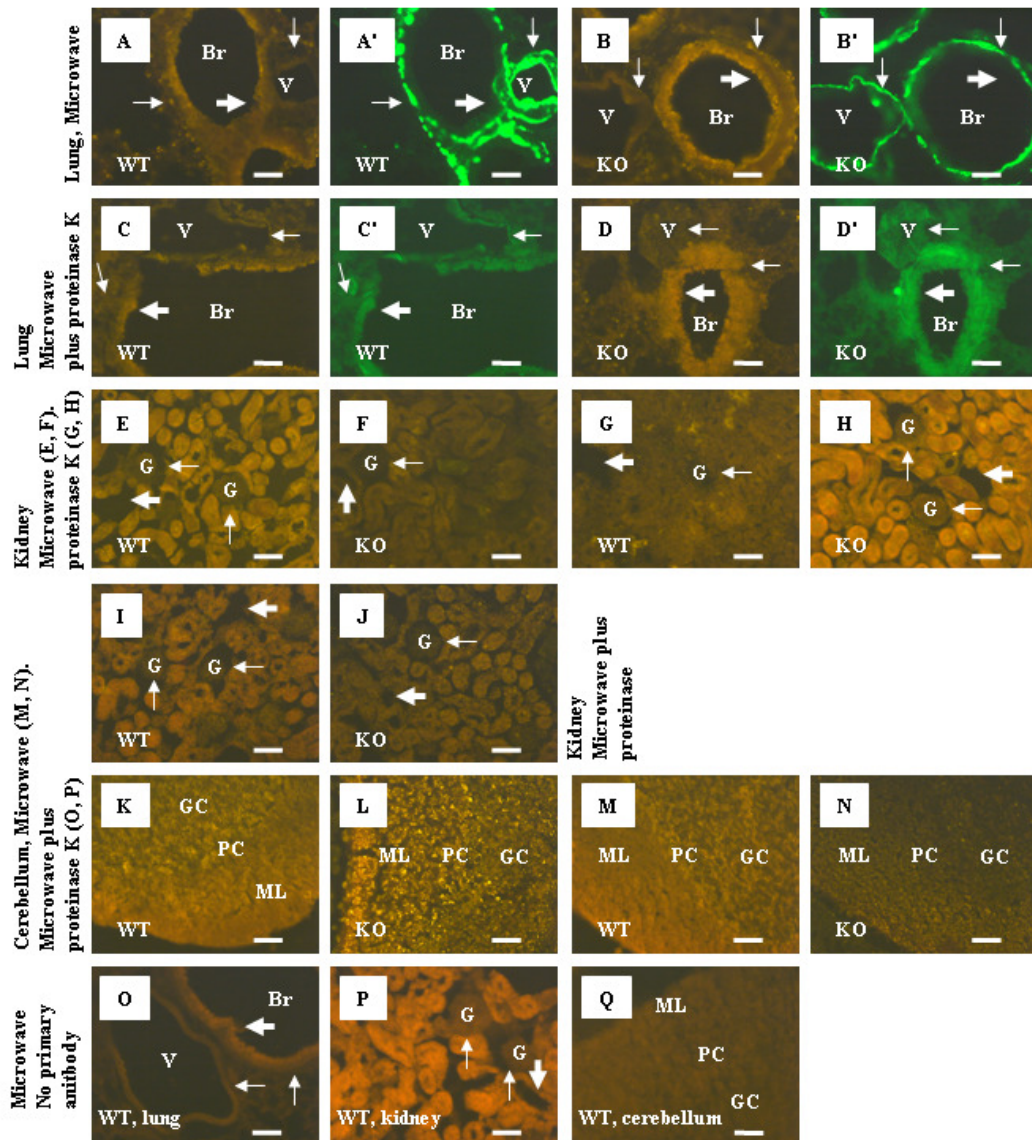


Fig. 3 NOX4 immunohistochemistry in the lung, kidney, and cerebellum.

First row: microwave treated lung, second row: microwave plus proteinase K treated lung, third row, E, F: microwave treated, and G, H: proteinase k treated, fourth row: microwave plus proteinase K treated kidney, fifth row, K, L: microwave treated, and M, N: microwave plus proteinase K treated cerebellum, sixth row: microwave treated, WT lung (O), kidney (P), and cerebellum (Q), secondary reagent controls. *Thick arrows*: bronchial epithelium, in case of lung and glomerulus in case of kidney samples. A'-D' represent staining with anti- α SMA antibody. *Thin arrows*: tracheal and vessels SMC in lung samples, and Bowman's capsule in kidney. Abbreviations: WT: wild-type, KO: knockout, Br: bronchus, V: vessel, G: glomerulus, GC: granule cell layer, PC: Purkinje cell layer, ML: molecular layer, bar: 50 μ m.

3.1.4 Aldosterone synthase immunohistochemistry in the adrenal gland

Western blot and immunohistochemistry analysis by available antibodies did not yield reliable results since staining patterns in KO and corresponding WT mice were indistinguishable. Moreover, real-time RT-PCR data also showed some residual mRNA expression in KO mice. To remove the ambiguity about the KO mice used, immunohistochemistry was performed on adrenal glands from female TASK-1 WT and KO mice with mouse monoclonal anti-aldosterone synthase antibody (gift from Prof. Celso E. Gomez-Sanchez), as female KO mice show disrupted adrenal gland zonation. Distribution of aldosterone synthase extends to deeper regions of the adrenal cortex instead of restraining to zona glomerulosa ^[155]. This KO mouse strain was used in our study, and in female WT, the labelling with aldosterone synthase antibody was confined to the zona glomerulosa (Fig. 4A), whereas, in female KO mice, staining was very weak and absent in that region. Instead it was distributed over the entire adrenal cortex (Fig. 4B). This phenotype confirmed that indeed TASK-1 KO mice were used, albeit with some residual mRNA content detected by RT-PCR.



Fig. 4 Aldosterone synthase immunohistochemistry, adrenal gland.

TASK-1 WT and KO mice samples showed quite different labelling patterns with anti-aldosterone synthase antibody. Labelling was absent in the WT sample treated without primary antibody (C). Abbreviations: ZG: zona glomerulosa, ZF: zona fasciculata, ZR: zona reticularis, WT: wild-type, KO: knockout, bar: 50 μ m.

3.2 Western blot analysis

3.2.1 Western blot analysis with anti-TASK-1, lot # AN 03

Western blot study gave different results with different antibodies. The molecular weight of the TASK-1 protein is 45.4 kDa. The polyclonal rabbit anti-TASK-1 antibody (lot # AN 03) labelled samples in the following organs and tissues from TASK-1 WT mice: lung, TE, trachea without epithelium (from which TE was abraded), heart and cerebellum (Fig. 5). Heart and cerebellum were taken as a positive control, as TASK-1 is highly expressed in these organs. All tested organs were also run without primary antibody to test the specificity of the secondary antibody. An unexpected band of 55 kDa and very weak labelling in heart samples indicated unspecific binding of this antibody.

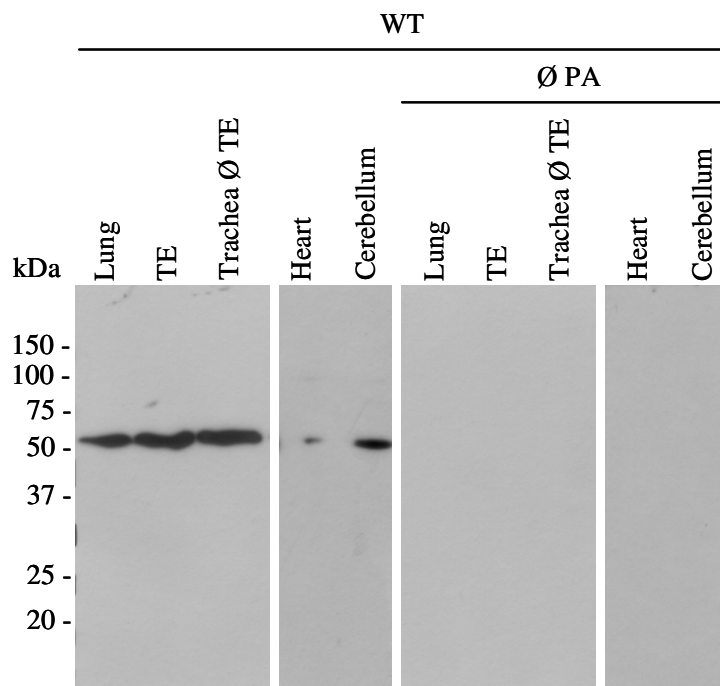


Fig. 5 Western blot, TASK-1 antibody, lot # AN 03.

An immunoreactive band of 55 kDa was observed. Abbreviations: kDa: kilodalton, TE: tracheal epithelium, Ø TE: without tracheal epithelium, Ø PA: without primary antibody, WT: wild-type.

3.2.2 Western blot analysis with anti-TASK-1, lot # AN 08

Lung, heart, and cerebellum from both TASK-1 KO and corresponding WT mice were investigated for TASK-1 protein expression with polyclonal rabbit anti-TASK-1 antibody but from different lot # AN 08. Bands on the membrane were observed in samples of all the above mentioned organs except cerebellum taken from both KO and WT animals (Fig. 6), and even more than one band were observed in lung samples in both cases (WT and KO). Here, labelling of KO samples questions the specificity and validity of this antibody, and absence of any band in cerebellar samples further adds to the antibody nonspecificity as TASK-1 is highly expressed in the cerebellum.

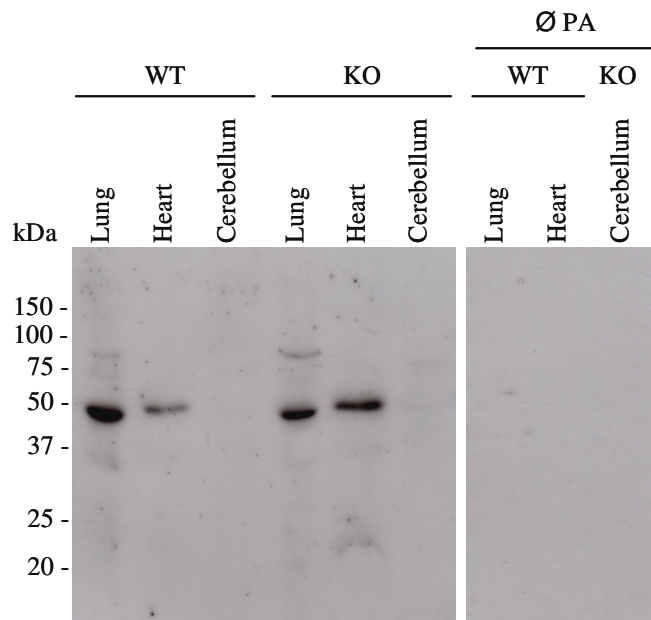


Fig. 6 Western blot, TASK-1 antibody, lot # AN 08.

A band of 45 kDa was observed, corresponding exactly to the molecular weight of TASK-1 protein. However, this labelling was noted both in WT and KO samples. Heart and cerebellum were used as a positive control. Abbreviations: kDa: kilodalton, Ø TE: without tracheal epithelium, Ø PA: without primary antibody, WT: wild-type, KO: knockout.

3.2.3 Western blot analysis with anti-TASK-1, lot # AN 02

Protein expression of TASK-1 in the lung from KO, heterozygous (HZ) and WT mice was examined using polyclonal rabbit anti-TASK-1 antibody, lot # AN 02. Strongly

immunolabelled bands were observed in heart samples as compared to cerebellum, and labelling of lung extracts was very weak or absent. Samples treated without primary antibody showed no band on the membrane. Detection of bands in KO samples and very weak labelling in lungs points towards the unspecificity of this antibody also.

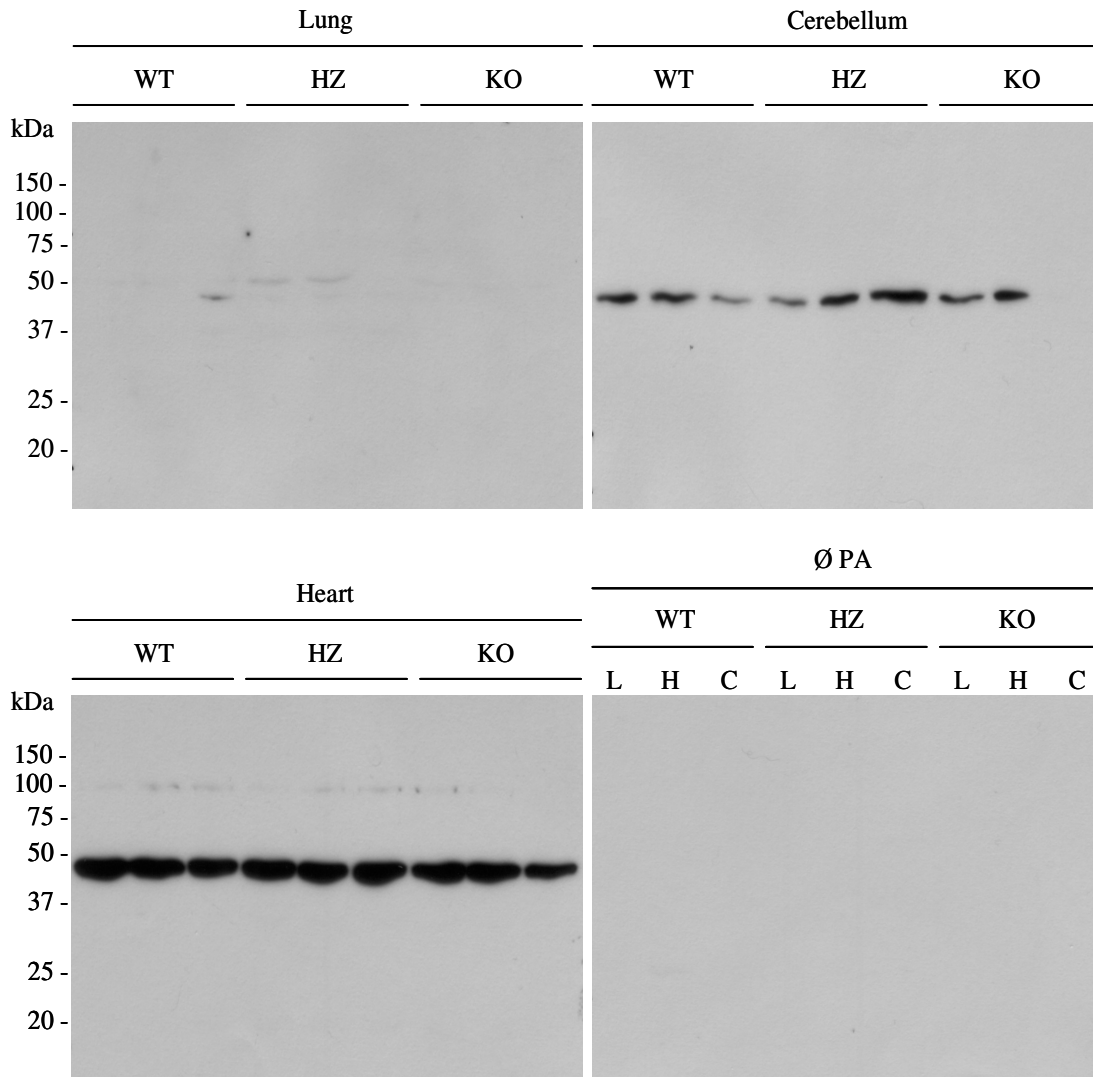


Fig. 7 Western blot, TASK-1 antibody, lot # AN 02.

A band of 45 kDa was observed. Heart and cerebellum were used as a positive control. Abbreviations: kDa. kilodalton, Ø PA: without primary antibody, WT: wild-type, KO: knockout, HZ: heterozygous, L, H, and C: lung, heart, and cerebellum, respectively.

3.2.4 Western blot analysis with anti-NOX4, Santa Cruz

Molecular weight of the NOX4 protein in mouse is 64.2 kDa (Gene bank accession No. NP_056575.1). Rabbit polyclonal anti-NOX4 (Santa Cruz, sc-30141) antibody was used

to detect the expression of NOX4 protein in extracts from lung, heart, cerebellum, fat, and kidney from both NOX4 KO and corresponding WT mice. All the samples showed labelling with NOX4 antibody from both KO and WT animals (Fig. 8). In contrast, labelling was absent in all the samples when treated without primary antibody. Labelling in the cerebellum was either absent or too weak to be seen on the membrane. Kidney ^[96] and fat ^[156] were used as positive controls, as NOX4 is expressed in these organs. Appearance of multiple bands on the membrane and labelling in KO demonstrate nonspecific labelling with this antibody as our RT-PCR data depicts no NOX4 mRNA expression in KO organs.

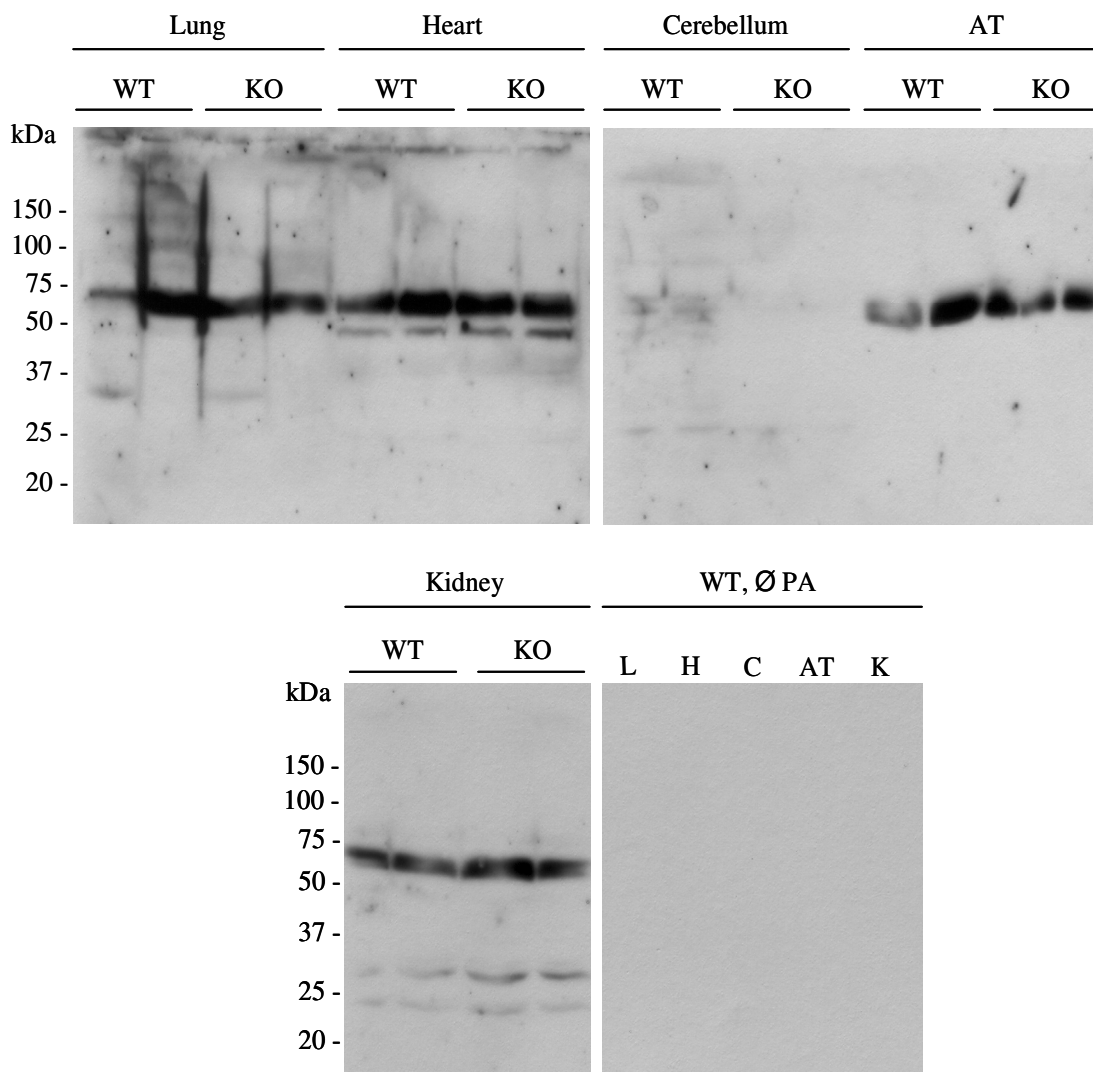


Fig. 8 Western blot, NOX4 antibody, Santa Cruz.

A band of about 70 kDa was labelled on the membrane. Abbreviations: kDa: kilodalton, Ø PA: without primary antibody, WT: wild-type, KO: knockout, L, H, C, and K: lung, heart, cerebellum, and kidney, respectively.

3.2.5 Western blot analysis with anti-NOX4, Biomol

Labelling with anti-NOX4 rabbit monoclonal (catalogue No. 3187-1, Biomol) antibody was observed in extracts from lung, heart, cerebellum and trachea ($n = 2$ each) from NOX4 KO and WT mice. No band appeared in the samples treated in the same way but without primary antibody. Kidney^[96] and AT^[156] were used as a positive controls being places of expression of NOX4 protein. The samples were treated with and without

protease inhibitors. Lung, AT, trachea, and heart samples exhibited double bands. In the heart, however, the second band was not so prominent and single bands appeared in kidney and cerebellum (Fig. 9). The labelling with NOX4 antibody could also not be considered as a specific because of appearance of double bands in the above mentioned samples, and most important, positive results obtained in all KO samples.

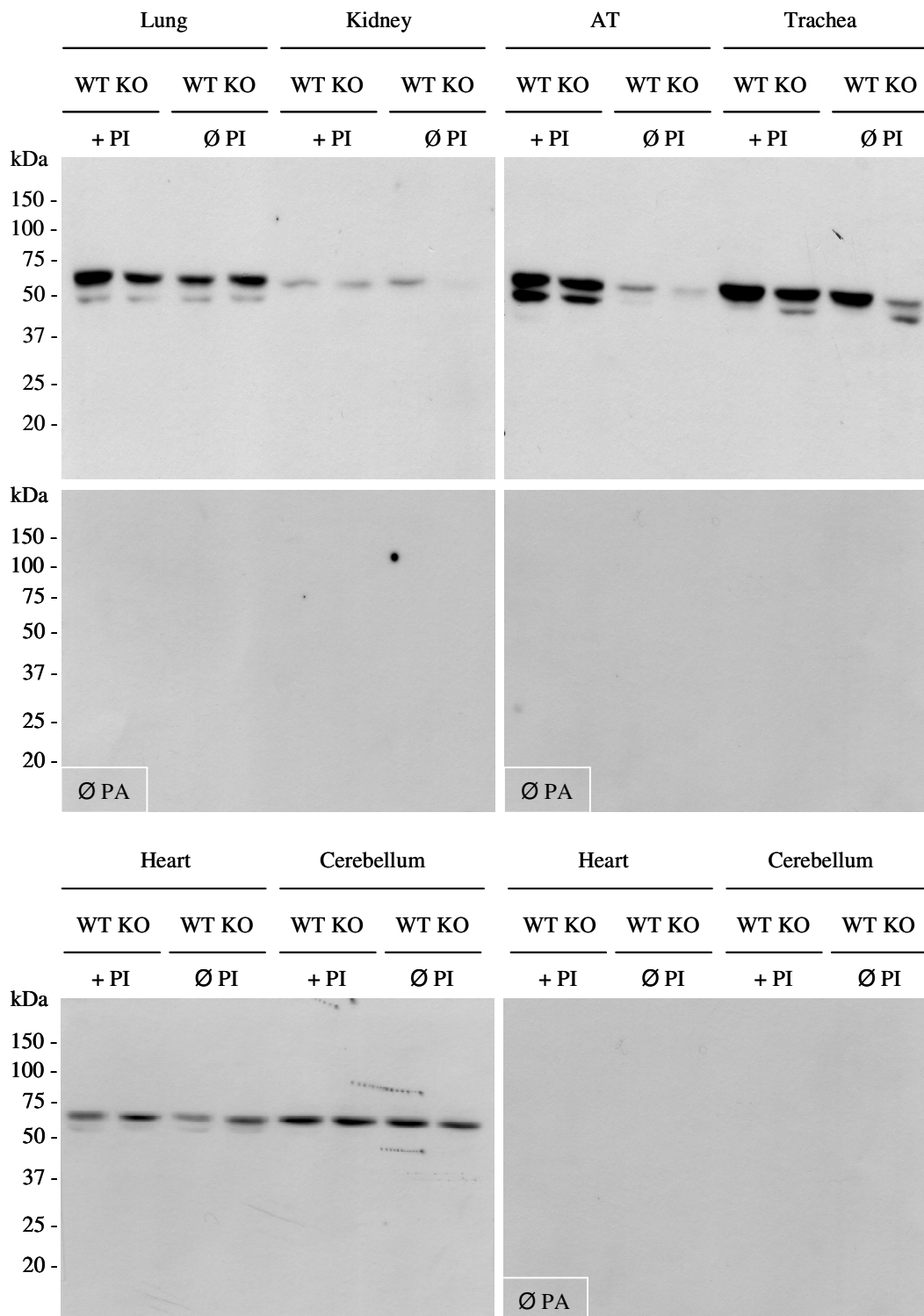


Fig. 9 Western blot, NOX4 antibody, Biomol.

A band of about 63 kDa was observed on the membrane. Abbreviations: AT: adipose tissue, kDa: kilodalton, Ø PA: without primary antibody, WT: wild-type, KO: knockout, + PI: with protease inhibitors, Ø PI: without protease inhibitors.

3.3 Validity of anti-TASK-1 lot # AN 02, analysed by 2-D gel electrophoresis

Immunoreactivities were detected by anti-TASK-1 lot # AN 02 antibody from cerebellum from TASK-1 WT and KO animals. The 2-D gel electrophoresis results also showed identical positive signals in above mentioned samples. Two spots were detected on each membrane from WT and KO samples, these spots were cut and on-membrane proteolytic digest was performed. The MS-analysis described spot 1, and spot 2 from WT and KO as glial fibrillary acidic protein isoform 2 (GFAP2), and mitochondrial cytochrome b-c1 complex subunit (cyt b (c1)), respectively. Furthermore, immobilized pH gradient (IPG)-strips covering 3-5.6 isoelectric point (PI) range were used for isoelectric focusing (IEF) separation of proteins. The reactivity was low and very little protein was detected on both WT and KO gels. Protein analysis by 2-D gel electrophoresis showed that above mentioned antibody did not bind to TASK-1 protein, which demonstrated nonspecificity of antibody.

3.4 Qualitative and quantitative RT-PCR

3.4.1 Expression of TASK-1, TASK-2, and TASK-3, analysed by RT-PCR

TASK-3 is reported to form a dimer with TASK-1 ^[57], and in this way it may compensate the absence of TASK-1 and start functioning in place of TASK-1 channel. TASK-3 mRNA expression was studied in lung, cerebellum, heart, TE (abraded by cotton swab), TM (collected by scissors) and kidney samples from TASK-1 WT mice and compared with TASK-1 and β -actin. In addition, TASK-2 mRNA expression was also studied in these samples. TASK-1, TASK-2, and β -actin were expressed in all the samples. TASK-3 was strongly expressed in the cerebellum, very weakly in TM, and in the rest of the samples it was absent or very low expressed as judged by the appearance of the bands in the gel (Fig. 10).

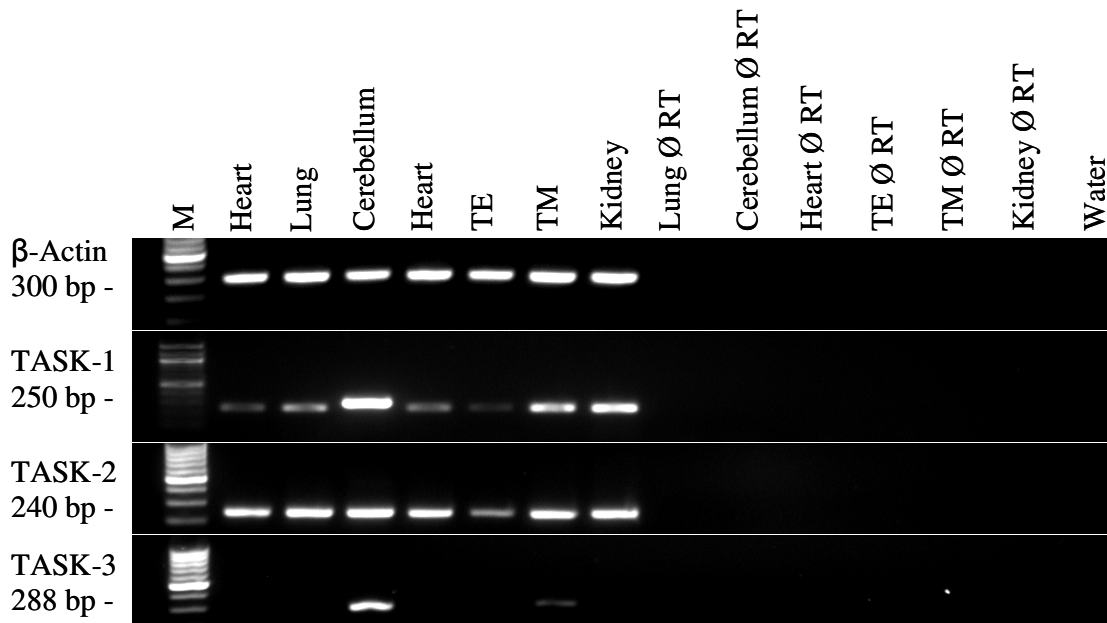


Fig. 10 Expression of TASK-1, TASK-2, and TASK-3, RT-PCR, agarose gel. β -Actin was used as a housekeeping for RT-PCR control and to compare its expression with other targets (TASK-1, TASK-2, and TASK-3). Heart was used as positive control for PCR and water was used without DNA template. Abbreviations: M: base pair size marker, \emptyset RT: control run without reverse transcriptase, TM: trachealis muscle, TE: tracheal epithelium.

3.4.2 Expression of TASK-1 mRNA in manually dissected tracheal epithelium and trachealis muscle

The trachealis muscle (TM) is a smooth muscle bridging the gap between the free ends of C-shaped cartilages at the posterior border of the trachea. It can be seen by naked eye or with a dissecting microscope, and was dissected manually using laboratory scissors. TE was collected by scrolling a cotton swab on the cut and opened surface of the trachea from TASK-1 WT mice. A band of 250 base pair (bp) size for TASK-1 and of 300 bp for β -actin was detected by RT-PCR from both TM and TE samples. Strong expression of TASK-1 mRNA in TE, TM and heart samples was observed. β -Actin, a housekeeping gene, was equally expressed in all the tested samples (Fig. 11).

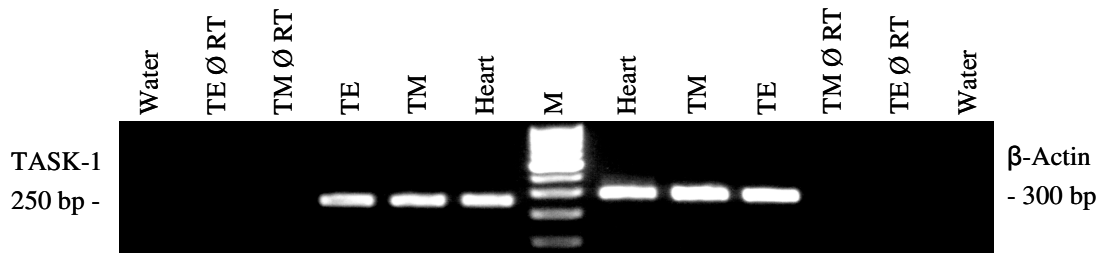


Fig. 11 Expression of TASK-1 in manually dissected tracheal epithelium and trachealis muscle, RT-PCR, agarose gel.

β -Actin, as a housekeeping gene, was used to control for the RT-PCR efficacy and to compare its expression with TASK-1 expression. Heart was included as a positive control for PCR, and water was run without DNA template. Abbreviations: M: base pair size marker, \emptyset RT: control run without reverse transcriptase, TM: trachealis muscle, TE: tracheal epithelium.

3.4.3 Laser-assisted microdissection and RT-PCR for TASK-1 mRNA detection in pulmonary cells

3.4.3.1 Laser-assisted cell picking

Laser-assisted microdissection was carried out to clearly define the localization of TASK-1 mRNA in the lungs from TASK-1 WT mice. Larger pulmonary arteries run adjacent to bronchi and small intra-acinar arteries run deep into the alveolar region. Bronchi, characterized with ciliated epithelium, can easily be distinguished from other lung structures. Cells from bronchi, larger and small pulmonary vessels were picked and studied (Fig. 12). Cells from only those vessels were picked which were having diameter 25-40 μm in small pulmonary vessels, and in larger pulmonary vessels it was 41-60 μm . About 60 profiles were picked for each sample and each profile might have different sample size.

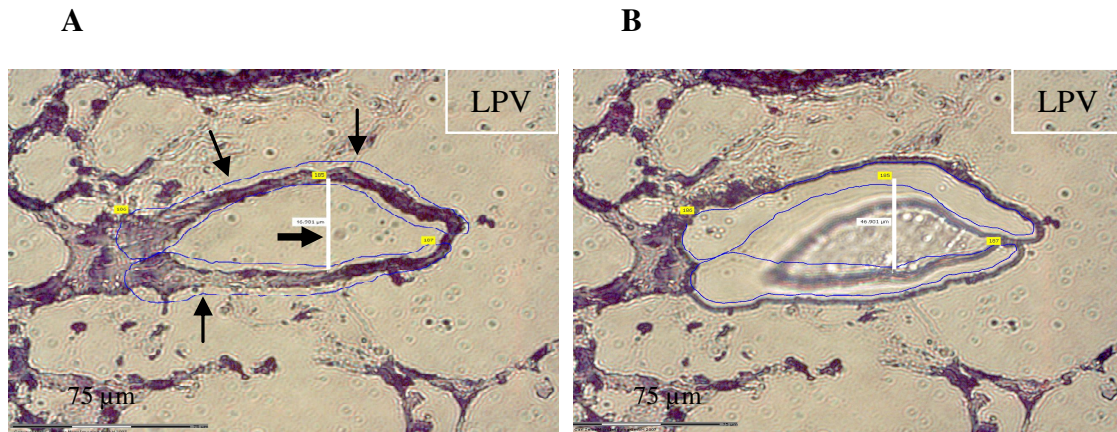


Fig. 12 Laser-assisted cell picking, larger pulmonary vessel.

The white line, indicated by a thick arrow, reflects the diameter of the vessel. It represents the maximum distance between intimal surfaces at a right angle (90°) to the longitudinal axis which follows the direction of the thick arrow. Thin arrows point to the path selected for the laser beam to cut the tissue. A: before picking, B: same vessel is absent as being catapulted by laser. LPV: larger pulmonary vessel.

3.4.3.2 Expression of TASK-1 mRNA in pulmonary structures

Expression of TASK-1 mRNA was detected in bronchi ($n = 1$) and larger pulmonary vessel ($n = 3$). However, in small pulmonary vessels ($n = 2$) expression in all samples was either absent or too low to be visible on the gel. Expression of TASK-1 mRNA was prominent in cardiomyocytes also picked by laser for a positive control for the whole laser-assisted cell picking process. β -Actin was used as an internal control and detected in all the samples run with it. No bands were obtained with β -actin and TASK-1 specific primers in all the samples run without reverse transcriptase/DNA template (Fig. 13).

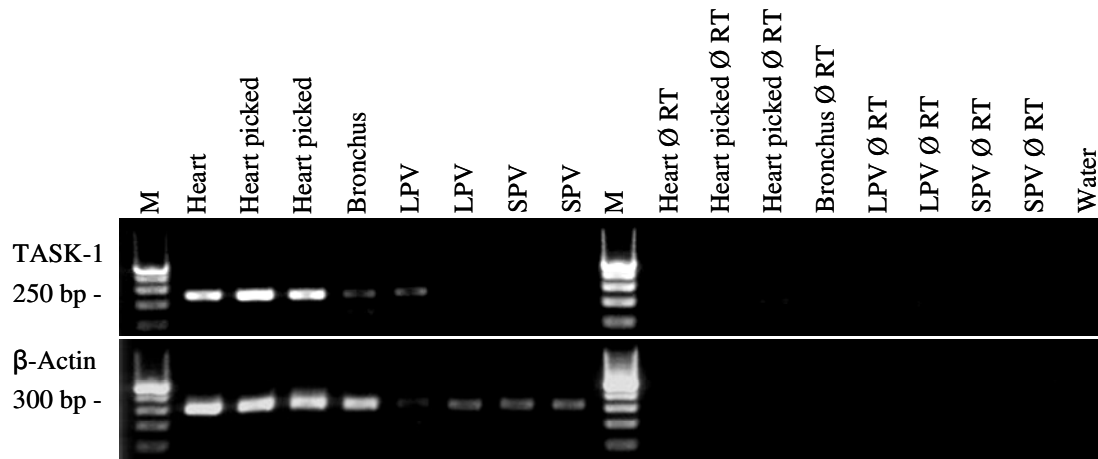


Fig. 13 Laser-assisted microdissection and RT-PCR, agarose gel.

β -Actin was used as a housekeeping gene for its comparison with TASK-1 and control for the RT-PCR efficacy. Heart was used a positive control for PCR and water control was run without DNA template. One sample from LPV gave positive band and one not. Abbreviations: M: base pair size marker, \emptyset RT: control run without reverse transcriptase, LPV: larger pulmonary vessel, SPV: small pulmonary vessel.

3.4.3.3 Expression of TASK-1 mRNA in tracheal epithelium

TASK-1 mRNA expression was studied by RT-PCR in laser-assisted microdissected tracheal epithelium (TE) from TASK-1 WT mice. Cardiomyocytes were also microdissected as a positive control for the whole laser-assisted microdissection process as TASK-1 highly expressed in cardiomyocytes ^[57]. β -Actin was used as an internal control and detected in all the samples. TASK-1 was expressed in TE but its expression was not as strong as seen in heart samples. However, laser microdissected samples run with β -actin gave equal band intensities on the gel (Fig. 14).

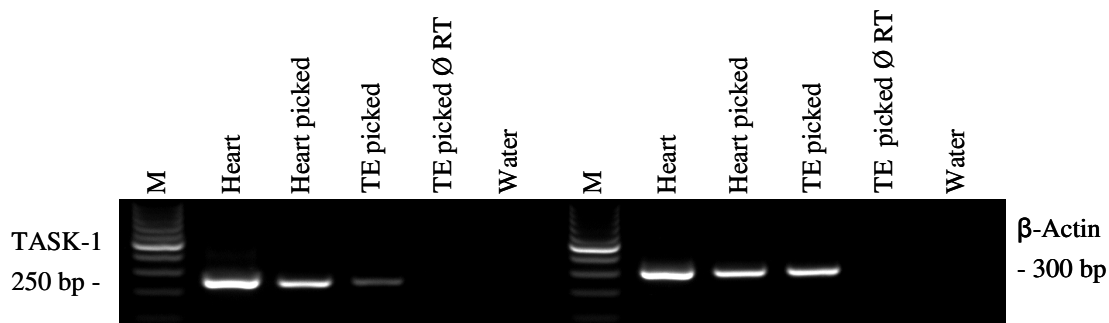


Fig. 14 Expression of TASK-1 in laser-microdissected tracheal epithelium, RT-PCR, agarose gel.

β -Actin was used as a housekeeping gene. Heart was used as a positive control for TASK-1 PCR, and water was without DNA template. Abbreviations: M: base pair size marker, Ø RT: control run without reverse transcriptase, TE: tracheal epithelium.

3.4.4 Expression of TASK-1 mRNA, analysed by real-time RT-PCR

Real-Time RT-PCR analysis of mRNA isolated from lung, heart, and cerebellum from both TASK-1 WT and KO mice revealed the expression of TASK-1 in all of these organs. Surprisingly, there was still TASK-1 mRNA detectable in TASK-1 KO mice. Residual mRNA content was $0.75 \pm 0.31\%$ (mean \pm S.D.; $n = 3$) in the cerebellum, $12.7 \pm 2.7\%$ (mean \pm S.D.; $n = 3$) in the lung, and $0.10 \pm 0.07\%$ (mean \pm S.D.; $n = 6$) in the heart. Agarose gel electrophoresis confirmed correct size of the amplified products (Fig. 15).

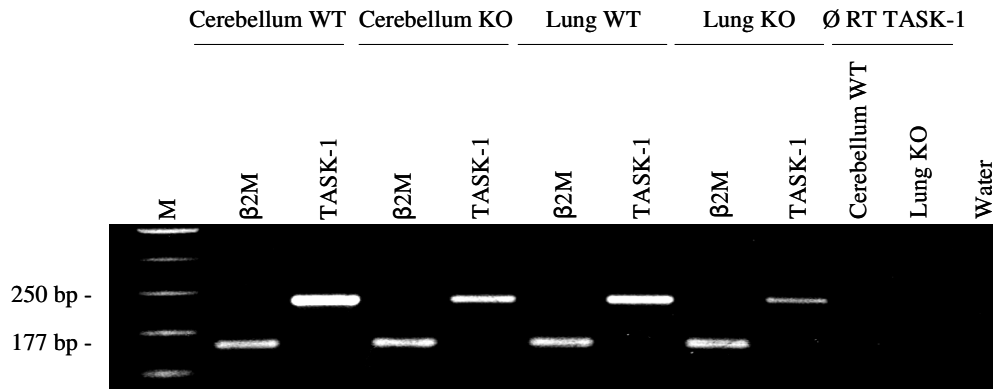


Fig. 15 Real-Time RT-PCR analysis of TASK-1 in cerebellum and lung.

β -2-Microglobulin (β 2M) was used as housekeeping gene for comparison with TASK-1 and to control for the real-time RT-PCR efficacy. Abbreviations: M: base pair size marker, \emptyset RT: control without reverse transcription step, WT: wild-type, KO: knockout, water: control without DNA template.

3.4.5 Expression of NOX4 mRNA in NOX4 KO mice, analysed by RT-PCR

NOX4 has been previously reported as a functional partner of TASK-1 ^[121]. NOX4 mRNA expression was studied in organs (lung, cerebellum, heart, adipose tissue, kidney, and trachea) from NOX4 KO mice and compared with corresponding WT mice. β -Actin was used as a control for RT-PCR and for comparison of mRNA expression between samples from WT and KO mice. It was equally expressed in all the samples both from WT and KO mice. A band of 126 bp revealing NOX4 specific amplicons, was detected from the all the WT samples, but not in the corresponding KO organs (Fig. 16).

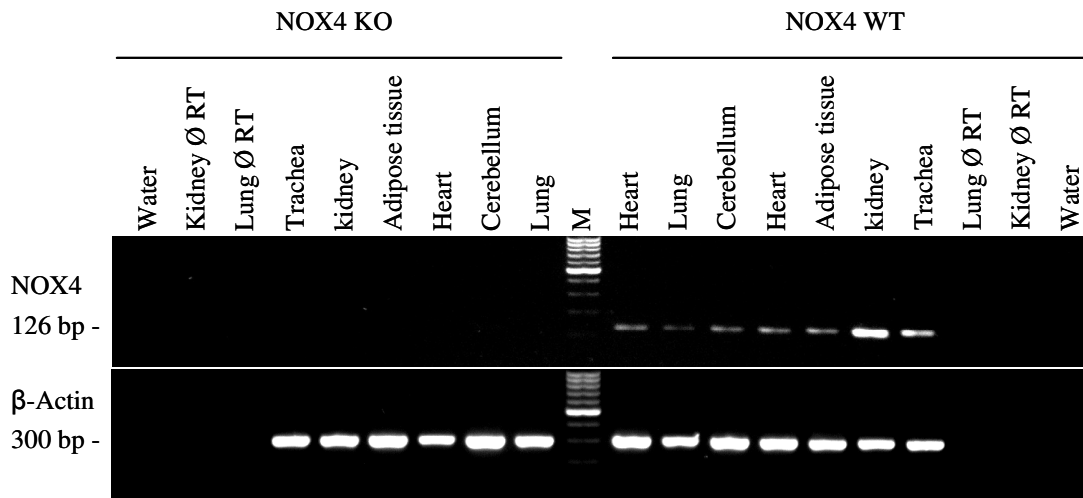


Fig. 16 Expression of NOX4 mRNA in NOX4 KO mice, RT-PCR, agarose gel. β -Actin was used as a housekeeping for RT-PCR control and to compare its expression with other targets (TASK-1, TASK-2, and TASK-3). Heart was used as positive control for PCR and water was used without DNA template. Abbreviations: M: base pair size marker, Ø RT: control run without reverse transcriptase.

3.5 Videomorphometric analysis of PCLS

TASK-1, NOX4 WT and KO mice were sacrificed by cervical dislocation. In PCLS, arteries with inner diameters 41-60 μm located close to bronchi, small intra-acinar arteries having inner diameters 25-40 μm located at gussets of alveolar septa next to alveolar ducts and bronchi with 150-250 μm inner diameters were subjected to videomorphometric analysis. Initially, the thromboxane analogue U46619 and muscarine induced constrictions of pulmonary arteries and bronchi, respectively. Wash-out of the drug from the chamber by perfusion either with medium and subsequent addition of the NO donor nipruss or by medium only induced vasodilatation and bronchodilation, respectively. These results show that intra-acinar, larger arteries and bronchi maintain their ability to vasoconstriction and dilatation in PCLS. To clarify the role of TASK-1 channels and its potential partner NOX4 in oxygen sensing, PCLS were exposed to hypoxic medium and reduction of luminal area of the vessels was observed. No changes in the luminal area of the vessels were observed in control incubations with normoxic gassed medium ($p\text{O}_2$: 160 mmHg) (Figs. 17-20). In case of bronchial analysis, PCLS were also exposed to hypoxic medium for 40 min. To check the viability of the

vessels and bronchi, PCLS were subsequently exposed to U46619 (Figs. 17-20) and muscarine (Fig. 21), respectively, which again resulted in a marked constriction, regardless whether the PCLS had been previously exposed to normoxic or hypoxic medium.

3.5.1 Videomorphometric analysis of pulmonary vessels in response to hypoxia in TASK-1 KO mice

Hypoxia induced an about 25% reduction of the luminal area of intra-acinar arteries in WT mice. In TASK-1 KO mice, HPV was not prevented (Fig. 17A). In larger vessels, hypoxia induced luminal area reduction was about 20% in WT mice. KO mice developed initial HPV that was not sustained. Significant differences in HPV between TASK-1 KO and WT mice were observed at 29-39 min after switching to hypoxic gassed medium (Fig. 17B).

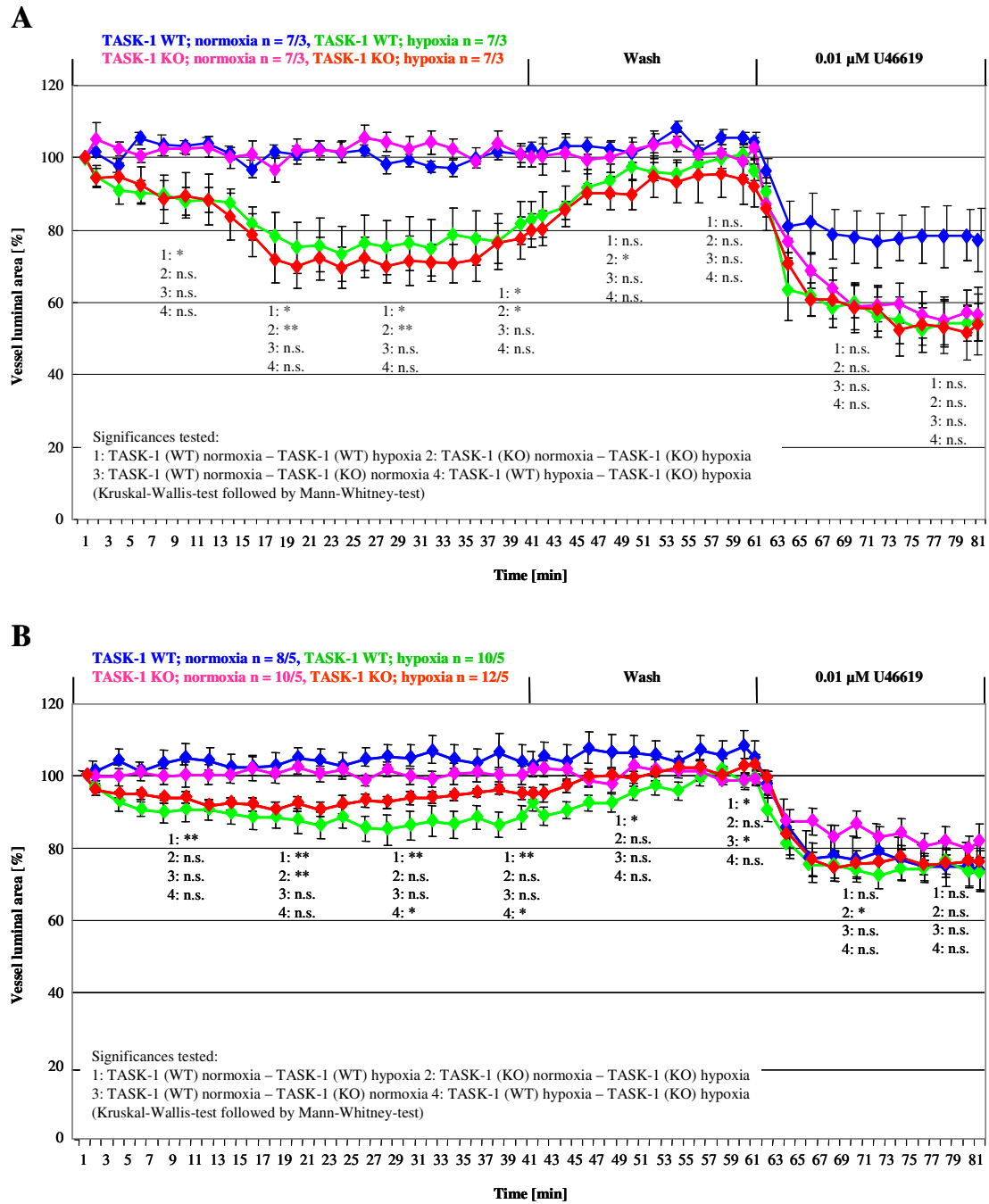


Fig. 17 Videomorphometry, HPV in TASK-1 KO and WT mice.

The luminal area of the vessels before exposure to hypoxia is set as 100% and changes in the luminal areas are presented as relative values. A: HPV in small intra-acinar pulmonary arteries, B: HPV in large pulmonary arteries. Data are presented as means \pm SEM. * $p \leq 0.05$, ** $p \leq 0.01$, n.s.: not significant, n: number of vessels/animals.

3.5.2 Videomorphometric analysis of pulmonary vessels in response to anandamide

In small intra-acinar arteries, anandamide induced constriction at one point under normoxia and significantly reduced HPV also at one time point (Fig. 18A). In larger arteries, it did not induce constrictions under normoxia and lead to a significantly reduced HPV at 29-39 min after switching to hypoxic gassed medium (Fig. 18B).

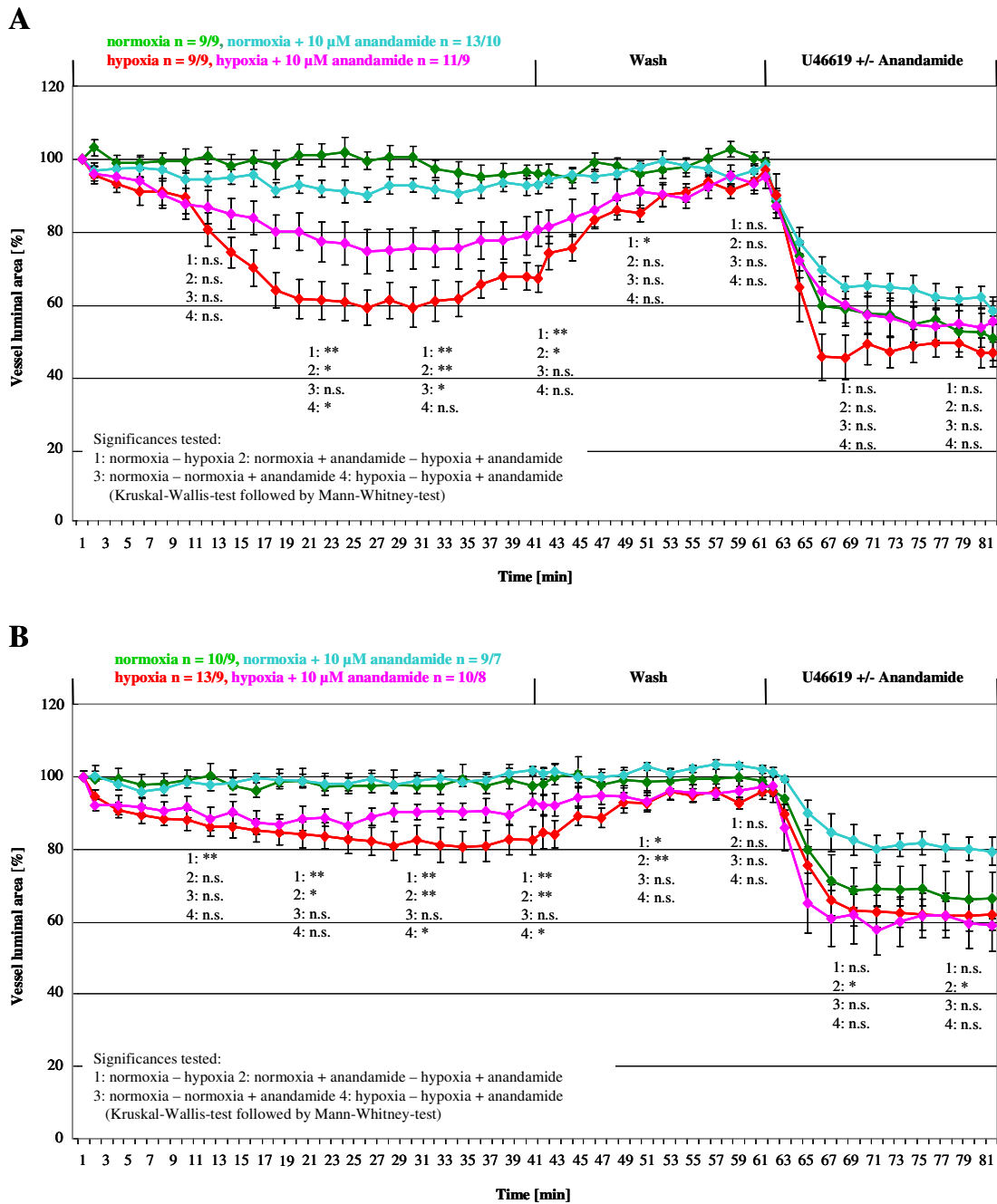


Fig. 18 Videomorphometry, effect of anandamide on PV under normoxia and hypoxia in TASK-1 WT mice.

The luminal area of the vessels before exposure to hypoxia or anandamide administration is set as 100% and changes in the luminal areas are presented as relative values. A: Effect of anandamide on PV under normoxia and hypoxia in small intra-acinar pulmonary arteries, B: Effect of anandamide on PV under normoxia and hypoxia in large pulmonary arteries. Data are presented as means \pm SEM. * $p \leq 0.05$, ** $p \leq 0.01$, n.s.: not significant, n: number of vessels/animals.

3.5.3 A293 causes contractions of vessels independent from TASK-1 channels

Effect of A293 (inhibitor of TASK-1 channel) on vasoconstriction was investigated under normoxic and hypoxic conditions. Moreover, under normoxic conditions, its effect was studied in TASK-1 KO mice. Under normoxic conditions, A293 caused significant constriction in WT small vessels, and no further constriction under hypoxic conditions was observed (Fig. 19A). Similarly, in larger vessels, it also caused significant constriction under normoxia and prevented further HPV (Fig. 19B). In KO animals, under normoxic conditions, the constrictory effect of A293 was not reduced. A significant vasoconstriction in both small intra-acinar (Fig. 19C) and larger (Fig. 19D) arteries was still observed. No changes in the luminal area of vessels were observed in control experiments with normoxia plus DMSO, the vehicle used for A293 application. These data show that vasoconstriction induced by A293 does not operate through TASK-1 channels.

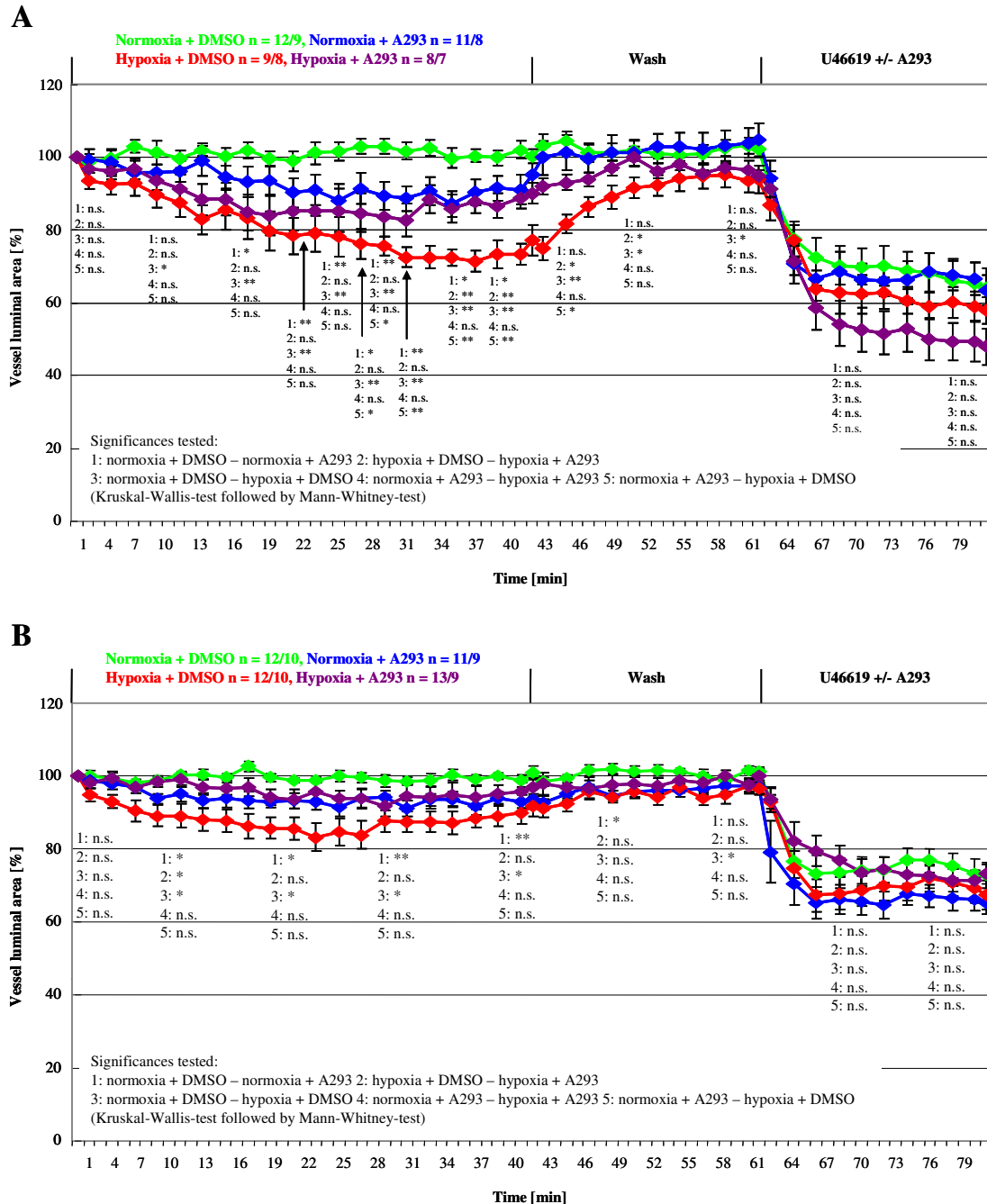


Fig. 19 Videomorphometry, effect of A293 on PV under normoxia and hypoxia in TASK-1 WT mice.

The luminal area of the vessels before exposure to hypoxia or A293 administration is set as 100% and changes in the luminal areas are presented as relative values. A: Effect of A293 on PV under normoxia and hypoxia in small intra-acinar pulmonary arteries, B: Effect of A293 on PV under normoxia and hypoxia in large pulmonary arteries. Data are presented as means \pm SEM. * $p \leq 0.05$, ** $p \leq 0.01$, n.s.: not significant, n: number of vessels/animals.

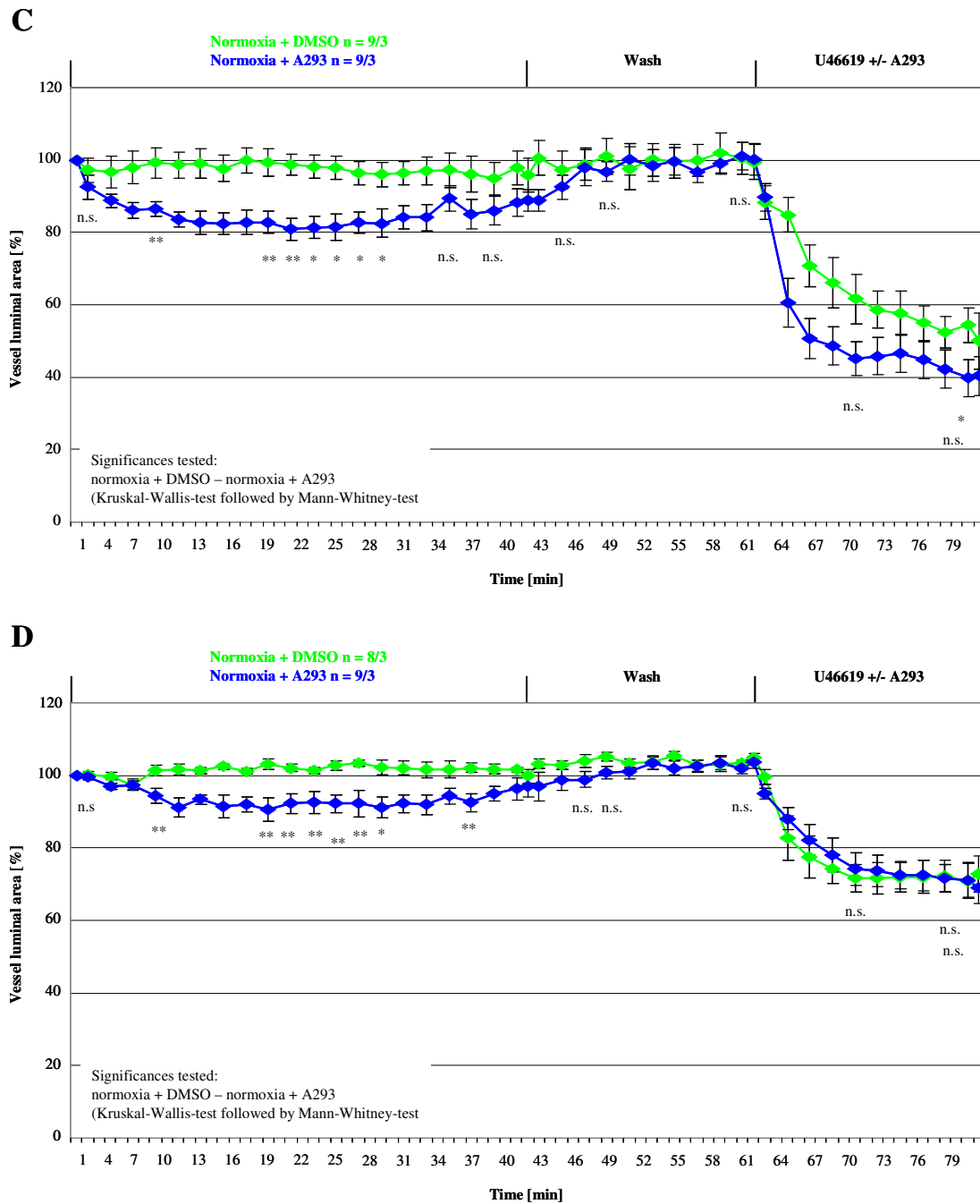


Fig. 19 Videomorphometry, effect of A293 on PV under normoxia in TASK-1 KO mice.

The luminal area of the vessels before A293 administration is set as 100% and changes in the luminal areas are presented as relative values. C: Effect of A293 on PV under normoxia in small intra-acinar pulmonary arteries, D: Effect of A293 on PV under normoxia in larger pre-acinar pulmonary arteries. Data are presented as means \pm SEM. * $p \leq 0.05$, ** $p \leq 0.01$, n.s.: not significant, n: number of vessels/animals.

3.5.4 Videomorphometric analysis of pulmonary vessels in response to hypoxia in NOX4 KO mice

PCLS from NOX4 WT and KO mice were incubated with hypoxic medium. In this set of experiments, exposure to hypoxia induced an about 40% reduction of the luminal area of intra-acinar arteries in WT mice. In PCLS taken from KO mice, a significant reduction in the hypoxic constriction of luminal area was observed (Fig. 20A). In WT larger vessels, reduction of the luminal area under hypoxia was about 20%, and in KO mice the constriction of the vessels was not reduced (Fig. 20B).

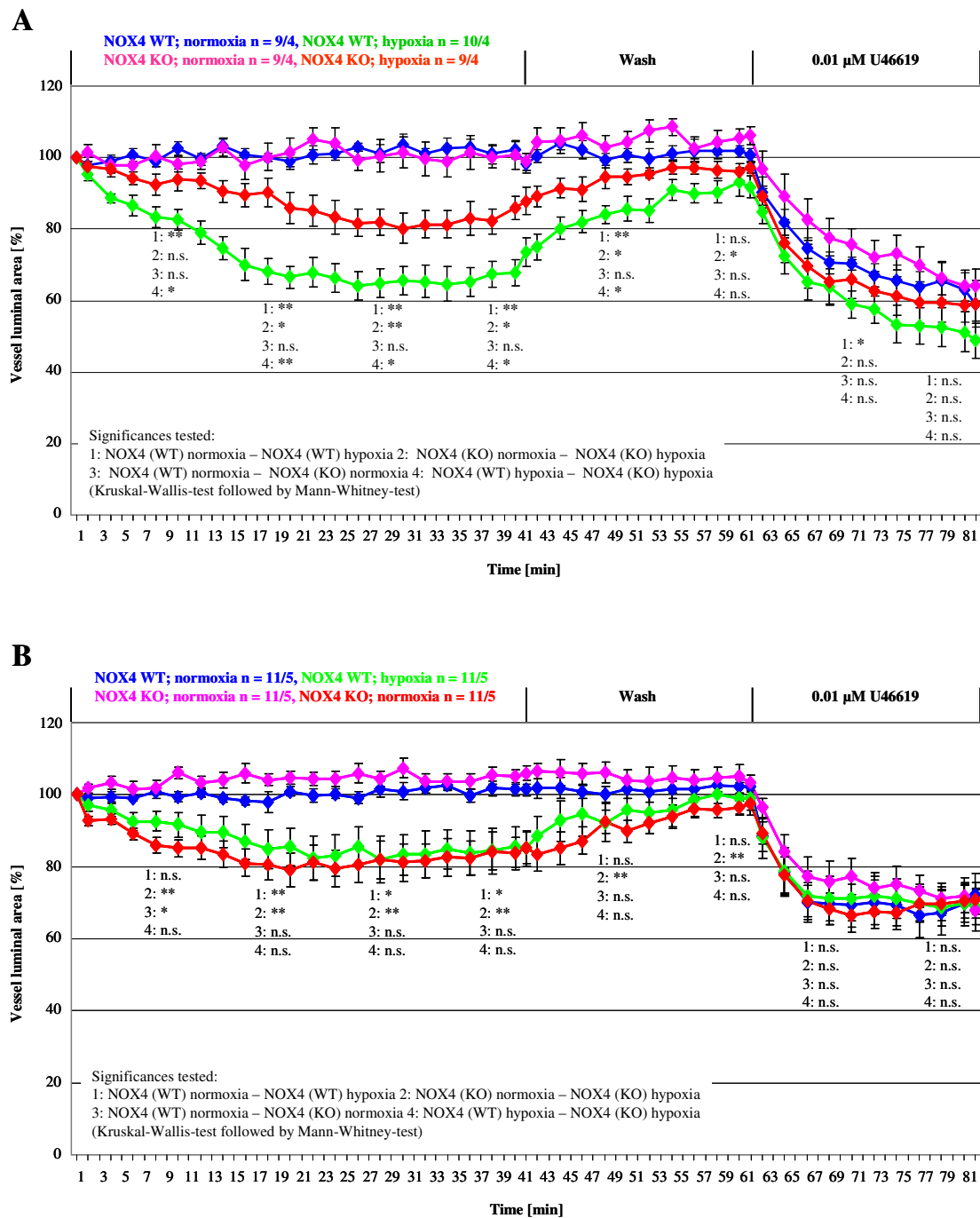


Fig. 20 Videomorphometry, HPV in NOX4 KO and WT mice.

The luminal area of the vessels before exposure to hypoxia is set as 100% and changes in the luminal areas are presented as relative values. A: HPV in small intra-acinar pulmonary arteries, B: HPV in large pulmonary arteries Data are presented as means \pm SEM. * $p \leq 0.05$, ** $p \leq 0.01$, n.s.: not significant, n: number of vessels/animals.

3.5.5 Effect of hypoxia and anandamide on bronchoconstriction

PCLS from TASK-1 WT were exposed to hypoxia and no reduction of bronchial luminal area was observed (Fig. 21A). Similarly, anandamide had no impact on bronchial diameter taken from PCLS analysis from TASK-1 WT and KO mice (Fig. 21B). These data show that hypoxia and TASK-1 do not regulate bronchoconstriction in mice.

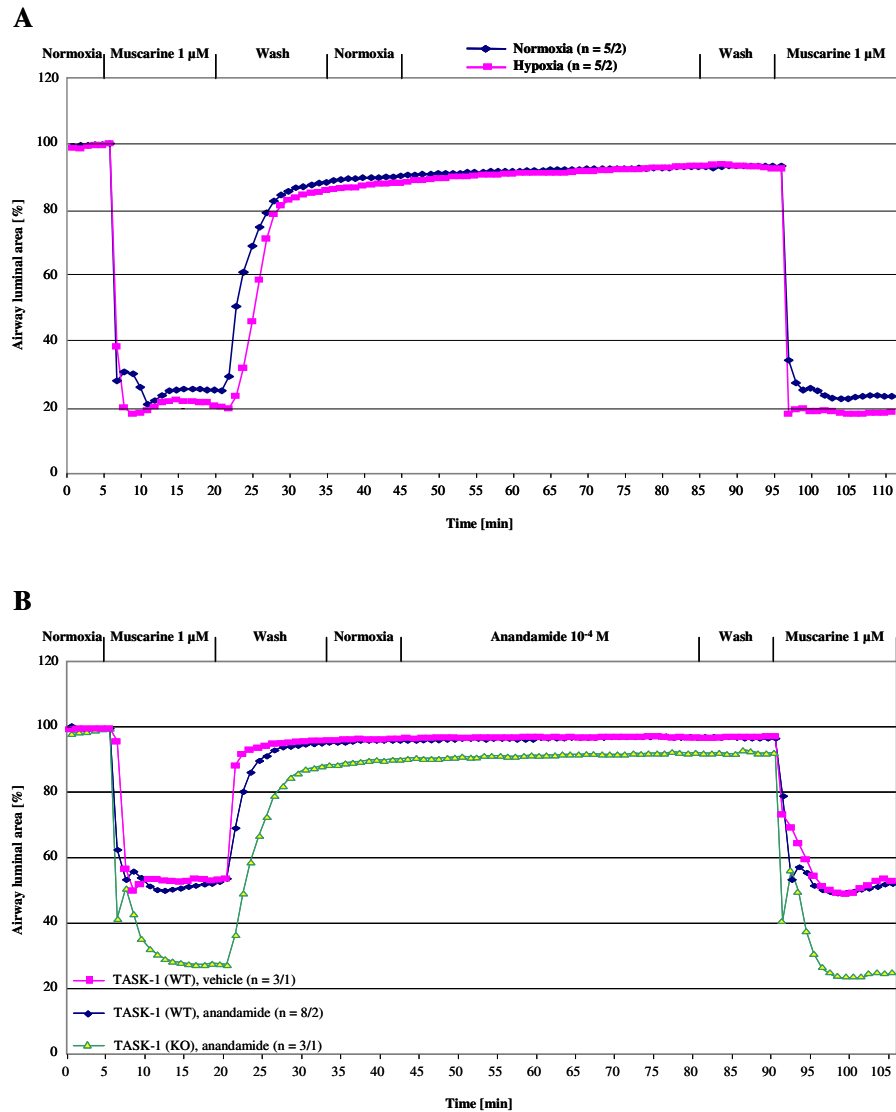


Fig. 21 Videomorphometry, effect of hypoxia and anandamide on bronchial diameter.

The luminal area of the airways before muscarine administration is set as 100% and changes in the luminal areas are presented as relative values. A: Effect of hypoxia on bronchial diameter, B: Effect of anandamide on bronchial diameter in TASK-1 WT and KO mice. n: number of bronchi/animals.

3.6 Measurement of cilia-driven PTS

3.6.1 Inhibition of TASK-1 channels does not affect cilia-driven PTS

TASK-1 inhibitors (anandamide and A293) did not induce an increase in PTS. Cumulative application of 1 μ M, 10 μ M and 100 μ M anandamide had no effect on PTS (Fig. 22A). Similarly, application of 100 nM, 200 nM, 500 nM and 1000 nM A293 did not affect the speed of particles (Fig. 22C). Vehicles for anandamide (Fig. 22B) and for A293 (Fig. 22D) had no effect on PTS. ATP applied at the end of experiment increased PTS significantly in all cases showing non-toxicity of the substances used. Concentrations of 100 μ M anandamide and 1000 nM A293 were used to further investigate the effects of avertin in the presence of inhibitors.

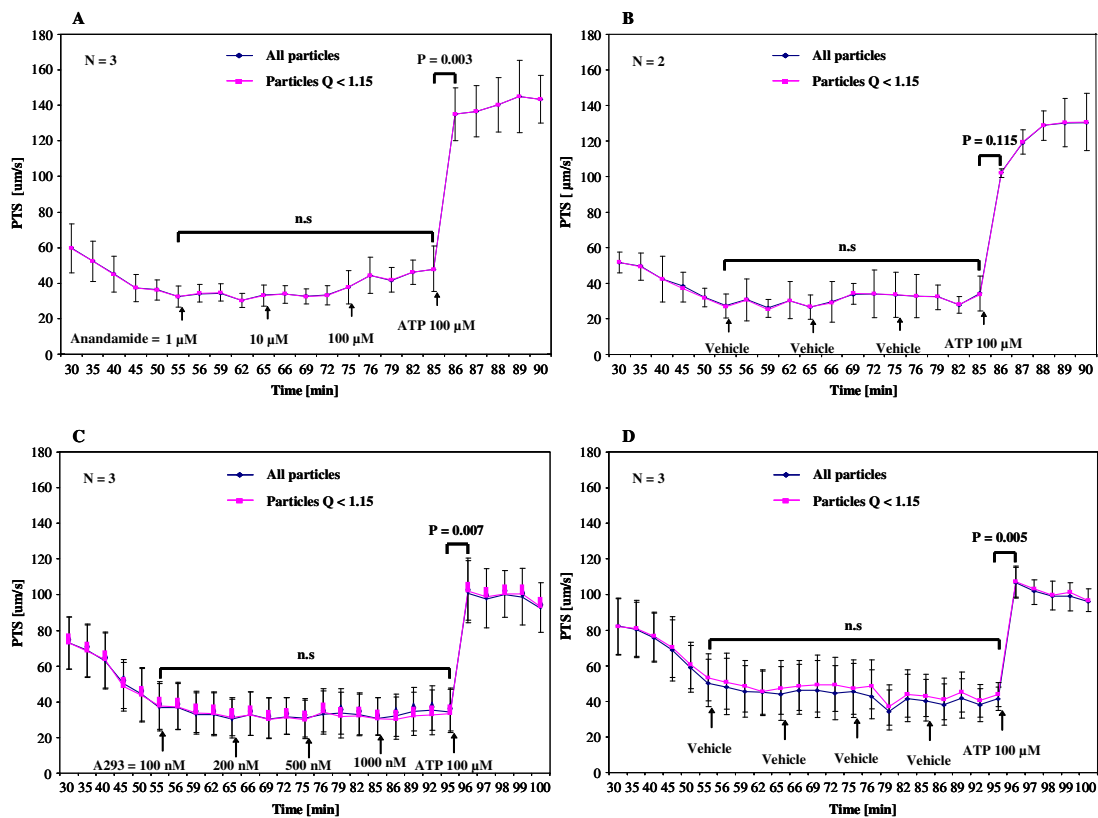


Fig. 22 Inhibition of TASK-1 channel does not affect the cilia-driven PTS.

B: vehicle: ethanol, D: vehicle: DMSO, Q < 1.15: those particles which from start to end point do not deviate more than 15% from their direct way, n.s: not significant, P values ≤ 0.05 are set in bold type (paired t-test), N = Number of tracheae. Values are means \pm SD.

3.6.2 Effect of anesthetics on the cilia-driven PTS

Anesthetics are reported to decrease cilia-driven PTS ^[158] and TASK-1 is their target molecule ^[159-163]. PTS was different depending upon the type of anesthetic and its concentration applied. Vaporized isoflurane (2%) had no effect on PTS (Fig. 23A) as vehicle (HEPES) alone also had no effect on PTS by its own (Fig. 23B). ATP applied at the end of experiments increased PTS significantly.

Another anesthetic, avertin, with unclear affinity to TASK-1 was studied at different concentrations. A concentration of 400 μ M avertin did not decrease and ATP increased PTS significantly, respectively (Fig. 23C). But when compared with vehicle (water), avertin induced decrease in PTS was significant ($P = 0.009$) and the effect of ATP remained unchanged. Avertin at 1 mM concentration significantly decreased PTS (Fig. 23D), and its effect was also significant when compared with vehicle ($P = 0.005$) and the effect of ATP on PTS was also reduced significantly in the presence of avertin ($P = 0.003$) showing some toxic effect of avertin at that concentration. Avertin at 4 mM concentration, robustly decreased PTS but after the application of ATP, no increase in PTS was observed (Fig. 23E), indicating that avertin might be toxic at that concentration. Vehicle (water) added instead of avertin, did not affect PTS (Fig. 23F). Effect of avertin at all concentrations (combined) was highly significant ($P \leq 0.001$). A concentration of 1 mM avertin was used for next experiments with inhibitors of TASK-1 channels and in TASK-1 KO mouse model.

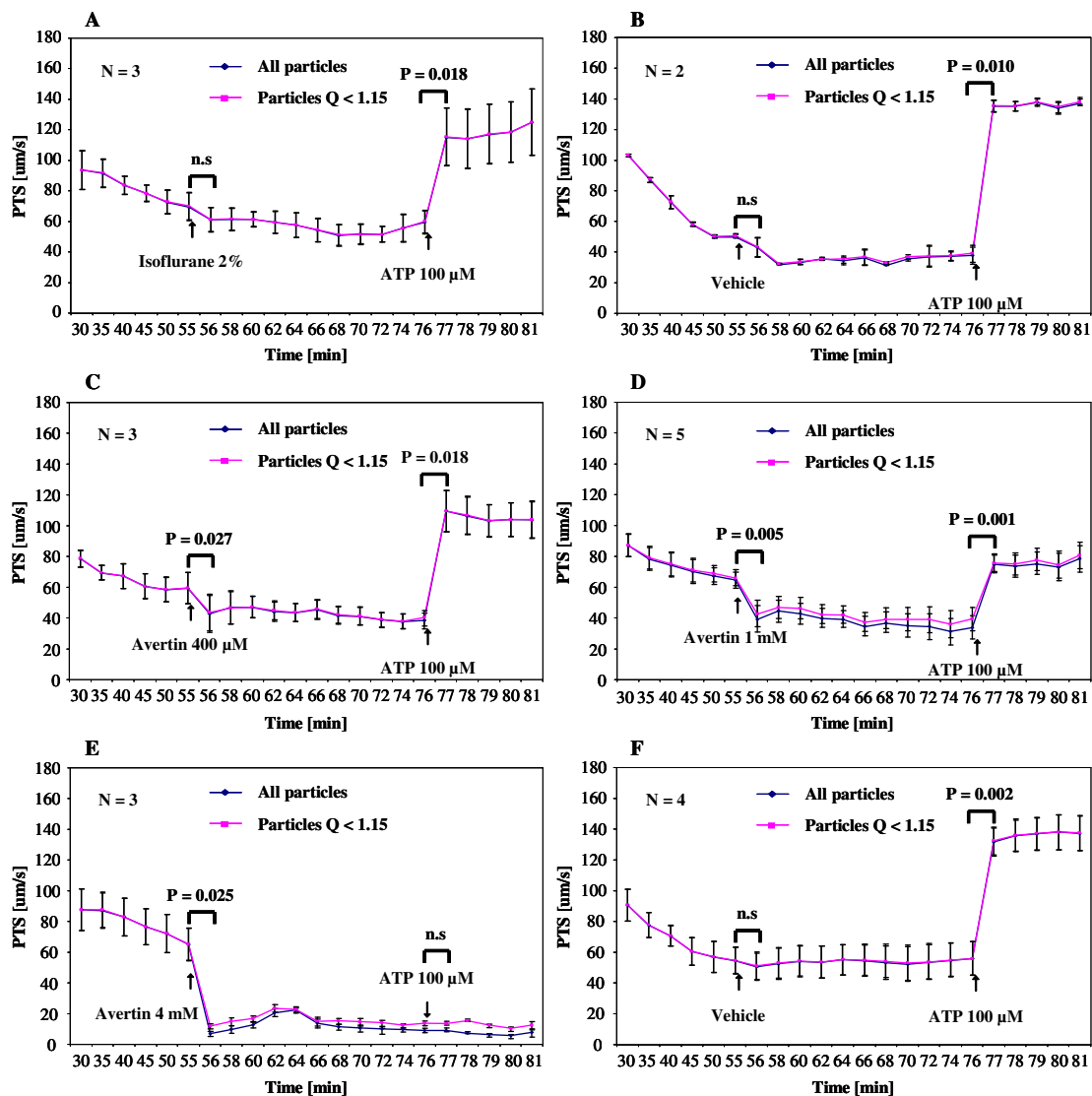


Fig. 23 Effect of anesthetics on the cilia-driven PTS.

B: vehicle: HEPES, F: vehicle: water, Q < 1.15: those particles which from start to end point do not deviate more than 15% from their direct way, n.s.: not significant, P values ≤ 0.05 are set in bold type (paired t-test), N = Number of tracheae. Values are means \pm SD.

3.6.3 Avertin-induced decrease in PTS persisted in the presence of TASK-1 inhibitors and in TASK-1 KO mice

TASK-1 channels inhibitors were applied before administration of avertin. In the presence of anandamide, avertin did not induce a significant decrease in PTS, and ATP application caused a significant increase in PTS (Fig. 24A). The same pattern was seen

when ethanol, the vehicle for anandamide, was used instead of anandamide, so that it was not considered as a specific effect (Fig. 24B). In the presence of A293, avertin decreased and ATP increased PTS significantly, respectively (Fig. 24C), and the effect of ATP was significantly reduced when compared with control. The vehicle added instead of A293 had no effect on PTS and did not affect ATP induced increase in PTS (Fig. 24D).

The avertin-induced decrease in PTS was still observed in TASK-1 KO mice (Fig. 24E). ATP administered at the end of experiment increased PTS significantly. The effect of avertin remained unchanged, and the ATP induced increase in PTS was significantly reduced ($P = 0.05$) when compared with vehicle (water, Fig. 24F). These data show that avertin did not decrease PTS through TASK-1 channels.

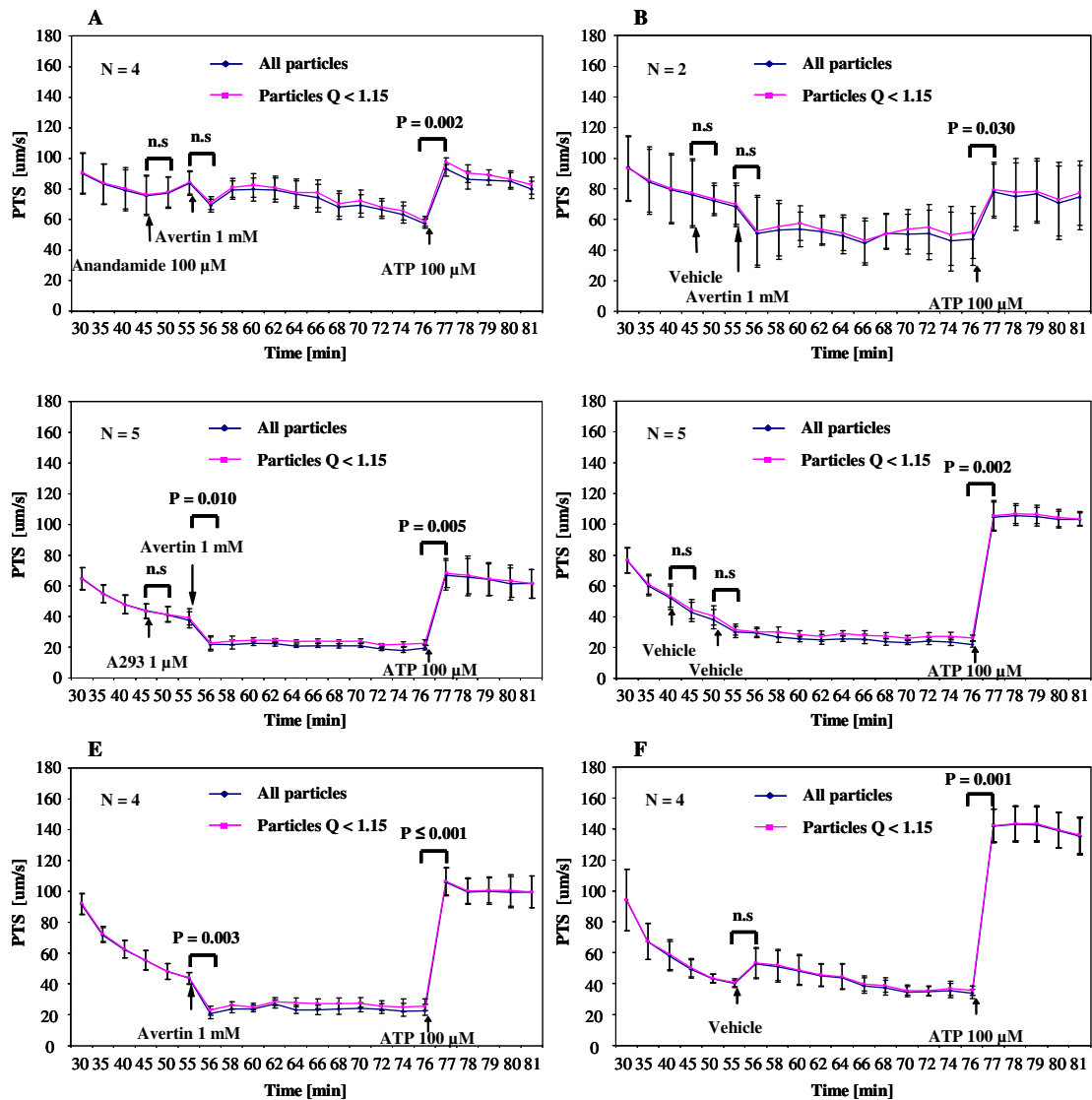


Fig. 24 Avertin-induced decrease in PTS in the presence of TASK-1 inhibitors and in TASK-1 KO mice.

B: vehicle: ethanol, D: vehicle: DMSO, and water, E: unchanged effect of avertin in TASK-1 KO, F: vehicle: water, Q < 1.15: those particles which from start to end point do not deviate more than 15% from their direct way, n.s: not significant, P values ≤ 0.05 are set in bold type (paired t-test), N = Number of tracheae. Values are means \pm SD.

4 DISCUSSION

4.1 Antibodies and TASK-1 KO mice validity

TASK-1 KO mice used in our study have been created by Aller et al. and described in a previous study ^[151]. Certain studies confer TASK-1 gene absence in the modulation of different physiological functions. In cerebellar granule neurons, absence of TASK-1 has been linked to alter the modulation of a leak conductance ^[151]. These mice exhibit increased motor impairment in rotarod and beam-walking test after application of diazepam and flurazepam and prolonged loss of righting reflex by propofol and pentobarbital ^[164], and CO₂-evoked increase in the carotid sinus nerve chemoafferent discharge ^[165]. Also, adrenal gland zonation and mineralocorticoid homeostasis disruption in female animals ^[155], increased sensitivity to thermal nociception in a hot-plate test and reduction of analgesic, sedative and hypothermic effects of WIN55212-2 ^[166] and reduction in blood pressure ^[167] have been reported in the same strain of KO mice.

Heitzmann et al. ^[155] detected amplicons in RT-PCR using TASK-1 specific primers in the adrenal gland of these KO mice (personal communication, R. Warth). Linden et al. ^[166] reported similar findings in the forebrain of KO mice (shown in Fig. 2). We also quantitatively measured TASK-1 mRNA from different tissues from TASK-1 KO mice, and 0.75% residual mRNA content was detected in the cerebellum, 0.1% in the heart and 12.7% in the lung. So, our real-time RT-PCR data are consistent with above mentioned studies. Even if any protein were translated from such low amounts of mRNA, it can be expected to be much reduced and might not be considered to be fully functional. Utku et al. ^[168] described 98% reduced protein translation from mRNA when it was downregulated to 80% in siRNA transfected cells. In general, studies carried out with siRNA transfected cells usually do not achieve downregulation of a certain gene up to 100%, and functionally effective studies are carried out when downregulation is accomplished up to > 80% ^[168-171]. To validate functional absence of TASK-1 in the mice used in our study, we used the same antibody (against aldosterone synthase) but from a different lot for immunohistochemistry and same methodology as used by Heitzmann et al. ^[155] to investigate for disruption of adrenal gland zonation in female TASK-1 KO mice. Labelling pattern of aldosterone synthase in zona glomerulosa in female TASK-1 WT mice was different from the corresponding female KO mice.

Labelling in WT was strictly confined to only zona glomerulosa whereas in KO it was very weak and irregular, and some labelling was also observed in zona reticulo-fasciculata (Fig. 4). However, this labelling was not as strong as reported by Heitzmann et al. ^[155] which may be attributed to the use of antibodies from different lots.

Detection of TASK-1 protein was attempted by using different TASK-1 antibodies. Different organs such as lung, cerebellum, and heart were studied from both TASK-1 WT and KO mice. Immunohistochemistry and western blot results showed labelling with TASK-1 antibodies in all these organs and this labelling neither vanished nor was reduced in the organs from KO mice. These results question the specificity and validity of these antibodies. In line with this observation, there are accumulating reports on a previously unexpected extent of non-specific reactions with antibodies as evidenced by the use of respective gene-deficient mice ^[151, 172, 173]. Alternatively, these antibody data may indicate the presence of TASK-1 protein also in KO mice. To solve this dilemma and remove the ambiguity of TASK-1 protein presence in KO mice, 2D gel electrophoresis was also performed using cerebellum from WT and KO mice. TASK-1 antibody from Alomone laboratory, lot # AN 02, was used for this purpose as it gave particularly strong labelling in the cerebellum. Data from 2D gel electrophoresis confirm the nonspecific binding of TASK-1 antibody in both organs, as the substrate to which TASK-1 antibody bound was not TASK-1 protein. Instead, the antibody labelled glial fibrillary acidic protein isoform 2 (GFAP2) and mitochondrial cytochrome b-c1 complex subunit (cyt b (c1)). In line with these observations, Aller et al. ^[151] had also reported on non-specific labelling in brain with TASK-1 antibodies in KO mice lacking TASK-1 mRNA.

Collectively, these data demonstrate functionally efficient deficiency in TASK-1 in the mouse strain used in this study, but lack of suitability of currently available TASK-1 antibodies for TASK-1 protein detection.

4.2 TASK-1 channels

Our data do not support a prominent role of TASK-1 channels in causing pulmonary vasoconstriction in response to change in O₂ concentration. The expression of this channel in rabbit ^[58], rat ^[59, 60] and human ^[61] PASMC has been described previously, and previous studies linked TASK-1 to the regulation of resting membrane potential

(Em) in PASMC [58, 59, 61]. Our study model was based upon the idea behind the role of TASK-1 channels being present in airways and PASMC. To conclusively explore the role of this channel, TASK-1 KO mice and inhibitors (anandamide and A293) were used in the present study. Based on data indicating expression of TASK-1 not only in pulmonary vessels and but also airways, changes in diameter of airways, small intra-acinar and larger pre-acinar arteries in response to hypoxia were measured.

The reactivity of the pulmonary vessels in response to different stimuli varies in different species and areas along the pulmonary vascular tree as small and large vessels are known to be different in receptor equipment and neurotransmitter sensitivity. In the rat, hypoxia induces constriction for a short period of time followed by relaxation in the pulmonary vessels with external diameter more than 300 μm . The vessels with external diameter below 300 μm respond to hypoxia with monophasic constriction. This differential response is attributed to the localization of electrophysiologically distinct types of K^+ -channels [181, 182]. Park et al. divided the rabbit pulmonary arterial system into large extralobar pulmonary arteries (diameter 2-3 mm), large intralobar pulmonary arteries (diameter 2-3 mm) and small intralobar pulmonary arteries (diameter 300-500 μm), and ascribed that in determining contractile responses of pulmonary arteries in the rabbit, location in pulmonary vessels was more important than the diameter itself [183]. Similarly, 5,6-epoxyeicosatrienoic acid relaxes extralobar but constricts intralobar rat pulmonary arteries [184]. Drexler et al. [87] identified significant differences in mechanical characteristics between the pulmonary trunk and the main arteries in the rat and suggested not to expect from each section of the extrapulmonary arterial system to behave identically. Hypoxia and the thromboxane analog U-46619 induced striking vasoconstriction in medium sized arteries (30-50 μm diameter), weak in small arteries having diameter less than 30 μm , and in venules no constriction was observed [81]. Moreover, Paddenberg et al. [185] reported that PAP did not depend upon the constriction of small intra-acinar arteries. So, small intra-acinar and larger pre-acinar arteries were studied separately in the present study to explore the role of TASK-1 channels in response to hypoxia. Furthermore, overall rise in PAP due to hypoxia was also measured from TASK-1 WT and corresponding KO mice including the use of inhibitors (anandamide and A293).

Oxygen dependent modulation of TASK-1 has been described differently in different organs and model systems. In transfected HEK293 cells, TASK-1 channel function of sensing O₂ was moderately inhibited ^[121]. In human brain, TASK-1 was potentially inhibited by hypoxia ^[186]. In contrast, no response to changes in O₂ tension was observed in TASK-1 expressing *Xenopus* oocytes ^[62] and the TASK-like current in adrenomedullary chromaffin cells was also O₂ insensitive ^[187]. Hypoxia causes rise in pulmonary vascular resistance, constriction of pulmonary vessels, pulmonary artery cell proliferation and ultimately can lead to PH ^[4, 20, 188-191]. PAP in response to hypoxia was measured in the laboratory of Prof. Norbert Weissmann, Excellence Cluster Cardio-Pulmonary System, Justus-Liebig-University, Giessen, in isolated, buffer perfused and ventilated lungs from TASK-1 WT and corresponding KO mice. There was no difference of rise in PAP under hypoxia between TASK-1 WT and KO mice, although there was a slight reduction in HPV at certain time points in larger pre-acinar arteries in PCLS prepared from KO mice. Most recently, Paddenberg et al. ^[185] demonstrated that HPV was prevented only in intra-acinar arteries in mitochondrial complex II heterozygous mice, and rise in hypoxic PAP remained unaffected in these mice. These findings can be assigned to the presence of a different muscularisation along the length of pulmonary arteries, and difference in sensitivity of cells to hormones, neurotransmitters, and hypoxia. The difference in response to hypoxia along the length of pulmonary arteries from heart to the capillaries can also be attributed to the presence of different proteins which sense changes in oxygen tension, their low and high expression, their translation from mRNA, and certain genes which regulate contraction of vessels. In a previous study ^[192], TRPC6 gene KO mice showed impaired PAP under acute hypoxic conditions. With respect to PH, different species can adapt to chronic hypoxic conditions and vascular remodeling is not induced. Pika, yak, snow pig, and llama ^[3, 193-195] represent such cases. Moreover, intensity and magnitude of hypoxia-induced changes vary according to the species, sex and the developmental stages of animal ^[196-199].

Hypoxia ^[61, 74] and blockers of TASK-1 channels ^[61, 157, 175-177] cause membrane depolarization, resulting in SMC constriction. Here, we investigated the effect of hypoxia and anandamide on bronchial constriction. Our data show that anandamide does not affect murine bronchial SMC at all, thus conflicting with the data from previous studies ^[178-180] where anandamide was described to induce bronchoconstriction

in guinea-pig. Our videomorphometric data from bronchus implicate that TASK-1 is not involved in the constriction of at least murine bronchial SMC. These results were quite unexpected as TASK-1 channels are expressed in bronchi, as shown by laser-assisted cell picking and subsequent RT-PCR, and their inhibition is supposed to cause bronchoconstriction. Either, TASK-1 mRNA is not translated into functional protein in murine bronchial SMC, which could not be directly investigated due to the proven unspecificity of all available TASK-1 antibodies, or TASK-1 is not linked to constriction in murine bronchial SMC.

Moreover, TASK-1 was proposed to regulate the vascular tone by cell membrane depolarization and thus causing PASMC contraction ^[58, 61, 157, 200]. In our study, when anandamide was used under hypoxia, hypoxic contraction was unaffected except at one time point in small intra-acinar and two in larger pre-acinar arteries. Response of vessels to anandamide under hypoxic conditions was more or less expected, and this is consistent with the results from a previous study ^[61]. Furthermore, to make the role of anandamide more clear, it was used in normoxic conditions where it could not induce constriction in vessels. So, our results from anandamide were conflicting with above mentioned studies ^[58, 61, 200] and we report that probably anandamide does inhibit TASK-1, but since it is not responsible for HPV, no effect resulted from that. The reason of different response of anandamide in our study and others may attribute towards the type of experiment model used, and the difference in TASK-1 being involved in these settings.

A293 was described for the first time as a blocker of TASK-1 channels in *Xenopus* oocytes by Putzke et al. ^[157]. They further demonstrated that a low concentration (200 nM) of A293 also inhibited TASK-1 channels in rat cardiomyocytes. Our data from A293 describe it as a strong pulmonary vasoconstrictor. Under normoxia, A293 induced significant contraction in small intra-acinar and large vessels. This reaction was in accord to the original hypothesis as A293 might have caused depolarization of cell membrane by blocking TASK-1 channel, leading to PASMC contraction. The role of A293 was further elaborated under hypoxic conditions and using TASK-1 KO mice. Constrictory effects of A293 and hypoxia were not additive, in that no further vasoconstriction was induced by hypoxia. To make the role of A293 more clear, it was used under normoxic conditions in KO mice, where its constrictory effect was not

vanished in both small intra-acinar and larger pre-acinar arteries. Our data from A293 demonstrate that it induces strong constriction of pulmonary vessels but not through TASK-1 channels.

In our experimental model, hypoxia induced constriction of intra-acinar and larger pre-acinar PASM. In TASK-1 KO mice, HPV was reduced significantly at certain time points only in large vessels but not in small intra-acinar arteries. In our study of NOX4 KO mice, HPV was reduced only in small intra-acinar arteries. Similar vessel-specific results were also presented by Paddenberg et al. ^[185] from mitochondrial complex II heterozygous mice, showing that the response of vessels varies among pre-acinar and intra-acinar arteries ^[87]. In a recent study, Manoury et al. ^[203] investigated the role of 2PK-channels in regulating contractility of PASM. They used TASK-1 KO mice, the same strain as used by us ^[151]. Effects of hypoxia and vasoconstrictors (phenylephrine, serotonin, prostaglandin F2 alpha, and endothelin-1) on pulmonary arteries were studied. Effects of hypoxia on pulmonary arteries could not be carried out by this group because in their experimental model hypoxia-induced vasoconstriction was very small in WT mice and could not be compared with KO. The study with other vasoactive agents mentioned above did not demonstrate any difference of response between WT and KO mice. So, this study is in complete harmony with our data that TASK-1 is not a key player in causing vasoconstriction in response to hypoxia and vasoconstrictors in mice.

Collectively, this study provides strong evidence that in mice the two-pore domain K⁺ channel, TASK-1, (a) is not involved in HPV of small intra-acinar arteries, (b) is marginally involved in maintenance of HPV of larger pre-acinar arteries, (c) does not affect overall rise in PAP due to hypoxia, and (d) plays no role in modulating muscarinic bronchoconstriction.

4.3 Relationship between TASK-1 and TASK-3

Different studies reported co-expression of TASK-3 and TASK-1 in different tissues and it has been suggested that these two subunits can form heterodimeric channels ^[51, 57, 151, 167, 201, 202]. Rajan et al. ^[201] reported 62% identity of TASK-1 with TASK-3 in human, and 54% identity in rat has been documented by Kim et al. ^[51]. In rat carotid body glomus cells, expression of TASK-1 and TASK-3 channels has also been

documented in a previous study where TASK-1/3 heteromer shall act as a site of sensing changes in O₂ tension ^[57]. TASK-3, like TASK-1, is also sensitive to pH ^[201]. So, TASK-3 may compensate in the absence of TASK-1 expression ^[151, 202]. Therefore, we also investigated the expression of TASK-3 channels by RT-PCR in different organs. Despite it was easily demonstrated in the cerebellum, we could not detect its expression in lung, heart and tracheal epithelium, suggesting that TASK-3 mRNA is either expressed at a very low level or not expressed at these sites. In contrast, TASK-1 was expressed in all of these samples. Previous studies about the TASK-3 expression report contradictory observations. Manoury et al. ^[202] described pulmonary arteries free of TASK-3 gene. Northern blot analysis using rat multiple tissue blots did not show TASK-3 transcripts in the following 12 organs: heart, skin, kidney, muscle, small intestine, small intestine, spleen, thymus, liver, lung, testis, and brain. However, by RT-PCR TASK-3 could be detected in most of the above mentioned organs including lungs ^[51]. RT-PCR study by Rajan et al. ^[201] implicated strong expression of TASK-3 in brain and almost no in lung and heart in guinea pig RNA samples. In a recent study, Manoury et al. ^[203] investigated the contractility of PASMC. They used two different types of TASK-1 KO mice, one was the same as used by us ^[151] and the other one was double KO (TASK-1/3) ^[165]. Effects of hypoxia and vasoconstrictors (phenylephrine, serotonin, prostaglandin F2 alpha, and endothelin-1) on pulmonary arteries were studied. Double KO mice were compared to TASK-1 KO mice to assess the role of TASK-3 in the absence of TASK-1 gene. No difference in response between WT and either strain of KO mice was observed. So, our data on the expression of TASK-3 is consistent with Rajan et al. ^[201] and Manoury et al. ^[203], and do not support heterodimerisation between TASK-1 and TASK-3, because of the absence of TASK-3, in the lung and tracheal epithelium. So, we can strongly argue that TASK-3, being absent or very poorly expressed in lung and tracheal epithelium, does not compensate TASK-1 absence at least at these locations. Our data, when compared with previous studies, also depict that the levels of expression of TASK-3 and other background K⁺ channels in the rat, mice and other species are not the same.

4.4 NOX4

The major finding of this study is that NOX4 is not an essential partner for TASK-1 to initiate HPV. Previous studies reported expression of NOX4 mRNA in vascular wall

cells to a significantly higher amount than other NOX enzymes ^[98, 99, 204-206]. NOX4, being prominently expressed in pulmonary arteries and upregulated under hypoxia ^[118], may contribute to pathophysiological changes in pulmonary arteries and vasculature ^[103, 107, 121, 124]. It acts as an oxygen sensor and is reported crucial in the regulation of TASK-1 activity in HEK293 cells ^[121].

To investigate the role of NOX4 as a potential oxygen sensor partner of TASK-1, NOX4 KO mice were used. NOX4 mRNA and protein expression were detected in the lung from mouse. NOX4 mRNA extraction from lung, heart, cerebellum, adipose tissue, kidney, and trachea, followed by RT-PCR and agarose gel electrophoresis showed that relative expression of NOX4 was high in the sample from kidney as compared to others, as it was also reported previously ^[96]. The expression of mRNA was absent in the above mentioned samples from the corresponding NOX4 KO mice, thereby validating both method and mouse strain.

Manish et al. ^[118] reported NOX4 localization in PASMC, and confocal imaging of immunolabelled cells revealed the presence of TASK-1 together with NOX4 in the plasma membranes in transfected HEK293 cells ^[121]. Moreover, colocalization of TASK-1 and NOX4 in the apical membranes of pulmonary NEB cells in the lungs of rabbits and rats was also revealed in previous reports ^[66, 207]. We detected TASK-1 mRNA expression in PASMC. Expression of TASK-1 in oxygen sensing cells like PASMC has also been reported previously ^[58, 59, 61, 201]. TASK-1 is also expressed in other oxygen sensing cells, such as carotid body type I cells ^[70] and NEB cell-derived H146 line ^[208]. A prominent response of pulmonary vessels to hypoxia is their constriction. So, our model was based on the concept of colocalization of TASK-1 and NOX4 proteins in pulmonary vessels and interaction between them. We considered PASMC to explore the functional relationship between TASK-1 and NOX4 proteins in response to changes in O₂ tension.

In our experimental set up, the response to hypoxia in small intra-acinar and larger pre-acinar pulmonary vessels was investigated separately. In TASK-1 and NOX4 WT mice, hypoxia induced constriction in both small and large arteries, albeit with some size-dependent differences. In TASK-1 KO mice, hypoxia-induced vasoconstriction was not altered in small intra-acinar arteries but significantly reduced at certain time points in larger pre-acinar arteries. In NOX4 KO mice, on the other hand, HPV was maintained

in larger pre-acinar arteries, whereas small intra-acinar arteries showed significant reduction in HPV only at certain time points. Hence, small intra-acinar and larger pre-acinar pulmonary vessels responded differently in NOX4 and TASK-1 KO mice. Consequently, our data from pulmonary vessels do not demonstrate NOX4 as a modulator of hypoxic response of TASK-1.

Reduction in HPV of small intra-acinar arteries was observed only in NOX4 KO mice. Furthermore, changes in PAP under hypoxic conditions were also measured from isolated perfused and ventilated mouse lungs in the laboratory of Prof. Norbert Weissmann, Excellence Cluster Cardio-Pulmonary System, Justus-Liebig-University, Giessen. Hypoxia induced an increase in PAP in both WT and NOX4 KO mice to the same extent. In a previous study Paddenberg et al. ^[185] observed a similar vessel-specific response from mitochondrial complex II heterozygous mice assigning to the presence of a different muscularisation along the length of pulmonary arteries, and difference in sensitivity of cells to hormones, neurotransmitters and hypoxia. The difference in response to hypoxia along the length of pulmonary arteries from heart to the capillaries can also be attributed to the presence of different proteins which sense changes in oxygen tension, their low and high expression, and their translation from mRNA. The data from isolated perfused and ventilated lungs show that NOX4 is not responsible for rise in overall PAP under hypoxia and has no connection with TASK-1 in this parameter in mice.

Our data are quite different from those of Lee et al. ^[121]. According to their data, in HEK293 cells, TASK-1 senses changes in O₂ tension and its activity was inhibited by hypoxia. Furthermore, inhibition of TASK-1 activity was modulated and augmented by NOX4. Inhibitors and siRNA of NOX4 nullified the function of TASK-1, leading to the conclusion that NOX4 regulates its oxygen sensing function. The reason behind this may be attributed to different experimental model used. Difference of direct and indirect effect on cells of substances could not be ignored. There may be a difference in response between from isolated and cultured cells and intact tissues ^[209]. P22phox, a subunit present in murine pulmonary arteries ^[118] associated with NOX4 was described to produce reactive oxygen species ^[210]. Park et al. ^[211] described p22 protein as a necessary partner for proper signalling from NOX4 to TASK-1 for hypoxic response. The reason for this difference in difference in function may be ascribable, at least in

part, to different type of species, cells and experimental conditions. Cells in cultured conditions may respond in a different mode than the cells when they are embedded in intact tissues ^[209].

In conclusion, in TASK-1 KO mice, HPV is reduced marginally in larger pre-acinar arteries and remains unaffected in small intra-acinar arteries. In case of NOX4 KO mice, HPV is reduced in small intra-acinar arteries and remains unaffected in larger pre-acinar arteries. So, TASK-1 and NOX4 behave independently in pulmonary vessels in mouse. Here NOX4 neither confers O₂ sensitivity to TASK-1 nor does it mediate responses to changes in O₂ tension in larger pre-acinar arteries. Moreover, NOX4 does not play a role in rise in overall PAP under hypoxic conditions.

4.5 Particle transport speed

The mechanism of regulation of CBF and MCC is complicated and still not fully understood. Many intrinsic factors are responsible for this regulation ^[158, 212-214], among them is ATP ^[212, 214]. The beating of cilia is regulated by many factors such as [Ca²⁺]_i ^[142-146], cAMP and cGMP ^[148-150]. The Ca²⁺ flux across the membrane is regulated by the depolarization and hyperpolarization of the cell membrane ^[15, 16, 25, 30, 32, 215]. Anesthetics reduce CBF ^[158] and target TASK-1 channels while activating them ^[159-163]. In the present study, we demonstrated TASK-1 mRNA expression in mouse tracheal epithelium. Hence, TASK-1 appeared as a candidate mediating the effects of anesthetics on CBF. This issue was addressed in the present study by measuring PTS on the surface of explanted mouse tracheas utilizing TASK-1 inhibitors (anandamide and A293), anesthetics (isoflurane and avertin), and TASK-1 KO and WT mice. Avertin used in our investigation is an anesthetic with an unclear affinity to TASK-1.

The inhibition of TASK-1 channels by anandamide and A293 did not increase the PTS. Similarly, isoflurane had no effect on PTS. Results from Hua et al. ^[216] also showed that isoflurane concentration up to 2.1% had very small effect on MCC in mice. They further reported that impaired MCC was observed when 3% isoflurane was used. In contrast, a previous study has pointed out that 2% isoflurane can significantly decrease CBF in cultured rat epithelial cells ^[158]. Similarity and difference between our results and those of Hua et al. ^[216] and Matsuura et al. ^[158], respectively, may be assigned, at least in part, due to different species, and experimental parameters used. Difference of

direct and indirect effect on cells of substances could not be ignored. There may be a difference in response between from isolated and cultured cells and intact tissues ^[209].

Effects of avertin on PTS were dose dependent. Avertin had slight reducing effect on PTS at 400 μ M concentration, and 4 mM avertin robustly decreased PTS. When ATP was applied after 4 mM avertin, no increase in PTS was observed, indicating that trachea had lost viability. Avertin at 1 mM concentration decreased PTS significantly, and the preparation still responded to ATP. Similarly, in a previous study, avertin was also described to play an important role in causing a robust decrease in MCC ^[158]. These first results from experiments performed with avertin match with the assumption that a decrease in PTS might be due to opening and closing of TASK-1 and Ca^{2+} channels, respectively. For further investigation, TASK-1 channels inhibitors were used before applying avertin but reduction in PTS was still observed. The role of TASK-1 channels in regulating PTS was further clarified by using TASK-1 KO mice. In the absence of TASK-1 gene, however, the effect of avertin was not abrogated. Collectively, the data from the experiments with TASK-1 inhibitors and with tracheas from TASK-1 gene mice show that TASK-1 is not the target molecule of avertin for modulation of PTS.

Previous studies described volatile anesthetics including isoflurane as cilioinhibitors, thus hindering MCC ^[158, 209, 212]. Our data from isoflurane and avertin also support the use of less than 2% isoflurane and 400 μ M avertin as an anesthetic reagent, as they have very small or no effect on MCC at these concentrations in mice. We demonstrate that TASK-1 is expressed in tracheal epithelium and is not involved in the regulation of PTS in mouse trachea. Decrease in PTS with avertin may not involve TASK-1 channels and some unknown mechanism is involved in that reduction of PTS and MCC in mouse. Moreover, previous studies, where TASK-1 is reported as target molecule of anesthetics ^[159-163], are contradictory to our data. We do not find a relation between avertin and TASK-1. Avertin does not target and activate TASK-1 in reducing PTS in mouse model.

4.6 Conclusions

Taken together, this study reflects multifactorial function of TASK-1 and suggests different species and organs might have different levels of expressions of these channels. Our present data strongly indicate that TASK-1 does neither regulate to a

significant extent HPV nor PTS or bronchoconstriction in mice. Still, it has to be considered that TASK-1 protein (a) possibly remains inactive after being synthesized, (b) becomes modified into another protein, (c) is not transported to the cell membrane in mice, (d) has very low expression that it is not fully functional, (e) function of TASK-1 protein in its absence may be compensated by another unknown protein, (f) TASK-1 KO mice might have adapted to counterbalance the absence of gene, (g) in mice, PASMC and tracheal epithelium, inhibition of TASK-1 channels may not further trigger activation of calcium channels and consequently PASMC constriction and increase in PTS are not induced. Additional studies from different species and organs are still required to clearly define TASK-1 channels and explore TASK-1 for better understanding of its role in HPV, PTS and relationship with TASK-3 and NOX4.

5 SUMMARY

TASK-1 is a member of the two pore domain K^+ channel family. Its closing causes a decrease in K^+ efflux, depolarization of cell membrane, opening of calcium channels and Ca^{2+} entry into the cell. This has been reported to occur under hypoxia while volatile anesthetics activate this channel. Consequently, TASK-1 may be involved in mechanisms of hypoxic pulmonary vasoconstriction (HPV) and anesthetics-induced inhibition of mucociliary clearance. In cell culture, the superoxide generating enzyme NOX4 has been considered as a functional partner of TASK-1 in O_2 sensing. On this background, we set out to investigate in mice (1) the role of TASK-1 channel in HPV and bronchial constriction, (2) the functional relation between TASK-1 and NOX4 in sensing changes in O_2 tension in pulmonary vessels, and (3) the role of TASK-1 in cilia driven particle transport on the tracheal mucosal surface.

Immunohistochemistry and western blot with different anti-TASK-1 and anti-NOX4 antibodies, real-time RT-PCR, RT-PCR, laser-assisted microdissection and subsequent RT-PCR studies were carried out on various organs from TASK-1 and NOX4 knockout (KO) and corresponding wild type (WT) mice. Effects of hypoxia on bronchi and of TASK-1 inhibitors in TASK-1 KO and corresponding WT mice, effects of hypoxia on small intra-acinar and larger pre-acinar pulmonary arteries of TASK-1 and NOX4 KO and corresponding WT mice, effects of TASK-1 inhibitors under normoxia and hypoxia on small intra-acinar and larger pre-acinar arteries of TASK-1 WT mice, and effects of A293 (TASK-1 inhibitor) under normoxia on small intra-acinar and larger pre-acinar arteries of TASK-1 KO mice were investigated by videomorphometric analysis. Changes in pulmonary arterial pressure induced by hypoxic ventilation were measured in isolated perfused and ventilated lungs from TASK-1 and NOX4 KO mice. Effects of inhibitors of TASK-1 and anesthetics on PTS were investigated.

Immunoreactivity patterns with TASK-1 and NOX4 antibodies were the same in different organs from both KO and WT mice, thus questioning the validity of the antibodies. Residual mRNA content was detected by quantitative PCR analysis in the cerebellum, lung, and heart from TASK-1 KO mice, thereby indicating background expression of a pseudogene or hitherto unknown gene duplication. Still, functional ablation of the TASK-1 gene was validated by demonstration of disrupted adrenal gland zonation, as previously reported. Laser-assisted cell picking and subsequent RT-PCR

showed TASK-1 mRNA expression in bronchi, tracheal epithelium, and larger pre-acinar arteries. No mRNA was detected from NOX4 KO mice samples by RT-PCR indicating these mice as true KO.

In videomorphometric analysis, the TASK-1 inhibitor anandamide induced constriction of small intra-acinar arteries at one time point under normoxia and significantly reduced HPV also at one time point in WT mice. In larger arteries, it did not induce constrictions under normoxia and lead to a significantly reduced HPV at 29-39 min after switching to hypoxic gassed medium. Under normoxia, A293 caused significant constriction in WT small vessels, and no further constriction under hypoxic conditions was observed. Similarly, in larger vessels, it also caused significant constriction under normoxia and prevented further HPV. In TASK-1 KO animals, under normoxic conditions, the constrictory effect of A293 was not reduced. A significant vasoconstriction in both small intra-acinar and larger arteries was still observed. In NOX4 KO mice, HPV was reduced in small arteries and remained unaffected in larger pre-acinar arteries. In muscarinic pre-constricted bronchi, hypoxia and anandamide induced no alteration of bronchial diameter. TASK-1 and NOX4 KO mice also responded normally in the hypoxic isolated perfused lung model. Data from cilia driven particle transport speed (PTS) experiments demonstrated that inhibitors of TASK-1 channels had no effect on PTS, and amongst anesthetics only avertin, but not isoflurane reduced basal PTS. In TASK-1 KO mice, neither basal nor ATP-stimulated PTS was affected and the avertin effect remained unchanged.

According to our data, TASK-1 channels do not play a prominent role in causing pulmonary vasoconstriction in response to change in O₂ concentration. It is not involved in HPV of small intra-acinar and marginally involved in HPV of larger pre-acinar arteries. TASK-1 and NOX4 behave independently in murine pulmonary vessels. Here, NOX4 neither confers O₂ sensitivity to TASK-1 nor does it mediate responses to changes in O₂ tension in larger pre-acinar arteries. Moreover, TASK-1 and NOX4 do not play a role in rise in overall pulmonary arterial pressure under hypoxic conditions. Hypoxia and TASK-1 do not regulate bronchoconstriction in mice. TASK-1 does not regulate PTS in mice, while avertin inhibits this mucociliary clearance mechanism independent from TASK-1.

6 ZUSAMMENFASSUNG

TASK-1 ist ein Mitglied der zweiporigen K^+ -Kanalfamilie. Sein Schluss resultiert in einer Abnahme des Kaliumausstroms, Depolarisierung der Zellmembran, Öffnung von Kalziumkanälen und Ca^{2+} -Einstrom in die Zelle. Es wurde berichtet, dass dies unter Hypoxie geschieht, wohingegen volatile Anästhetika den Kanal aktivieren. Dementsprechend könnte TASK-1 in die Mechanismen der hypoxischen pulmonalen Vasokonstriktion (HPV) und der durch Anästhetika induzierten Hemmung der mukoziliären Clearance involviert sein. Aufgrund von Zellkulturexperimenten wurde angenommen, dass das Superoxid generierende Enzym NOX4 bei der zellulären Sauerstoffmessung als funktioneller Partner von TASK-1 fungiert. Vor diesem Hintergrund sollten in der Maus untersucht werden: 1.) die Rolle von TASK-1 in der HPV und Bronchokonstriktion, 2.) der funktionelle Zusammenhang zwischen TASK-1 und NOX4 im Sauerstoffsensormechanismus pulmonaler Gefäße und 3.) die Rolle von TASK-1 im zilienvermittelten Partikeltransport auf der trachealen Schleimhautoberfläche.

An verschiedenen Organen von TASK-1 und NOX4 knockout (KO) und korrespondierenden Wildtyp (WT) Mäusen wurden Immunhistochemie und Western Blot mit verschiedenen TASK-1- und NOX4-Antikörpern, Real-time RT-PCR, RT-PCR, sowie laserassistierte Mikrodissektion mit nachfolgender RT-PCR durchgeführt. Die Effekte von Hypoxie und von TASK-1-Inhibitoren wurden videomorphometrisch in Bronchi, kleinen intra-azinären und größeren prä-azinären pulmonalen Arterien untersucht. In isoliert perfundierten und ventilierten Lungen von TASK-1 und NOX4 KO und WT Mäusen wurden hypoxiebedingte Änderungen des pulmonal-arteriellen Druckes untersucht. Effekte von TASK-1-Inhibitoren und Anästhetika auf die Partikeltransportgeschwindigkeit wurden in isolierten Tracheen analysiert.

Antikörper gegen TASK-1 und NOX4 erwiesen sich als unspezifisch, da sie sowohl im Western Blot als auch in der Immunhistochemie die gleichen Ergebnisse in KO und WT Mäusen zeigten. Quantitative PCR-Analyse zeigte einen residualen mRNA-Gehalt im Kleinhirn, Lunge und Herz von TASK-1 KO Mäusen, welches als ein Hinweis auf eine Hintergrundexpression eines Pseudogens oder auf eine bisher unbekannte Genduplikation gedeutet wird. Dennoch zeigten sich die TASK-1 KO Mäuse als

diesbezüglich funktionell inaktiv, was durch den Nachweis einer gestörten Zonierung der Nebenniere validiert werden konnte, welches aufgrund von Befunden einer anderen Arbeitsgruppe mit dem funktionellen Verlust des Gens assoziiert ist. Laserassistierte Mikrodisektion und nachfolgende RT-PCR zeigen TASK-1 mRNA-Expression in Bronchien, Trachealepithel und größeren prä-azinären Lungengefäßen. In NOX4 KO Mäusen war kein residueller mRNA-Gehalt nachweisbar.

Der TASK-1-Inhibitor Anandamid induzierte nur zu einem der untersuchten Zeitpunkte eine Kontraktion kleiner intra-azinärer Arterien unter Normoxie und reduzierte zu einem weiteren Zeitpunkt signifikant die HPV. In größeren Arterien induzierte er keine Konstriktion unter Normoxie und führte zu einer signifikant reduzierten HPV zwischen der 29. und 39. Minute unter hypoxischer Begasung. Der Inhibitor A293 bewirkte eine signifikante Konstriktion in normoxischen kleinen Gefäßen, die durch zusätzliche Hypoxie nicht weiter verstärkt wurde. Eine vergleichbare Reaktion zeigte sich in größeren Gefäßen. Der konstriktorische Effekt von A293 war in TASK-1 KO Tieren unverändert. In NOX4 KO Mäusen war die HPV in kleinen Arterien geschmälert und blieb unbeeinflusst in größeren prä-azinären Arterien. TASK-1 und NOX4 KO Mäuse zeigten keine Veränderungen im Modell der isoliert perfundierten Lunge. Hypoxie und Anandamid hatten keinen Einfluss auf den bronchialen Durchmesser nach Präkonstriktion durch Muskarin. In der Analyse des ziliengetriebenen Partikeltransports zeigten TASK-1-Inhibitoren keinen Effekt, und unter den getesteten Anästhetika bewirkte Avertin, aber nicht Isofluran, eine Verringerung der basalen Transportgeschwindigkeit. Dieser Avertin-Effekt blieb in TASK-1 KO Mäusen bestehen.

Nach dieser Datenlage spielt TASK-1 keine wesentliche Rolle im Mechanismus der HPV. Es ist bei der HPV kleiner intra-azinärer Gefäße unbeteiligt und nur marginal in die HPV größerer prä-azinärer Gefäße involviert. Im Rahmen der HPV agieren TASK-1 und NOX4 unabhängig im pulmonalen Gefäßsystem der Maus. NOX4 vermittelt weder O₂-Sensitivität von TASK-1, noch vermittelt es hypoxische Antworten in größeren prä-azinären Gefäßen. Beide, TASK-1 und NOX4, sind nicht für den pulmonalen arteriellen Druckanstieg unter hypoxischer Beatmung verantwortlich. Hypoxie und TASK-1 regulieren ebenfalls nicht die Bronchokonstriktion in der Maus. Der mukoziliäre

Clearance-Mechanismus wird nicht über TASK-1 reguliert. Das Anästhetikum Avertin inhibiert diese mukoziliären Reinigungsmechanismen, aber unabhängig von TASK-1.

7 REFERENCES

1. Peacock, A. J., Murphy, N. F., McMurray, J. J., Caballero, L., Stewart, S. (2007) An epidemiological study of pulmonary arterial hypertension. *Eur Respir J* 30(1), 104-109.
2. Humbert, M., Sitbon, O., Simonneau, G. (2004) Treatment of pulmonary arterial hypertension. *N Engl J Med* 351(14), 1425-1436.
3. Stenmark, R., Fagan, K., Frid, M. G. (2006) Hypoxia-induced pulmonary vascular remodeling: cellular and molecular mechanisms. *Circ Res* 99(7), 675-691.
4. Jeffery, T. K. and Wanstall, J. C. (2001) Pulmonary vascular remodeling: a target for therapeutic intervention in pulmonary hypertension. *Pharmacol Ther* 92(1), 1-20.
5. Veeraghavan, S., Koss, M. N., Sharma, O. P. (1999) Pulmonary veno-occlusive disease. *Curr Opin Pulm Med* 5(5), 310-313.
6. Carbone, R., Bossone, E., Bottino, G., Monselise, A., Rubenfire, M. (2005) Secondary pulmonary hypertension—diagnosis and management. *Eur Rev Med Pharmacol Sci* 9(6), 331-342.
7. Hyduk, A., Croft, J. B., Ayala, C., Zheng, K., Zheng, Z. J., Mensah, G. A. (2005) Pulmonary hypertension surveillance—United States, 1980-2002. *MMWR Surveill Summ* 54(5), 1-28.
8. Naeije, R. (2005) Pulmonary hypertension and right heart failure in chronic obstructive pulmonary disease. *Proc Am Thorac Soc* 2(1), 20-22.
9. Roy, R. and Couriel, J. M. (2006) Secondary pulmonary hypertension. *Paediatr Respir Rev* 7(1), 36-44.
10. Stenmark, K. R. and Abman, S. H. (2005) Lung vascular development: implications for the pathogenesis of bronchopulmonary dysplasia. *Annu Rev Physiol* 67, 623-661.
11. Strange, C. and Highland, K. B. (2005) Pulmonary hypertension in interstitial lung disease. *Curr Opin Pulm Med* 11(5), 452-455.
12. Wigley, F. M., Lima, J. A., Mayes, M., McLain, D., Chapin, J. L., Ward-Able, C. (2005) The prevalence of undiagnosed pulmonary arterial hypertension in subjects with connective tissue disease at the secondary health care level of

- community-based rheumatologists (the UNCOVER study). *Arthritis Rheum* 52(7), 2125-2132.
13. Gilroy, J., Cahalan, J. L., Berman, R., Newman, M. (1963) Cardiac and pulmonary complications in Duchenne's progressive muscular dystrophy. *Circulation* 1, 484-493.
 14. Simonneau, G., Galiè, N., Rubin, L. J., Langleben, D., Seeger, W., Domenighetti, G., Gibbs, S., Lebrec, D., Speich, R., Beghetti, M., Rich, S., Fishman, A. (2004) Clinical classification of pulmonary hypertension. *J Am Coll Cardiol* 43, 5-12.
 15. Brimiouille, S., LeJeune, P., Naeije, R. (1996) Effects of hypoxic pulmonary vasoconstriction on pulmonary gas exchange. *J Appl Physiol* 81(4), 1535-1543.
 16. Thomas, H. M. and Garrett, R. C. (1982) Strength of hypoxic vasoconstriction determines shunt fraction in dogs with atelectasis. *J Appl Physiol* 53(1), 44-51.
 17. Arribas, S. M., Hillier, C., Gonzalez, C., McGrory, S., Dominiczak, A. F., McGrath, J. C. (1997) Cellular aspects of vascular remodeling in hypertension revealed by confocal microscopy. *Hypertension* 30(6), 1455-1464.
 18. Belknap, J. K., Orton, E. C., Ensley, B., Tucker, A., Stenmark, K. R. (1997) Hypoxia increases bromodeoxyuridine labeling indices in bovine neonatal pulmonary arteries. *Am J Respir Cell Mol Biol* 16(4), 366-371.
 19. Stenmark, K. R., Davie, N., Frid, M., Gerasimovskaya, E., Das, M. (2006) Role of the adventitia in pulmonary vascular remodeling. *Physiology (Bethesda)* 21, 134-145.
 20. Kobs, R. W., Muvarak, N. E., Eickhoff, J. C., Chesler, N. C. (2005) Linked mechanical and biological aspects of remodeling in mouse pulmonary arteries with hypoxia-induced hypertension. *Am J Physiol Heart Circ Physiol* 288(3), 1209-1217.
 21. Stenmark, K. R. and Mecham, R. P. (1997) Cellular and molecular mechanisms of pulmonary vascular remodeling. *Annu Rev Physiol* 59, 89-144.
 22. Parks, W. C., Mecham, R. P., Crouch, E. C., Orton, E. C., Stenmark, K. R. (1989) Response of lobar vessels to hypoxic pulmonary hypertension. *Am Rev Respir Dis* 140(5), 1455-1457.
 23. Chen, C. P., Yang, Y. C., Su, T. H., Chen, C. Y., Aplin, J. D. (2005) Hypoxia and transforming growth factor-beta 1 act independently to increase extracellular

- matrix production by placental fibroblasts. *J Clin Endocrinol Metab* 90(2), 1083-1090.
24. Papakonstantinou, E., Aletras, A. J., Roth, M., Tamm, M., Karakiulakis, G. (2003) Hypoxia modulates the effects of transforming growth factor-beta isoforms on matrix-formation by primary human lung fibroblasts. *Cytokine* 24(1-2), 25-35.
 25. Platoshyn, O., Golovina, V. A., Bailey, C. L., Limsuwan, A., Krick, S., Juhaszova, M., Seiden, J. E., Rubin, L. J., Yuan, J. X. (2000) Sustained membrane depolarization and pulmonary artery smooth muscle cell proliferation. *Am J Physiol Cell Physiol* 279(5), 1540-1549.
 26. Mauban, J. R., Remillard, C. V., Yuan, J. X. (2005) Hypoxic pulmonary vasoconstriction: role of ion channels. *J Appl Physiol* 98, 415-420.
 27. Moudgil, R., Michelakis, E. D., Archer, S. L. (2005) Hypoxic pulmonary vasoconstriction. *J Appl Physiol* 98(1), 390-403.
 28. Remillard, C. V. and Yuan, J. X. High altitude pulmonary hypertension: role of K⁺ and Ca²⁺ channels. *High Alt Med Biol* 6(2), 133-146.
 29. Gelband, C. H. and Gelband, H. (1997) Ca²⁺ release from intracellular stores is an initial step in hypoxic pulmonary vasoconstriction of rat pulmonary artery resistance vessels. *Circulation* 96(10), 3647-3654.
 30. Salvaterra, C. and Goldman, W. (1993) Acute hypoxia increases cytosolic calcium in cultured pulmonary arterial myocytes. *Am J Physiol Lung Cell Mol Physiol* 264, 323-328.
 31. Somlyo, A. P. and Somlyo, A. V. (1994) Signal transduction and regulation in smooth muscle. *Nature* 372(6503), 231-236.
 32. Gabashvili, I. S., Sokolowski, B. H., Morton, C. C., Giersch, A. B. (2007) Ion channel gene expression in the inner ear. *J Assoc Res Otolaryngo* 8(3), 305-328.
 33. Littleton, J. T. and Ganetzky, B. (2000) Ion channels and synaptic organization: analysis of the *Drosophila* genome. *Neuron* 26(1), 35-43.
 34. Mathie, A. (2010) Ion channels as novel therapeutic targets in the treatment of pain. *J Pharm Pharmacol* 62(9), 1089-1095
 35. Lesage, F. and Lazdunski, M. (2000) Molecular and functional properties of two-pore-domain potassium channels. *Am J Physiol Renal Physiol* 279(5), 793-801.

36. Lesage, F., Guillemare, E., Fink, M., Duprat, F., Lazdunski, M., Romey, G., Barhanin, J. (1996) TWIK-1, a ubiquitous human weakly inward rectifying K⁺ channel with a novel structure. *EMBO J* 15(5), 1004-1011.
37. Goldstein, S. A. (2011) K2P potassium channels, mysterious and paradoxically exciting. *Sci Signal* 4(184), 35.
38. Yanni, J., Tellez, J. O., Maczewski, M., Mackiewicz, U., Beresewicz, A., Billeter, R., Dobrzynski, H., Boyett, M. R. (2011) Changes in ion channel gene expression underlying heart failure-induced sinoatrial node dysfunction. *Circ Heart Fail* 4(4), 496-508.
39. Fink, M., Duprat, F., Lesage, F., Reyes, R., Romey, G., Heurteaux, C., Lazdunski, M. (1996) Cloning, functional expression and brain localization of a novel unconventional outward rectifier K⁺ channel. *EMBO J* 15(24), 6854-6862
40. Alloui, A., Zimmermann, K., Mamet, J., Duprat, F., Noel, J. (2006) TREK-1, a K⁺ channel involved in polymodal pain perception. *EMBO J* 25(11), 2368-2376.
41. Noel, J., Zimmermann, K., Busserolles, J., Deval, E., Alloui, A. (2009) The mechano-activated K⁺ channels TRAAK and TREK-1 control both warm and cold perception. *EMBO J* 28(9), 1308-1318.
42. Duprat, M., Lesage, F., Fink, M., Reyes, R., Heurteaux, C., Lazdunski, M. (1997) TASK, a human background K⁺ channel to sense external pH variations near physiological pH. *EMBO J* 16(17), 5464-5471.
43. Kim, D., Fujita, A., Horio, Y., Kurachi, Y. (1998) Cloning and functional expression of a novel cardiac two-pore background K⁺ channel (cTBAK-1). *Circ Res* 82(4), 513-518.
44. Fink, M., Lesage, F., Duprat, F., Heurteaux, C., Reyes, R., Fosset, M., Lazdunski, M. (1998) A neuronal two P domain K⁺ channel stimulated by arachidonic acid and polyunsaturated fatty acids. *EMBO J* 17(12), 3297-3308.
45. Reyes, R., Duprat, F., Lesage, F., Fink, M., Salinas, M., Farman, N., Lazdunski, M. (1998) Cloning and expression of a novel pH-sensitive two pore domain K⁺ channel from human kidney. *J Biol Chem* 273(47), 30863-30869.
46. Bayliss, D. A. and Barrett, P. Q. (2008) Emerging roles for two-pore-domain potassium channels and their potential therapeutic impact. *Trends Pharmacol Sci* 29(11), 566-575.
47. Chavez, R. A., Gray, A. T., Zhao, B. B., Kindler, C. H., Mazurek, M. J., Mehta, Y., Forsayeth, J. R., Yost, C. S. (1999) TWIK-2, a new weak inward rectifying

- member of the tandem pore domain potassium channel family. *J Biol Chem* 274(12), 7887-7892.
48. Salinas, M., Reyes, R., Lesage, F., Fosset, M., Heurteaux, C., Romey, G., Lazdunski, M. (1999) Cloning of a new mouse two-P domain channel subunit and a human homologue with a unique pore structure. *J Biol Chem* 274(17), 11751-11760.
 49. Coetzee, W. A., Amarillo, Y., Chiu, J., Chow, A., Lau, D., McCormack, T., Moreno, H., Nadal, M. S., Ozaita, A., Pountney, D., Saganich, M., Vega-Saenz de Miera, E., Rudy, B. (1999) Molecular diversity of K⁺ channels. *Ann NY Acad Sci* 868, 233-285.
 50. Jan, L. Y. and Jan, Y. N. (1997) Voltage-gated and inwardly rectifying potassium channels. *J Physiol (Lond)* 505, 267-282.
 51. Kim, Y., Bang, H., Kim, D. (2000) TASK-3, a new member of the tandem pore K(+) channel afamily. *J Biol Chem* 275(13), 9340-9347.
 52. Millar, J. A., Barratt, L., Southan, A. P., Page, K. M., Fyffe, R. E., Robertson, B., Mathie, A. (2000) A functional role for the two-pore domain potassium channel TASK-1 in cerebellar granule neurons. *Proc Natl Acad Sci USA* 97(7), 3614-3618.
 53. Talley, E. M., Lei, Q., Sirois, J. E., Bayliss, D. A. (2000) TASK-1, a two-pore domain K1 channel, is modulated by multiple neurotransmitters in motoneurons. *Neuron* 25(2), 399-410.
 54. Brickley, S. G., Revilla, V., Cull-Candy, S. G., Wisden, W., Rarrant, M. (2001) Adaptive regulation of neuronal excitability by a voltage-independent potassium conductance. *Nature* 409(6816), 88-92.
 55. Decher, N., Maier, M., Dittrich, W., Gassenhuber, J., Brüggemann, A., Busch, A. E., Steinmeyer, K. (2001) Characterization of TASK-4, a novel member of the pH-sensitive, two-pore domain potassium channel family. *FEBS Lett* 492(1-2), 84-90.
 56. Kim, D. and Gnatenco, C. (2001) TASK-5, a new member of the tandem-pore K(+) channel family. *Biochem Biophys Res Commun* 284(4), 923-930.
 57. Kim, D., Cavanaugh, E. J., Kim, I., Carroll, J. L. (2009) Heteromeric TASK-1/TASK-3 is the major oxygen-sensitive background K⁺ channel in rat carotid body glomus cells. *J Physiol* 587, 2963-2975.

58. Gurney, A. M., Osipenko, O. N., MacMillan, D., McFarlane, K. M., Tate, R. J., Kempson, F. E. (2003) Two-pore domain K channel, TASK-1, in pulmonary artery smooth muscle cells. *Circ Res* 93(10), 957-964.
59. Gardener, M. J., Johnson, I. T., Burnham, M. P., Edwards, G., Heagerty, A. M., Weston, A. H. (2004) Functional evidence of a role for two-pore domain potassium channels in rat mesenteric and pulmonary arteries. *Br J Pharmacol* 142(1), 192-202.
60. Manoury, B., Etheridge, S. L., Reid, J., Gurney, A. M. (2009) Organ culture mimics the effects of hypoxia on membrane potential, K (+) channels and vessel tone in pulmonary artery. *Br J Pharmacol* 158(3), 848-861.
61. Olschewski, A., Li, Y., Tang, B., Hanze, J., Eul, B., Bohle, R. M., Wilhelm, J., Morty, R. E., Brau, M. E., Weir, E. K., Kwapiszewska, G., Klepetko, W., Seeger, W., Olschewski, H. (2006) Impact of TASK-1 in human pulmonary artery smooth muscle cells. *Circ Res* 98(8), 1072-1080.
62. Patel, A. J. and Honore, E. (2001) Molecular physiology of oxygen-sensitive potassium channels. *Eur Respir J* 18, 221-227.
63. Jiang, C. and Haddad, G. G. (1994) A direct mechanism for sensing low oxygen levels by central neurons. *Proc Natl Acad Sci USA* 91, 7198-7201.
64. Weir, E. and Will, J. (1982) Oxidants: a new group of pulmonary vasodilators. *Clin Resp Physiol* 18(1), 81-85.
65. Mühlhölzer, J., Tiefenbach, M., López-Barneo, J., Piruat, J. I., García-Flores, P., Pfeil, U., Gries, B., Mühlhölzer, C., Weigand, M. A., Kummer, W., Weissmann, N., Paddenberg, R. (2010) Mitochondrial complex II participates in normoxic and hypoxic regulation of α -keto acids in the murine heart. *J Mol Cell Cardiol* 49(6), 950-961.
66. Cave, A. C., Brewer, A. C., Narayanapanicker, A., Ray, R., Grieve, D. J., Walker, S., Shah, A. M. (2006) NADPH oxidases in cardiovascular health and disease. *Antioxid Redox Signal* 8(5-6), 691-728.
67. Geiszt, M. (2006) NADPH oxidases: new kids on the block. *Cardiovasc Res* 71(2), 289-299.
68. Wang, D., Youngson, C., Wong, V. (1996) NADPH-oxidase and a hydrogen peroxide-sensitive K⁺ channel may function as an oxygen sensor complex in airway chemoreceptors and small cell lung carcinoma cell lines. *Proc Natl Acad Sci USA* 93(23), 13182-13187.

69. Perez-Garcia, M. T., Lopez-Lopez, J. R., Riesco, A. M. (2000) Viral gene transfer of dominant negative Kv4 construct suppresses an O₂-sensitive K⁺ current in chemoreceptor cells. *J Neurosci* 20(15), 5689-5695.
70. Buckler, K., Williams, B., Honore', E. (2000) An oxygen-, acid and anaesthetic-sensitive TASK-like background potassium channel in rat arterial chemoreceptor cells. *J Physiol* 525, 135-142.
71. Perez-Garcia, M. T., Lopez-Lopez, J. R., Gonzalez, C. (1999) Kvbeta1.2 subunit coexpression in HEK293 cells confers O₂ sensitivity to Kv4.2 but not to Shaker channels. *J Gen Physiol* 113(6), 897-907.
72. Conforti, L. and Millhorn, D. E. (1997) Selective inhibition of a slow-inactivating voltage-dependent K channel. *J Physiol* 502, 293-305.
73. Conforti, L., Bodi, I., Nisbet, J. W., Millhorn, D. E. (2000) O₂-sensitive K⁺ channels: role of the Kv1.2 -subunit in mediating the hypoxic response. *J Physiol* 3, 783-793.
74. O'Kelly, I., Stephens, R. H., Peers, C., Kemp, P. J. (1999) Potential identification of the O₂-sensitive K⁺ current in a human neuroepithelial body-derived cell line. *Am J Physiol* 276, 96-104.
75. Patel, A. J., Lazdunski, M., Honore', E. Kv2.1/Kv9.3, (1997) a novel ATP-dependent delayed-rectifier K⁺ channel in oxygen-sensitive pulmonary artery myocytes. *EMBO J* 16(22), 6615-6625.
76. Archer, S. L., Souil, E., Dinh-Xuan, A. T. (1998) Molecular identification of the role of voltage-gated K⁺ channels, Kv1.5 and Kv2.1, in hypoxic pulmonary vasoconstriction and control of resting membrane potential in rat pulmonary artery myocytes. *J Clin Invest* 101(11), 2319-2330.
77. Hulme, J. T., Coppock, E. A., Felipe, A., Martens, J. R., Tamkun, M. M. (1999) Oxygen sensitivity of cloned voltage gated K⁺ channels expressed in the pulmonary vasculature. *Circ Res* 85(6), 489-497.
78. Osipenko, O. N., Tate, R. J., Gurney, A. M. (2000) Potential role for kv3.1b channels as oxygen sensors. *Circ Res* 86(5), 534-540.
79. Reid, L. and Simon, G. (1958) The peripheral pattern in the normal bronchogram and its relation to peripheral pulmonary anatomy. *Thorax* 13(2), 103-109.
80. Hislop, A. and Reid, L. (1978) Normal structure and dimensions of the pulmonary arteries in the rat. *J Anat* 125, 71-83.

81. Tabuchi, A., Mertens, M., Kuppe, H., Pries, A. R., Kuebler, W. M. (2008) Intravital microscopy of the murine pulmonary microcirculation. *J Appl Physiol* 104(2), 338-346.
82. Kay, J. M. (1983) Comparative morphologic features of the pulmonary vasculature in mammals. *Am Rev Respir Dis* 128, 53-57.
83. Michel, R. P. (1982) Arteries and veins of the normal dog lung: qualitative and quantitative structural differences. *Am J Anat* 164(3), 227-241.
84. al-Tinawi, A., Krenz, G. S., Rickaby, D. A., Linehan, J. H., Dawson, C. A. (1994) Influence of hypoxia and serotonin on small pulmonary vessels. *J Appl Physiol* 76(1), 56-64.
85. Kato, M. and Staub, N. C. (1996) Response of small pulmonary arteries to unilobar hypoxia and hypercapnia. *Circ Res* 19(2), 426-440.
86. Nagasaka, Y. Bhattacharya, J. Nanjo, S. Gropper, M. A., Staub, N. C. (1984) Micropuncture measurement of lung microvascular pressure profile during hypoxia in cats. *Circ Res* 54(1), 90-95.
87. Drexler, E. S., Quinn, T. P., Slifka, A. J., McCowan, C. N., Bischoff, J. E., Wright, J. E., Ivy, D. D., Shandas, R. (2007) Comparison of mechanical behavior among the extrapulmonary arteries from rats. *J Biomech* 40(4), 812-819.
88. Lambeth, J. D. (2004) NOX enzymes and the biology of reactive oxygen. *Nat Rev Immunol* 4(3), 181-189.
89. Sumimoto, H. (2008) Structure, regulation and evolution of Nox-family NADPH oxidases that produce reactive oxygen species. *Febs J* 275(13), 3249-3277.
90. Bedard, K. and Krause, K. H. (2007) The NOX family of ROS-generating NADPH oxidases: physiology and pathophysiology. *Physiol Rev* 87(1), 245-313.
91. Martyn, K. D., Frederick, L. M., von Loehneysen, K., Dinauer, M. C., Knaus, U. G. (2006) Functional analysis of Nox4 reveals unique characteristics compared to other NADPH oxidases. *Cell Signal* 18(1), 69-82.
92. Serrander, L. (2007) NOX4 activity is determined by mRNA levels and reveals a unique pattern of ROS generation. *Biochem J* 406(1), 105-114.

93. Dikalov, S. I. (2008) Distinct roles of Nox1 and Nox4 in basal and angiotensin II stimulated superoxide and hydrogen peroxide production. *Free Radic Biol Med* 45(9), 1340-1351.
94. Nisimoto, Y., Jackson, H. M., Ogawa, H., Kawahara, T., Lambeth, J. D. (2010) Constitutive NADPH-dependent electron transferase activity of the Nox4 dehydrogenase domain. *Biochemistry* 49(11), 2433-2442.
95. Suh, Y. A., Arnold, R. S., Lassegue, B., Shi, J., Xu, X., Sorescu, D., Chung, A. B., Griendling, K. K., Lambeth, J. D. (1999) Cell transformation by the superoxide generating oxidase Mox1. *Nature* 401(6748), 79-82.
96. Geiszt, M., Kopp, J. B., Varnai, P., Leto, T. L. (2000) Identification of renox, an NAD(P)H oxidase in kidney. *Proc Natl Acad Sci USA* 97(14), 8010-8014.
97. Shiose, A., Kuroda, J., Tsuruya, K., Hirai, M., Hirakata, H., Naito, S. (2001) A novel superoxide-producing NAD(P)H oxidase in kidney. *J Biol Chem* 276(2), 1417-1423.
98. Ago, T., Kitazono, T., Ooboshi, H., Iyama, T., Han, Y. H., Takada, J. (2004) Nox4 as the major catalytic component of an endothelial NAD(P)H oxidase. *Circulation* 109(2), 227-233.
99. Clempus, R. E., Sorescu, D., Dikalova, A. E., Pounkova, L., Jo, P., Sorescu, G. P. (2007) Nox4 is required for maintenance of the differentiated vascular smooth muscle cell phenotype. *Arterioscler Thromb Vasc Biol* 27(1), 42-48.
100. Ago, T., Kuroda, J., Pain, J., Fu, C., Li, H., Sadoshima, J. (2010) Upregulation of Nox4 by hypertrophic stimuli promotes apoptosis and mitochondrial dysfunction in cardiac myocytes. *Circ res* 106(7), 1253-1264.
101. Zhang, M., Brewer, A. C., Schroder, K., Santos, C. X., Grieve, D. J., Wang, M. (2010) NADPH oxidase-4 mediates protection against chronic load-induced stress in mouse hearts by enhancing angiogenesis. *Proc Natl Acad Sci USA* 107(42), 18121-18126.
102. Hoidal, J. R., Brar, S. S., Sturrock, A. B., Sanders, K. A., Dinger, B., Fidone, S., Kennedy, T. P. (2003) The role of endogenous NADPH oxidases in airway and pulmonary vascular smooth muscle function. *Antioxid Redox Signal* 5(6), 751-758.
103. Sturrock, A., Cahill, B., Norman, K., Huecksteadt, T. P., Hill, K., Sanders, K., Karwande, S. V., Stringham, J. C., Bull, D. A., Gleich, M., Kennedy, T. P., Hoidal, J. R. (2006) Transforming growth factor-beta1 induces Nox4 NAD(P)H

- oxidase and reactive oxygen species-dependent proliferation in human pulmonary artery smooth muscle cells. *Am J Physiol Lung Cell Mol Physiol* 290(4), 661-673.
104. Kummer, W. and Acker, H. (1995) Immunohistochemical demonstration of four subunits of neutrophil NAD(P)H oxidase in type I cells of carotid body. *J Appl Physiol* 78(5), 1904-1909.
105. Youngson, C., Nurse, C., Yeager, H., Cutz, E. (1993) Oxygen sensing in airway chemoreceptors. *Nature* 365(6442), 153-155.
106. Hohler, B., Holzapfel, B., Kummer, W. (2000) NADPH oxidase subunits and superoxide production in porcine pulmonary artery endothelial cells. *Histochem Cell Biol* 114(1), 29-37.
107. Cai, H., Griendling, K. K., Harrison, D. G. (2003) The vascular NAD(P)H oxidases as therapeutic targets in cardiovascular diseases. *Trends Pharmacol Sci* 24(9), 471-478.
108. Babior, B. M., Lambeth, J. D., Nauseef, W. (2002) The neutrophil NADPH oxidase. *Arch Biochem Biophys*. 397(2), 342-344.
109. Bendall, J. K., Cave, A. C., Heymes, C., Gall, N., Shah, A. M. (2002) Pivotal role of a gp91(phox)-containing NADPH oxidase in angiotensin II-induced cardiac hypertrophy in mice. *Circulation* 105(3), 293-296.
110. Byrne, J. A., Grieve, D. J., Bendall, J. K., Li, J. M., Gove, C., Lambeth, J. D., Cave, A. C., Shah, A. M. (2003) Contrasting roles of NADPH oxidase isoforms in pressure overload versus angiotensin II-induced cardiac hypertrophy. *Circ Res* 93(9), 802-805.
111. Nakagami, H., Takemoto, M., Liao, J. K. (2003) NADPH oxidase-derived superoxide anion mediates angiotensin II-induced cardiac hypertrophy. *J Mol Cell Cardiol* 35(7), 851-859.
112. Satoh, M., Ogita, H., Takeshita, K., Mukai, Y., Kwiatkowski, D. J., Liao, J. K. (2006) Requirement of Rac1 in the development of cardiac hypertrophy. *Proc Natl Acad Sci USA* 103(19), 7432-7437.
113. Doerries, C., Grote, K., Hilfiker-Kleiner, D., Luchtefeld, M., Schaefer, A., Holland, S. M., Sorrentino, S., Manes, C., Schieffer, B., Drexler, H., Landmesser, U. (2007) Critical role of the NAD(P)H oxidase subunit p47phox for left ventricular remodeling/dysfunction and survival after myocardial infarction. *Circ Res* 100(6), 894-903.

114. Looi, Y. H., Grieve, D. J., Siva, A., Walker, S. J., Anilkumar, N., Cave, A. C., Marber, M., Monaghan, M. J., Shah, A. M. (2008) Involvement of Nox2 NADPH oxidase in adverse cardiac remodeling after myocardial infarction. *Hypertension* 51(2), 319-325.
115. Sorescu, D., Weiss, D., Lassegue, B., Clempus, R. E., Szocs, K., Sorescu, G. P., Valppu, L., Quinn, M. T., Lambeth, J. D., Vega, J. D., Taylor, W. R., Griendling, K. K. (2002) Superoxide production and expression of nox family proteins in human atherosclerosis. *Circulation* 105(12), 1429-1435.
116. Brandes, R. P. (2003) Role of NADPH oxidases in the control of vascular gene expression. *Antioxid Redox Signal* 5(6), 803-811.
117. Ambasta, R. K., Kumar, P., Griendling, K. K., Schmidt, H. H., Busse, R., Brandes, R. P. (2004) Direct interaction of the novel Nox proteins with p22phox is required for the formation of a functionally active NADPH oxidase. *J Biol Chem* 279(44), 45935-45941.
118. Mittal, M., Roth, M., König, P., Hofmann, S., Dony, E., Goyal, P., Selbitz, A. C., Schermuly, R. T., Ghofrani, H. A., Kwapiszewska, G., Kummer, W., Klepetko, W., Hoda, M. A., Fink, L., Hänze, J., Seeger, W., Grimminger, F., Schmidt, H. H., Weissmann, N. (2007) Hypoxia-dependent regulation of nonphagocytic NADPH oxidase subunit NOX4 in the pulmonary vasculature. *Circ Res* 101(3), 258-267.
119. Li, S., Tabar, S. S., Malec, V., Eul, B. G., Klepetko, W., Weissmann, N., Grimminger, F., Seeger, W., Rose, F., Hänze, J. (2008) NOX4 regulates ROS levels under normoxic and hypoxic conditions, triggers proliferation, and inhibits apoptosis in pulmonary artery adventitial fibroblasts. *Antioxid Redox Signal* 10(10), 1687-1698
120. Cross, A. R., Henderson, L., Jones, O. T., Delpiano, M. A., Hentschel, J., Acker, H. (1990) Involvement of an NAD(P)H oxidase as a pO₂ sensor protein in the rat carotid body. *Biochem J* 272(3), 743-747.
121. Lee, Y. M., Kim, B. J., Chun, Y. S., So, I., Choi, H., Kim, M. S., Park, J. W. (2006) NOX4 as an oxygen sensor to regulate TASK-1 activity. *Cell Signal* 18(4), 499-507.
122. Robinson, N. P., Venning, L., Kyle, H., Widdicombe, J. G. (1986) Quantitation of the secretory cells of the ferret tracheobronchial tree. *J Anat* 145, 173-188.

123. Rhodin, J. and Dalhamn, T. (1956) Electron microscopy of the tracheal ciliated mucosa in rat. *Z Zellforsch Mikrosk Anat* 44(4), 345-412.
124. Sbarbati, A. and Osculati, F. (2005) The taste cell-related diffuse chemosensory system. *Prog Neurobiol* 75(4), 295-307.
125. Sbarbati, A., Bramanti, P., Benati, D., Merigo, F. (2010) The diffuse chemosensory system: Exploring the iceberg toward the definition of functional roles. *Prog Neurobiol* 91(1), 77-89.
126. Krasteva, G., Canning, B. J., Hartmann, P., Veres, T. Z., Papadakis, T., Mühlfeld, C., Schliecker, K., Tallini, Y. N., Braun, A., Hackstein, H., Baal, N., Weihe, E., Schütz, B., Kotlikoff, M., Ibanez-Tallon, I., Kummer, W. (2011) Cholinergic chemosensory cells in the trachea regulate breathing. *Proc Natl Acad Sci USA* 108(23), 9478-9483.
127. Sleight, M. A., Blake, J. R., Liron, N. (1988) The Propulsion of Mucus by Cilia. *Am Rev Respir Dis* 137(3), 726-741.
128. Williams, R., Rankin, N., Smith, T., Galler, D., Seakins, P. (1996) Relationship between humidity and temperature of inspired gas and the function of the airway mucosa. *Crit Care Med* 24(11), 1920-1929.
129. Estes, R. J. and Meduri, G. U. (1995) The Pathogenesis of Ventilator-Associated Pneumonia: I. Mechanisms of Bacterial Transcolonization and Airway Inoculation. *Intensive Care Med* 21(4), 365-383.
130. Gheber, L., Priel, Z., Aflalo, C., Shoshan-Barmatz, V. (1995) Extracellular ATP binding proteins as potential receptors in mucociliary epithelium: characterization using [32P]39-O-(4-benzoyl) benzoyl ATP, a photoaffinity label. *J Membr Biol* 147(1), 83-93.
131. Weiss, T., Gheber, L., Shoshan-Barmatz, V., Priel, Z. (1992) Possible mechanism of ciliary stimulation by extracellular ATP: involvement of calcium-dependent potassium channels and exogenous Ca²⁺. *J Membr Biol* 127(3), 185-193.
132. Aiello, E., Kennedy, J., Hernandez, C. (1991) Stimulation of frog ciliated cells in culture by acetylcholine and substance P. *Comp Biochem Physiol C Pharmacol Toxicol Endocrinol* 99(3), 497-506.
133. Gheber, L. and Priel, Z. (1994) Metachronal activity of cultured mucociliary epithelium under normal and stimulated conditions. *Cell Motil Cytoskeleton* 28(4), 333-345.

134. Slaughter, M. and Aiello, E. (1982) Cholinergic nerves stimulate mucociliary transport, ciliary activity, and mucus secretion in the frog palate. *Cell Tissue Res* 227(2), 413-421.
135. Maruyama, I. (1984) Conflicting effects of noradrenalin on ciliary movement of frog palatine mucosa. *Eur J Pharmacol* 97(3-4), 239-245.
136. Sastry, B. V. R. and Sadavongvivad, C. (1978) Cholinergic systems in non-nervous tissues. *Pharmacol Rev* 30(1), 65-132.
137. Mao, H. and Wong, L. B. (1995) Depolarization of membrane is associated with an increase in ciliary beat frequency (CBF). *Biochem Biophys Res Commun* 215(3), 1014-1021.
138. Salathe, M. and Bookman, R. J. (1999) Mode of Ca^{2+} action on ciliary beat frequency in single ovine airway epithelial cells. *J Physiol (Lond)* 520, 851-865.
139. Yang, B., Schlosser, R. J., McCaffrey, T. V. (1996) Dual signal transduction mechanisms modulate ciliary beat frequency in upper airway epithelium. *Am J Physiol Lung Cell Mol Physiol* 270, 745-751.
140. Klein, M. K., Haberberger, R.V., Hartmann, P., Faulhammer, P., Lips, K. S., Krain, B., Wess, J., Kummer, W., König, P. (2009) Muscarinic receptor subtypes in cilia-driven transport and airway epithelial development. *Eur Respir J* 33(5), 1113-1121.
141. Rasmussen, H. and Rasmussen, J. E. (1990) Calcium as intracellular messenger: from simplicity to complexity. *Curr Top Cell Regul* 31, 1-109.
142. Korngreen, A. and Priel, Z. (1994) Simultaneous measurement of ciliary beating and intracellular calcium. *Biophys J* 67(1), 1-4.
143. Villalon, M., Hinds, T. R., Verdugo, P. (1989) Stimulus-response coupling in mammalian ciliated cells. Demonstration of two mechanisms of control for cytosolic $[Ca^{2+}]_i$. *Biophys J* 56(6), 1255-1258.
144. Evans, T. C. and Nelson, D. L. (1989) The cilia of *Paramecium tetraurelia* contain both Ca^{2+} -dependent and Ca^{2+} -inhibitable calmodulin binding proteins. *Biochem J* 259(2), 358-396.
145. Salathe, M. and Bookman, R. J. (1995) Coupling of $[Ca^{2+}]_i$ and ciliary beating in cultured tracheal epithelial cells. *J Cell Sci* 108, 431-440.
146. Salathe, M., Lipson, E. J., Ivonnet, P. I., Bookman, R. J. (1997) Muscarinic signaling in ciliated tracheal epithelial cells: dual effects on Ca^{2+} and ciliary beating. *Am J Physiol Lung Cell Mol Physiol* 272, 301-310.

147. Nakahari, T. (2007) Regulation of ciliary beat frequency in airways: shear stress, ATP action, and its modulation. *Am J Physiol Lung Cell Mol Physiol* 292(3), 612-613.
148. Uzlaner, N. and Priel, Z. (1999) Interplay between the NO pathway and elevated $[Ca^{2+}]_i$ enhances ciliary activity in rabbit trachea. *J Physiol* 516, 179-190.
149. Ma, W., Silberberg, S. D., Priel, Z. (2002) Distinct axonemal processes underlie spontaneous and stimulated airway ciliary activity. *J Gen Physiol* 120(6), 875-885.
150. Zagoory, O., Priel, A. X., Priel, Z. (2002) The mechanism of ciliary stimulation by acetylcholine: roles of calcium, PKA, and PKG. *J Gen Physiol* 119(4), 329-339.
151. Aller, M. I., Veale, E. L., Linden, A. M., Sandu, C., Schwaninger, M., Evans, L. J., Korpi, E. R., Mathie, A., Wisden, W., Brickley, S. G. (2005) Modifying the subunit composition of TASK channels alters the modulation of a leak conductance in cerebellar granule neurons. *J Neurosci* 25(49), 11455-11467.
152. Forssmann, W. G., Ito, S., Weihe, E., Aoki, A., Dym, M., Fawcett, D. W. (1977) An improved perfusion fixation method for the testis. *Anat Rec* 188(3), 307-314.
153. Martin, C., Uhlig, S., Ullrich, V. (1996) Videomicroscopy of methacholine induced contraction of individual airways in precision-cut lung slices. *Eur Respir J* 9(12), 2479-2487.
154. Pfaff, M., Powaga, N., Akinci, S., Schütz, W., Banno, Y., Wiegand, S., Kummer, W., Wess, J., Haberberger, R. V. (2005) Activation of the SPHK/S1P signalling pathway is coupled to muscarinic receptor-dependent regulation of peripheral airways. *Respir Res* 6, 48-61.
155. Heitzmann, D., Derand, R., Jungbauer, S., Bandulik, S., Sterner, C., Schweda, F., El Wakil, A., Lalli, E., Guy, N., Mengual, R., Reichold, M., Tegtmeier, I., Bendahhou, S., Gomez-Sanchez, C. E., Aller, M. I., Wisden, W., Weber, A., Lesage, F., Warth, R., Barhanin, J. (2008) Invalidation of TASK1 potassium channels disrupts adrenal gland zonation and mineralocorticoid homeostasis. *EMBO J* 27(1), 179-187.
156. Mouche, S., Mkaddem, S. B., Wang, W., Katic, M., Tseng, Y. H., Carnesecchi, S., Steger, K., Foti, M., Meier, C. A., Muzzin, P., Kahn, C. R., Ogier-Denis, E., Szanto, I. (2007) Reduced expression of the NADPH oxidase NOX4 is a

- hallmark of adipocyte differentiation. *Biochim Biophys Acta* 1773(7), 1015-1027.
157. Putzke, C., Wemhöner, K., Sachse, F. B., Rinné, S., Schlichthörl, G., Li, X. T., Jaé, L., Eckhardt, I., Wischmeyer, E., Wulf, H., Preisig-Müller, R., Daut, J., Decher, N. (2007) The acid-sensitive potassium channel TASK-1 in rat cardiac muscle. *Cardiovasc Res* 75(1), 59-68.
 158. Matsuura, S., Shirakami, G., Iida, H., Tanimoto, K., Fukuda, K. (2006) The effect of sevoflurane on ciliary motility in rat cultured tracheal epithelial cells: a comparison with isoflurane and halothane. *Anesth Analg* 102(6), 1703-1708.
 159. Bayliss, D. A., Sirois, J. E., Talley, E. M. (2003) The TASK family: two-pore domain background K⁺ channels. *Mol Interv* 3(4), 205-219.
 160. Patel, A. J., Honore, E., Lesage F., Fink M., Romey, G., Lazdunski, M. (1999) Inhalational anesthetics activate two-pore-domain background K⁺ channels. *Nat Neurosci* 2(5), 422-426.
 161. Meadows, H. J. and Randall, A. D. (2001) Functional characterisation of human TASK-3, an acid-sensitive two-pore domain potassium channel. *Neuropharmacology* 40(4), 551-559.
 162. Sirois, J. E., Lei, Q., Talley, E. M., Lynch, I.I.C., Bayliss, D. A. (2000) The TASK-1 two-pore domain K⁺ channel is a molecular substrate for neuronal effects of inhalation anesthetics. *J Neurosci* 20(17), 6347-6354.
 163. Washburn, C. P., Sirois, J. E., Talley, E. M., Guyenet, P. G., Bayliss, D. A. (2002) Serotonergic neurons express TASK channel transcripts and a TASK-like pH- and halothane-sensitive K⁺ conductance. *J Neurosci* 22(4), 1256-1265.
 164. Linden, A. M., Aller, M. I., Leppä, E., Rosenberg, P. H., Wisden, W., Korpi, E. R. (2008) K⁺ channel TASK-1 knockout mice show enhanced sensitivities to ataxic and hypnotic effects of GABA(A) receptor ligands. *J Pharmacol Exp Ther* 327(1), 277-286.
 165. Trapp, S., Aller, M. I., Wisden, W., Gourine, A. V. (2008a) A role for TASK-1 (KCNK3) channels in the chemosensory control of breathing. *J Neurosci* 28(35), 8844-8850.
 166. Linden, A. M., Aller, M. I., Leppä, E., Vekovischeva, O., Aitta-Aho, T., Veale, E. L., Mathie, A., Rosenberg, P., Wisden, W., Korpi, E. R. (2006) The in vivo contributions of TASK-1-containing channels to the actions of inhalation

- anesthetics, the alpha (2) adrenergic sedative dexmedetomidine, and cannabinoid agonists. *J Pharmacol Exp Ther* 317(2), 615-626.
167. Muhammad, S., Aller, M. I., Maser-Gluth, C., Schwaninger, M., Wisden, W. (2010) Expression of the *kcnk3* potassium channel gene lessens the injury from cerebral ischemia, most likely by a general influence on blood pressure. *Neuroscience* 167(3), 758-764.
168. Utku, Y., Dehan, E., Ouerfelli, O., Piano, F., Zuckermann, R. N., Pagano, M., Kirshenbaum, K. (2006) A peptidomimetic siRNA transfection reagent for highly effective gene silencing. *Mol Biosyst* 2(6-7), 312-317.
169. Kang, S. G., Roh, Y. M., Kang, M. L., Kim, Y. S., Yoo, H. S. (2010) Mouse neuronal cells expressing exogenous bovine PRNP and simultaneous downregulation of endogenous mouse PRNP using siRNAs. *Prion* 4(1), 32-37.
170. Grabowska, A. M., Hughes, J., Watson, S. A. (2007) Use of interfering RNA to investigate the role of endogenous gastrin in the survival of gastrointestinal cancer cells. *Br J Cancer* 96(3), 464-473.
171. Zhang, P., Su, J., King, M. E., Maldonado, A. E., Park, C., Mende, U. (2011) Regulator of G protein signaling 2 is a functionally important negative regulator of angiotensin II-induced cardiac fibroblast responses. *Am J Physiol Heart Circ Physiol* 301(1), 147-156.
172. Jositsch, G., Papadakis, T., Haberberger, R. V., Wolff, M., Wess, J., Kummer, W. (2009) Suitability of muscarinic acetylcholine receptor antibodies for immunohistochemistry evaluated on tissue sections of receptor gene-deficient mice. *Naunyn Schmiedebergs Arch Pharmacol* 379(4), 389-395.
173. Jensen, B. C., Swigart, P. M., Simpson, P. C. (2009) Ten commercial antibodies for alpha-1-adrenergic receptor subtypes are nonspecific. *Naunyn Schmiedebergs Arch Pharmacol* 379(4), 409-412.
174. Lewis, A., Hartness, M. E., Chapman, C. G., Fearon, I. M., Meadows, H. J., Peers, C., Kemp, P. J. (2001) Recombinant hTASK1 is an O₂-sensitive K⁺ channel. *Biochem Biophys Res Commun* 285, 1290-1294.
175. Maingret, F., Patel, A. J., Lazdunski, M., Honore, E. (2001) The endocannabinoid anandamide is a direct and selective blocker of the background K⁺ channels TASK-1. *EMBO J* 20, 47-54.

176. Barbuti, A., Ishii, S., Shimizu, T., Robinson, R. B., Feinmark, S. J. (2002) Block of the background K(+) channel TASK-1 contributes to arrhythmogenic effects of platelet-activating factor. *Am J Physiol Heart Circ Physiol* 282, 2024-2030.
177. Streit, A. K., Netter, M. F., Kempf, F., Walecki, M., Rinné, S., Bollepalli, M. K., Preisig-Müller, R., Renigunta, V., Daut, J., Baukowitz, T., Sansom, M. S., Stansfeld, P. J., Decher, N. (2011) A specific two-pore domain potassium channel blocker defines the structure of the TASK-1 open pore. *J Biol Chem* 286, 13977-13984.
178. Spina, D., Tucker, R. C., Page, C. P. (2000) Effect of the putative vanilloid receptor agonist, anandamide on the baseline tone in the guinea-pig bronchus. *Proc Aust Soc Clin Exp Pharmacol Toxicol* 7, 60.
179. Craib, S. J., Ellington, H. C., Pertwee, R. G., Ross, R. A. (2001) A possible role of lipoxygenase in the activation of vanilloid receptors by anandamide in the guinea-pig bronchus. *Br J Pharmacol* 134, 30-37.
180. Harrison, S., De Petrocellis, L., Trevisani, M., Benvenuti, F., Bifulco, M., Geppetti, P., Di Marzo, V. (2003) Capsaicin-like effects of N-arachidonoyl-dopamine in the isolated guinea pig bronchi and urinary bladder. *Eur J Pharmacol* 475, 107-114.
181. Archer, S. L., Huang, J. M., Reeve, H. L., Hampl, V., Tolarova, S., Michelakis, E., Weir, E. K. (1996) Differential distribution of electrophysiologically distinct myocytes in conduit and resistance arteries determines their response to nitric oxide and hypoxia. *Circ Res* 78, 431-442.
182. Archer, S. L., Wu, X. C., Thébaud, B., Nsair, A., Bonnet, S., Tyrrell, B., McMurtry, M. S., Hashimoto, K., Harry, G., Michelakis, E. D. (2004) Preferential expression and function of voltage-gated, O₂-sensitive K⁺ channels in resistance pulmonary arteries explains regional heterogeneity in hypoxic pulmonary vasoconstriction: ionic diversity in smooth muscle cells. *Circ Res* 95, 308-318.
183. Park, M. K., Kang, T. M., Uhm, D. Y., Lee, S. J., Lee, S. H., Ho, W. K., Earm, Y. E. (1999) Different contractile properties between intralobar and extralobar pulmonary arteries of the rabbit. *J Smooth Muscle Res* 35, 1-10.
184. Stephenson, A. H., Sprague, R. S., Losapio, J. L., Lonigro, A. J. (2003) Differential effects of 5,6-EET on segmental pulmonary vasoactivity in the rabbit. *Am J Physiol Heart Circ Physiol* 284, 2153-2161.

185. Paddenberg, R., Tiefenbach, M., Faulhammer, P., Goldenberg, A., Gries, B., Pfeil, U., Lips, K. S., Piruat, J. I., López-Barneo, J., Schermuly, R. T., Weissmann, N., Kummer, W. (2012) Mitochondrial complex II is essential for hypoxia-induced pulmonary vasoconstriction of intra- but not of pre-acinar arteries. *Cardiovasc Res* 93(4), 702-10.
186. Kemp, P. J., Peers, C., Lewis, A., Miller, P. (2004) Regulation of recombinant human brain tandem P domain K⁺ channels by hypoxia: a role for O₂ in the control of neuronal excitability?. *J Cell Mol Med* 8, 38-44.
187. Johnson, R. P., O'Kelly, I. M., Fearon, I. M. (2004) System-specific O₂ sensitivity of the tandem pore domain K⁺ channel TASK-1. *Am J Physiol Cell Physiol* 286, 391-397.
188. Durmowicz, A. G. and Stenmark, K. R. (1999) Mechanisms of structural remodeling in chronic pulmonary hypertension. *Pediatr Rev* 20, 91-102.
189. Shimoda, L. A., Sham, J. S., Sylvester, J. T. (2000) Altered pulmonary vasoreactivity in the chronically hypoxic lung. *Physiol Res* 49, 549-560.
190. Kobs, R. W. and Chesler, N. C. (2006) The mechanobiology of pulmonary vascular remodeling in the congenital absence of eNOS. *Biomech Model Mechanobiol* 5, 217-225.
191. Casserly, B., Mazer, J. M., Vang, A., Harrington, E. O., Klinger, J. R., Rounds, S., Choudhary, G. (2011) C-type natriuretic peptide does not attenuate the development of pulmonary hypertension caused by hypoxia and VEGF receptor blockade. *Life Sci* 2011 89, 460-466.
192. Weissmann, N., Dietrich, A., Fuchs, B., Kalwa, H., Ay, M., Dumitrascu, R., Olschewski, A., Storch, U., Mederos, y., Schnitzler, M., Ghofrani, H. A., Schermuly, R. T., Pinkenburg, O., Seeger, W., Grimminger, F., Gudermann, T. (2006) Classical transient receptor potential channel 6 (TRPC6) is essential for hypoxic pulmonary vasoconstriction and alveolar gas exchange. *Proc Natl Acad Sci USA* 103(50), 19093-19098.
193. Durmowicz, A. G., Hofmeister, S., Kadyraliev, T. K., Aldashev, A. A., Stenmark, K. R. (1993) Functional and structural adaptation of the yak pulmonary circulation to residence at high altitude. *J Appl Physiol* 74, 2276-2285.
194. Meyrick, B. (2001) The pathology of pulmonary artery hypertension. *Clin Chest Med* 22, 393-404.

195. Rhodes, J. (2005) Comparative physiology of hypoxic pulmonary hypertension: historical clues from brisket disease. *J Appl Physiol* 98, 1092-1100.
196. Wu, Z. S., Hall, S. M., Haworth, S. G. (2002) Pulmonary vascular remodeling in hypoxic hypertension in newborn pigs. *Hunan Yi Ke Da Xue Xue Bao* 27, 114-116.
197. Dempsey, E. C., Das, M., Frid, M. G., Stenmark, K. R. (1996) Unique growth properties of neonatal pulmonary vascular cells: importance of time- and site-specific responses, cell-cell interaction, and synergy. *J Perinatol* 16, 2-11.
198. Haworth, S. G. and Hislop, A. A. (2003) Lung development-the effects of chronic hypoxia. *Semin Neonatol* 8, 1-8.
199. Rabinovitch, M., Gamble, W. J., Miettinen, O. S., Reid, L. (1981) Age and sex influence on pulmonary hypertension of chronic hypoxia and on recovery. *Am J Physiol* 240, 62-72.
200. Leonoudakis, D., Gray, A. T., Winegar, B. D., Kindler, C. H., Harada, M., Taylor, D. M., Chavez, R. A., Forsayeth, J. R., Yost, C. S. (1998) An open rectifier potassium channel with two pore domains in tandem cloned from rat cerebellum. *J Neurosci* 18, 868-877.
201. Rajan, S., Wischmeyer, E., Xin Liu, G., Preisig-Müller, R., Daut, J., Karschin, A., Derst, C. (2000) TASK-3, a novel tandem pore domain acid-sensitive K⁺ channel. An extracellular histidine as pH sensor. *J Biol Chem* 275, 16650-16657.
202. Berg, A. P., Talley, E. M., Manger, J. P., Bayliss, D. A. (2004) Motoneurons express heteromeric TWIK-related acid-sensitive K⁺ (TASK) channels containing TASK-1 (KCNK3) and TASK-3 (KCNK9) subunits. *J Neurosci* 24, 6693-6702.
203. Manoury, B., Lamalle, C., Oliveira, R., Reid, J., Gurney, A. M. (2011) Contractile and electrophysiological properties of pulmonary artery smooth muscle are not altered in TASK-1 knockout mice. *J Physiol* 589 (13), 3231-3246.
204. Lassegue, B. and Clempus, R. E. (2003) Vascular NAD(P)H oxidases: specific features, expression, and regulation. *Am J Physiol Regul Integr Comp Physiol* 285(2), 277-297.
205. Haurani, M. J., Cifuentes, M. E., Shepard, A. D., Pagano, P. J. (2008) Nox4 oxidase over expression specifically decreases endogenous Nox4 mRNA and

- inhibits angiotensin II-induced adventitial myofibroblast migration. *Hypertension* 52(1), 143-149.
206. Miller, A. A., Drummond, G. R., Schmidt, H. H., Sobey, C. G. (2005) NADPH oxidase activity and function are profoundly greater in cerebral versus systemic arteries. *Circ Res* 97(10), 1055-1062.
207. Pan, J., Yeager, H., Cutz, E. (2008) Immunohistochemical localization and multigene expression profiling of O₂ sensor components in airway chemoreceptors. *FASEB J* 22, 1122.6.
208. Hartness, M. E., Lewis, A., Searle, G. J., O'Kelly, I., Peers, C., Kemp, P. J. (2001) Combined antisense and pharmacological approaches implicate hTASK as an airway O₂ sensing K(+) channel. *J Biol Chem* 276, 26499-26508.
209. Wanner, A., Salathé, M., O'Riordan, T. G. (1996) Mucociliary clearance in the airways. *Am J Respir Crit Care Med* 154, 1868-1902.
210. Wang, D., De Deken, X., Milenkovic, M., Song, Y., Pirson, I., Dumont, J. E., Miot, F. (2005) Identification of a novel partner of duox: EFP1, a thioredoxin-related protein. *J Biol Chem* 280(4) 3096-3103.
211. Park, S. J., Chun, Y. S., Park, K. S., Kim, S. J., Choi, S. O., Kim, H. L., Park, J. W. (2009) Identification of subdomains in NADPH oxidase-4 critical for the oxygen-dependent regulation of TASK-1 K⁺ channels. *Am J Physiol Cell Physiol* 297, 855-864.
212. Lee, K. S. and Park, S. S. (1980) Effect of halothane, enflurane, and nitrous oxide on tracheal ciliary activity in vitro. *Anesth Analg* 59(6), 426-430.
213. Salathe, M. (2002) Effects of β -agonists on airway epithelial cells. *J Allergy Clin Immunol* 110(6), 275-281.
214. Hastie, A. T., Dicker, D. T., Hingley, S. T., Kueppers, F., Higgins, M. L., Weinbaum, G. (1986) Isolation of cilia from porcine tracheal epithelium and extraction of dynein arms. *Cell Motil Cytoskeleton* 6(1), 25-34.
215. Imaizumi, Y., Torii, Y., Ohi, Y., Nagano, N., Atsuki, K., Yamamura, H., Muraki, K., Watanabe, M., Bolton, T. B. (1998) Ca²⁺ images and K⁺ current during depolarization in smooth muscle cells of the guinea-pig vas deferens and urinary bladder. *J Physiol* 510, 705-719.
216. Hua, X., Zeman, K. L., Zhou, B., Hua, Q., Senior, B. A., Tilley, S. L., Bennett, W. D. (2010) Noninvasive real-time measurement of nasal mucociliary

clearance in mice by pinhole gamma scintigraphy. *J Appl Physiol* 108(1), 189-196.

8 DECLARATION

„Hiermit erkläre ich, dass ich die vorliegende Arbeit selbständig und ohne unzulässige Hilfe oder Benutzung anderer als der angegebenen Hilfsmittel angefertigt habe. Alle Textstellen, die wörtlich oder sinngemäß aus veröffentlichten oder nichtveröffentlichten Schriften entnommen sind, und alle Angaben, die auf mündlichen Auskünften beruhen, sind als solche kenntlich gemacht. Bei den von mir durchgeführten und in der Dissertation erwähnten Untersuchungen habe ich die Grundsätze guter wissenschaftlicher Praxis, wie sie in der „Satzung der Justus-Liebig-Universität Gießen zur Sicherung guter wissenschaftlicher Praxis“ niedergelegt sind, eingehalten sowie ethische, datenschutzrechtliche und tierschutzrechtliche Grundsätze befolgt. Ich versichere, dass Dritte von mir weder unmittelbar noch mittelbar geldwerte Leistungen für Arbeiten erhalten haben, die im Zusammenhang mit dem Inhalt der vorgelegten Dissertation stehen, oder habe diese nachstehend spezifiziert. Die vorgelegte Arbeit wurde weder im Inland noch im Ausland in gleicher oder ähnlicher Form einer anderen Prüfungsbehörde zum Zweck einer Promotion oder eines anderen Prüfungsverfahrens vorgelegt. Alles aus anderen Quellen und von anderen Personen übernommene Material, das in der Arbeit verwendet wurde oder auf das direkt Bezug genommen wird, wurde als solches kenntlich gemacht. Insbesondere wurden alle Personen genannt, die direkt und indirekt an der Entstehung der vorliegenden Arbeit beteiligt waren. Mit der Überprüfung meiner Arbeit durch eine Plagiatserkennungssoftware bzw. ein internetbasiertes Softwareprogramm erkläre ich mich einverstanden.“

Giessen, 21.03.2012

Ort, Datum



Unterschrift

**Der Lebenslauf wurde aus der elektronischen
Version der Arbeit entfernt.**

**The curriculum vitae was removed from the
electronic version of the paper.**

- 2006 – 2008 Lecturer at Department of Zoology, University of the Punjab Lahore, Pakistan.
- 2004 – 2006 Masters (MPhil) thesis in forensic science research laboratory at National Centre of Excellence in Molecular Biology, University of the Punjab Lahore, Pakistan. Thesis title: “Analysis of 15 Y-STRs in the Pathan population for forensic uses”.
- 1999 – 2001 Masters (MSc) thesis in evolutionary laboratory and fossils display and research centre at Department of Zoology, University of the Punjab Lahore, Pakistan. Thesis title: “Studies on fossil remains of the siwalik cervids”.

Awards

1. Travel grant from Institute of Anatomy and Cell Biology, Justus-Liebig-University, Giessen to attend and participate in annual conference of German Physiological Society (DPG), March 22-25, 2012, Dresden, Germany.
2. Travel grant from Institute of Anatomy and Cell Biology, Justus-Liebig-University, Giessen to attend and participate in annual conference of ATS, May 13-18, 2011, Denver, USA.
3. Grant from Institute of Anatomy and Cell Biology, Justus-Liebig-University, Giessen to attend 88th annual meeting of DPG, March 22-25, 2009, Giessen, Germany.
4. Received scholarship from Higher Education Commission (HEC) Pakistan for PhD from Germany.

Publications

1. Murtaza, G., Akhtar, M., Nayyer, A. Q. 2002. *Cervus rewati* explored for the first time from the Middle Siwaliks of Pakistan. *Sci Int.* (Lahore), 14(2): 125-128.

2. Murtaza, G., Akhtar, M., Nayyer, A. Q. 2002. Fossil remains of *Cervus sivalensis* Lydekker, from Middle Siwaliks of Pakistan. *Punjab Univ J Zool.* 17: 139-145.
3. Murtaza, G., Akhtar, M., Nayyer, A. Q. 2002. Fossil remains of *Cervus simplicidens* Lydekker from the Punjab province of Pakistan. *Punjab Univ J Zool.* 17: 71-76.
4. Murtaza, G., Akhtar, M., Nayyer, A. Q. 2003. First record of *Cervus* from Kallar Kahar, Chakwal district, the Punjab Province, Pakistan. *Sci Int.* (Lahore), 15(4): 363-364.
5. Arshad, M., Ansari, R., Rauf, A., Murtaza, G., Akhtar, M., Nayyer, A. Q. 2003. Dental morphological studies of *Cormohipparion theobaldi* (Lydekker), *Sci Int.* (Lahore), 15(2): 157-160.

Abstracts

1. Murtaza, G., Pfeil, U., Faulhammer, P., Goldenberg, A., Paddenberg, R., Kummer, W. 2012. The two-pore-domain K⁺-channel, TASK-1, does not mediate anesthetics induced effects on cilia-driven particle transport in the mouse trachea. Submitted and will be published in *Acta Physiologica.* 204: 689.
2. Murtaza, G., Pfeil, U., Faulhammer, P., Goldenberg, A., Weissmann, N., Paddenberg, R., Kummer, W. 2011. Two-pore domain K⁺-channel, TASK-1, is not crucial for hypoxic pulmonary vasoconstriction in the mouse. *Am J Respir Crit Care Med.* 183: A5485.

Poster / oral presentations at conferences

1. Murtaza, G., Pfeil, U., Faulhammer, P., Goldenberg, A., Paddenberg, R., Kummer, W. 2012. The two-pore-domain K⁺-channel, TASK-1, does not mediate anesthetics induced effects on cilia-driven particle transport in the mouse trachea. *Ninety first annual meeting of German Physiological Society Dresden, Germany, March 22-25, 2012.* Poster presentation.
2. Murtaza, G., Pfeil, U., Faulhammer, P., Goldenberg, A., Weissmann, N., Paddenberg, R., Kummer, W. 2011. Hypoxic pulmonary vasoconstriction is still operative in mice with target disruption of two-pore domain K⁺-Channel,

- TASK-1. *Fourth GGL annual conference Giessen, Germany, September 21-22, 2011*. Poster presentation.
3. Murtaza, G., Pfeil, U., Faulhammer, P., Goldenberg, A., Weissmann, N., Paddenberg, R., Kummer, W. 2011. Two-pore domain K⁺-channel, TASK-1, is not crucial for hypoxic pulmonary vasoconstriction in the mouse. *Second international ECCPS symposium Bad Nauheim, Germany, June 16-18, 2011*. Poster presentation.
 4. Murtaza, G., Pfeil, U., Faulhammer, P., Goldenberg, A., Weissmann, N., Paddenberg, R., Kummer, W. 2011. Two-pore domain K⁺-channel, TASK-1, is not crucial for hypoxic pulmonary vasoconstriction in the mouse. *International conference of ATS Denver, USA, May 13-18, 2011*. Poster and oral presentation.
 5. Murtaza, G., Pfeil, U., Faulhammer, P., Goldenberg, A., Weissmann, N., Warth, R., Paddenberg, R., Kummer, W. 2010. Two-pore domain K⁺-channel, TASK-1, is not crucial for hypoxic pulmonary vasoconstriction. *Third GGL annual conference Giessen, Germany, September 29-30, 2010*. Poster presentation.
 6. Murtaza, G., Faulhammer, P., Goldenberg, A., Weissmann, N., Brandes, R., Paddenberg, R., Kummer, W. 2009. Two-pore domain K⁺-channel, TASK-1, in pulmonary vessels and airways. *Second GGL annual conference, Giessen, Germany, September 30-October 1, 2009*. Poster presentation.

Symposiums / Workshops / Conferences Attended

1. Ninety First Annual Meeting of German Physiological Society. March 22-25, 2012, Dresden, Germany.
2. Fourth Annual Conference of GGL. September 21-22, 2011, Giessen, Germany.
3. Second International Symposium of ECCPS (Excellence Cluster Cardio-Pulmonary System). June 16-18, 2011, Bad Nauheim, Germany.
4. International Conference of ATS (American Thoracic Society). May 13-18, 2011, Denver, USA.
5. K₂P-Kanäle - vom Molekül zur Physiologie und Pathophysiologie Symposium. October 07-09, 2010, Marburg, Germany.
6. Third Annual Conference of GGL. September 29-30, 2010, Giessen, Germany.
7. Cardiac Physiology & Experimental Cardiology Workshop. September 16-17, 2010, Rauschholzhausen, Germany.

8. Annual Retreat of MBML (Molecular Biology of Medicine and Lung). May 28-29, 2010, Rauischholzhausen, Germany.
9. Seventy Sixth Annual Meeting of German Cardiac Society. April 08-10, 2010, Mannheim, Germany.
10. Chronic Obstructive Pulmonary Disease (COPD) Workshop. December 10-11, 2009, Marburg, Germany.
11. First Von Behring-Röntgen Symposium, Neurotransmission then, now and tomorrow - The lessons of Loewi - November 18-19, 2009, Marburg, Germany.
12. Second Annual Conference of GGL. September 30-October 1, 2009, Giessen, Germany.
13. Eighty Eighth Annual Meeting of German Physiological Society. March 22-25, 2009, Giessen, Germany.

Membership in Professional Societies

1. European Respiratory Society (ERS)
2. International Society of Zoological Sciences (ISZS)
3. The New York Academy of Sciences (NYAS)
4. British Science Association (BSA)
5. American Thoracic Society (ATS)

10 ACKNOWLEDGEMENTS

All praises, gratitude, and thanks to the grace of **ALLAH ALMIGHTY**, WHO is the ultimate source of knowledge to mankind. Bow in obeiscene, I before my Lord, WHO bestows me to fortitude and impetus to accomplish this task and elucidate a drop of already existing ocean of knowledge. Then all praises to His Messenger **HAZRAT MUHAMMAD** (*Peace Be Upon Him*), Who is an eternal beacon of guidance, and persuasion and source of knowledge for humanity.

I owe a great debt of deepest respect and sincere gratitude to **Prof. Dr. Wolfgang Kummer**, for the vision and foresight which inspired me to conceive this research project. He provided me this opportunity to work in Human Biology with all laboratory facilities and helped at all stages of research work and thesis writing. His kind and helping behaviour coupled with friendly and benevolent attitude towards science was a source of enthusiasm and inspiration for me. The work presented in this manuscript was accomplished under his supervision with patient and enthusiastic guidance, affectionate and friendly attitude, and studious and intellectual approach.

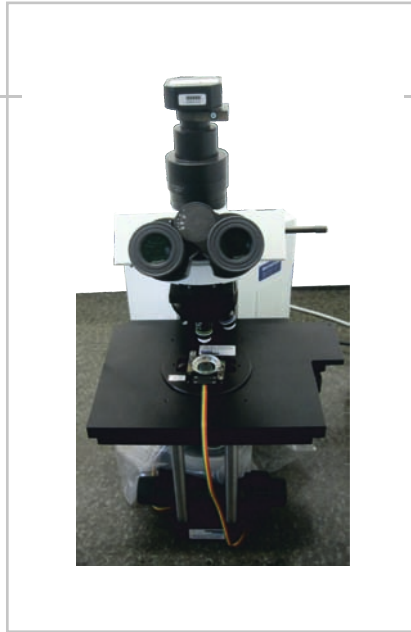
Many thanks and gratitude also go to **Prof. Dr. Nobert Weissmann**, and **Prof Dr. Günter Lochnit** for conducting important experiments for my research work in their laboratories. I would also like to appreciate **Prof. Dr. Ralf Brandes** and **Prof. Dr. Richard Warth** for providing me knockout mice to complete my research work. I would like to thank **Dr. Renate Paddenberg**, **Dr. Uwe Pfeil**, **Mr. Amir Rafique**, and **Dr. Gabriela Krasteva** for their valuable suggestions, guidance, and support in bringing out research work successfully. I especially appreciate **Anna Goldenberg**, **Petra Faulhammer**, **Barbara Gries**, **Martin Bodenbenner-Türich**, and **Tamara Papadakis** for providing me technical assistance during the whole period of my research work. They have always been ready to help me with an encouraging attitude.

It seems impossible for me to go ahead without paying thanks to **Higher Education Commission (HEC) Pakistan**, and **German Academic Exchange Service (DAAD) Germany**. The completion of research work and thesis compilation would not have been possible without the financial support provided by HEC and the collaboration of DAAD. I can not express my sincere praise enough for **International Giessen**

Graduate Centre for the Life Sciences (GGL) which has been always source of knowledge and guidance for me.

My heartfelt thanks and appreciation to my wife **Razia Sultana** for her patience, encouragement, support, and care and my daughter **Eshaal Murtaza** who had always been around to share her infinite joy and sitting with me during literature search and thesis writing.

I also extend my special thanks to brothers, sisters, and friends for their continuous and wholehearted cooperation, encouragement, and constructive suggestion at various stages of the study. Also thanks to everyone for supporting my work and help during the study until it is fully completed.



édition scientifique
VVB LAUFERSWEILER VERLAG

VVB LAUFERSWEILER VERLAG
STAUFENBERGRING 15
D-35396 GIESSEN

Tel: 0641-5599888 Fax: -5599890
redaktion@doktorverlag.de
www.doktorverlag.de

ISBN: 978-3-8359-5937-8



9 7 8 3 8 3 5 1 9 5 9 3 7 8